# Automated Detection and Classification of Brain Tumor from MRI Images using Machine Learning Methods


*By*

Ghulam Gilanie

CIIT/FA14-PCS-007/LHR

PhD Thesis

In

Computer Science

COMSATS University Islamabad

Lahore Campus-Pakistan

Fall, 2018


**COMSATS University Islamabad**

# Automated Detection and Classification of Brain Tumor from MRI Images using Machine Learning Methods

A Thesis Presented to

COMSATS University Islamabad

In partial fulfillment

of the requirement for the degree of

## PhD (Computer Science)

By

Ghulam Gilanie

CIIT/FA14-PCS-007/LHR

Fall, 2018

# Automated Detection and Classification of Brain Tumor from MRI Images using Machine Learning Methods

A Post Graduate Thesis submitted to the Department of Computer Science as partial fulfillment of the requirement for the award of Degree of Ph.D in Computer Science.


| Name | Registration Number |
|---|---|
| Ghulam Gilanie | CIIT/FA14-PCS-007/LHR |

**Supervisor**

Dr. Usama Ijaz Bajwa

Assistant Professor, Department of Computer Science

COMSATS University Islamabad, Lahore Campus

**Co-Supervisor**

Prof. Dr. Zulfiqar Habib

Chairman, Department of Computer Science

COMSATS University Islamabad, Lahore Campus

## Certificate of Approval

This is to certify that the research work presented in this thesis, entitled "Automated Detection and Classification of Brain Tumor from MRI Images using Machine Learning Methods" was conducted by Mr. Ghulam Gilanie, CIIT/FA14-PCS-007/LHR, under the supervision of Dr. Usama Ijaz Bajwa. No part of this thesis has been submitted anywhere else for any other degree. This thesis is submitted to the Department of Computer Science, COMSATS University Islamabad, Lahore Campus, in the partial fulfillment of the requirements for the degree of Doctor of Philosophy in the field of Computer Science.

Student Name: Mr. Ghulam Gilanie Signature: _____

**Examination Committee:**

Signature: _____ Signature: _____

External Examiner 1:

Dr. Abdul Jalil
Professor
Department of Electrical Engineering
International Islamic University, Islamabad

External Examiner 2:

Dr. Adnan Abid
Associate Professor
Department of Computer Science
University of Management and Technology, Lahore

Signature: _____ Signature: _____

Dr. Usama Ijaz Bajwa
Supervisor
Assistant Professor
Department of Computer Science
COMSATS University Islamabad
Lahore Campus

Dr. Ghulam Rasool
HoD
Associate Professor
Department of Computer Science
COMSATS University Islamabad
Lahore Campus

Signature: _____

Prof. Dr. Syed Asad Hussain
Dean, Faculty of Information Science & Technology
COMSATS University Islamabad

## Author's Declaration

I Ghulam Gilanie, CIIT/FA14-PCS-007/LHR, hereby state that my PhD thesis titled "Automated Detection and Classification of Brain Tumor from MRI Images using Machine Learning Methods" is my own work and has not been submitted previously by me for taking any degree from this university i.e. COMSATS University Islamabad or any anywhere else in the country/world.

At any time if my statement is found to be incorrect even after I graduate the University has the right to withdraw my PhD degree.

Date: 14-05-2019

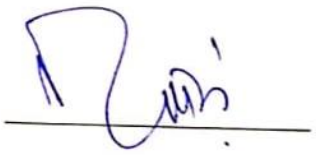

**Ghulam Gilanie**

CIIT/FA14-PCS-007/LHR

## Plagiarism Undertaken

I solemnly declare that research work presented in the thesis titled "Automated Detection and Classification of Brain Tumor from MRI Images using Machine Learning Methods" is solely my research work with no significant contribution from any other person. Small contribution/help wherever taken has been duly acknowledged and that complete thesis has been written by me.

I understand the zero tolerance policy of HEC and COMSATS University Islamabad towards plagiarism. Therefore, I as an author of the above titled thesis declare that no portion of my thesis has been plagiarized and any material used as reference is properly referred/cited.

I undertake that if I am found guilty of any formal plagiarism in the above titled thesis even after award of PhD degree, the University reserves the right to withdraw/revoke my PhD degree and that HEC and the University has the right to publish my name on the HEC/University website on which names of students are placed who submitted plagiarized thesis.

Date: 14-05-2019

**Ghulam Gilanie**

CIIT/FA14-PCS-007/LHR

# Certificate

It is certified that Mr. Ghulam Gilanie CIIT/FA14-PCS-007/LHR has carried out all the work related to this thesis under my supervision at the Department of Computer Science, COMSATS University Islamabad, Lahore Campus and the work fulfills the requirement for award of PhD degree.

Date: 20-05-2019

Supervisor:

Dr. Usama Ijaz Bajwa
Assistant Professor,
Department of Computer Science

Head of Department:

Dr. Ghulam Rasool
Associate Professor,
Department of Computer Science

# DEDICATION

## Dedicated to

## The Holy Prophet MUHAMMAD ﷺ

## انتساب

سرکارِ دو عالَم، حُضُورِ اکرم، سیّدِ عالَم، نورِ مُجسّم، شاہِ بنی آدم، رسولِ مُحتشم، رَحمتِ عالَم، سرکارِ خیر الاَنام، نبیِّ کریم، محبوبِ ربِّ عظیم، رء وف رحیم، سرکارِ نامدار، مدینے کے تاجدار، دو عالَم کے مالِک ومختار، شَہَنشاہِ اَبرار، بِاِذنِ پروَردگار، سرکارِ عالی وقار، حُضُور سراپا نور، شافِعِ یومُ النُّشُور، فیض گنجور، شاہِ غیور، حُضورِ انور، شافِعِ مَحشر، مدینے کے تاجور، بِاِذنِ ربِّ اکبر، غیبوں سے باخبر، محبوبِ داوَر عَزَّ وَجَلَّ وَصَلَّی اللہ تَعَالٰی علیہ وَاٰلہٖ وَسلَّم

سرکارِ مدینہ، سلطانِ باقرینہ، قرارِ قلب وسینہ، فَیض گنجینہ، صاحِبِ مُعَطَّر پسینہ، باعثِ نُزولِ سکینہ، راحَتِ قلب وسینہ، سلطانِ مکّۂ مُکَرَّمہ، تاجدارِ مدینۂ منوّرہ، اللہ کے حبیب، حبیبِ لبیب، دانائے غُیُوب، مُنَزَّہٌ عَنِ الْعُیُوب، اللہ کے محبوب، اللہ کے پیارے رسول، رسولِ مقبول، سیّدہ آمِنہ کے گلشن کے مہکتے پھول عَزَّ وَجَلَّ وَصَلَّی اللہ تَعَالٰی علیہ وَاٰلہٖ وَسلَّم ورضی اللہ تَعَالٰی عنہا

میٹھے میٹھے مکّی مَدَنی آقا، حضرتِ سیِّدُنا محمدِ مصطفٰے، حُضُورِ اقدس، نبیِّ رَحمت، تاجدارِ رسالت، شَہَنشاہِ نُبُوَّت، پیکرِ جُود وسخاوت، سراپا رَحمت، شَفیعِ امّت، محبوبِ ربُّ العزّت، میرے میٹھے مدینے کے عظمت والے سلطان، سلطانِ دو جہان، شَہَنشاہِ کون ومکان، رَحمتِ عالَمیان، سرورِ ذیشان، محبوبِ رَحمٰن، شفیعِ مُجرِمان، نبیوں کے سُلطان، سردارِ دو جہان، شَہَنشاہِ زمین وآسمان، امامُ الاَنصارِ وَالْمُہاجِرین، مُحِبُّ الْفُقَراءِ وَالْمَساکین، جنابِ رَحْمَۃٌ لِّلْعٰلمین، رَحمتِ کونَین، سلطانِ حَرَمین، نانائے حَسَنَین عَزَّ وَجَلَّ وَصَلَّی اللہ تَعَالٰی علیہ وَاٰلہٖ وَسلَّم ورضی اللہ تَعَالٰی عنہما

کے نام

# ACKNOWLEDGMENTS

I am nothing without the support and blessings of Almighty **Allah**, my faith in the pious and peaceful religion Islam and faith in the last messenger of **Allah**, **Hazrat Muhammad (P.B.U.H)** strengthened me to carried out each and every bit of my life and so as in this work.

I would like to thank my supervisor **Dr. Usama Ijaz Bajwa** for providing me the opportunity to work on the brain MRI images for tumor detection, colorization of gray scale brain MRI images and brain tumor classification. I specially thank to my co-supervisor **Prof. Dr. Zulfiqar Habib**. It was during my discussions with him that I finally decided a research topic, which focused on brain MRI. His continued mentorship has made it possible the research project. His depth of knowledge on computational paradigms, encouragement, suggestions for improvement and supervision helped me to carried out this research productively.

I would also like to thank **Prof. Dr. Muhammad Shahid Naweed, Dr. Muhammad Aksam Iftikhar, Dr. Muhammad Waqas Anwar** and **Mr. M. Attique Rafique** for their intelligence, wit, vision and impeccable professionalism who provided an endless supply of visionary ideas.

I am deeply thankful and want to express my honest appreciations to my dear friends **Mr. Qaisar Hassan, Dr. Rana Tanveer Ahmed**, and **Mr. Muhammad Adeel Saqib** for their friendship, idea generation, providing jolly and entertainment oriented environment. I appreciate their priceless time, moral support and assistance.

Exceptional thanks for **Prof. Dr. Mustansar Mahmood Waraich** of Bahawal Victoria Hospital, Bahawalpur, Pakistan and his staff who spent time in explaining their jobs, explaining their needs, in evaluating this method, providing me valuable connotation for future work, providing MRI Data, sharing anonymized data, radiological consultation, expert opinion, validation of outcomes, further biological required assistance and gold truths for the patients already successfully treated.

Others who have helped along the way are my students Mr. Asad Razzaq, Mr. Atif Sajjad, Mr. Usman Mushtaq, Mr. Naweed Kanwar, Mr. Aftab Saeed, Mr. Saif Ullah Tarrar,

Muhammad Nasir, Mr. Hamza Rafique, who have endured far too many teaching experiments.

I'd also like to mention, Mr. Muhammad Mashhood, Mr. Muhammad Adrees Graywal and Mr. Adnan Hameed Qureshi, in thinly veiled attempts to make me miss a putt, constantly asked, "Is that my PhD done yet?" Particularly effective was Mr. Muhammad Sami of Dahranwala (my school fallow).

I remember the generosity and encouragement of the eminent PSP officer **Mr. Mirza Faran Baig** and owe the dev of his kindness, which I can never return.

My heartfelt thanks go to my great father **Raja Habib Ullah Janjua**, my beloved ami jan **Safia Nasreen**, my wife **Ms Saba Parveen**, my doll **Ayesha Noor**, my lovely sons **Mr. Muhammad Shareque Janjua** and **Mr. Muhammad Abdullah Janjua** and my sisters **Ms Shaguftah Anjuam**, **Ms Shahistah Habib** and **Dr. Sumera Kanwal** for believing in me and inspiring me during my **Ph.D**.

And, in saving the best for last, a special note of thanks and appreciation to my **late Chachu Jan Raja Muhammad Afzal Janjua** and my elder brother **Dr. Hafeez Ullah Janjua** who have been involved in this work from the start and provided loving support every step of the way.

I couldn't have done it without all of you.

**Ghulam Gilanie**

**CIIT/FA14-PCS-007/LHR**

# ABSTRACT


## Automated Detection and Classification of Brain Tumor from MRI Images using Machine Learning Methods

The focus of this thesis is to report an automated, efficient, and robust method of brain tumor detection and classification from Magnetic Resonance Images (MRI) images. Clinically, it is a challenging issue faced by the researchers working in this domain. In routine health care units, Magnetic Resonance (MR) scanners are being used to generate a massive number of brain slices, underlying the anatomical details. Pathological assessment from this medical data is being carried out manually by the radiologists or neuro-oncologists. Due to huge volume of brain anatomical data produced by MRI scanners, it is almost impossible to manually analyze every slice. Conclusively, if automated protocols are executed for auto-interpretation; not only the radiologist will be assisted but also a better pathological assessment process would be expected. Several methods have been suggested to address this problem, but still, accuracy, robustness and optimization is still an open issue to address. The development of such automated procedures is difficult due to complex organization of brain cells, several types of tumor, difference in medical traits of a specific ethnicity and many more factors. To achieve the target, research has been started from reviewing the most popular and prominent state-of-the-art methods. Based upon the reviewed literature, automated brain tumor detection and classification techniques have been reported with high computational cost, low classification rates, detection and classification of only one or a few of brain tumor types, lack of robustness, etc. Therefore, step wise research and experiments based upon empirical scientific methodology have been performed in order to achieve the objectives of brain tumor classification.

In the first step, a research activity has been performed to report a colorization method with the aims to enhance the visualization, cell characterization and interpretation of brain cells. The high dimensional brain data scanned through MRI embodied in gray scale, if converted, represented, mapped and/or visualized in colored versions, irrefutably, more definitive and more accurate the pathological assessment process will be. Several methods have been reported to represent brain MRI data in color with high computational

complexity. In this research activity, an efficient method of colorization using frequencies from visible range of color spectrum, has been proposed to embody the variations and sensitivity of the brain MRI images. The experiments have been performed on a locally developed dataset. Side by side visual comparison based on multiple MRI sequences of identical subjects by domain experts have proved the adequate success and fruitfulness of the story. The reported method of colorization as a protocol has also been deployed in Department of Radiology and Diagnostic Images, Bahawal Victoria, Hospital, Bahawalpur (BVHB), Pakistan. Radiologists are using this tool for visual interpretation and monitoring of the patients for their assessment and clinical decision making.

In second step, an automated approach using Gabor filter and Support Vector Machines (SVMs), for the classification of brain MRI slices as normal or abnormal has been reported. Accuracy, sensitivity, specificity and AUC-value have been used as standard quantitative measures to evaluate the proposed algorithm. To the best of our knowledge, this is the first study in which experiments have been performed on The Whole Brain Atlas - Harvard Medical School (HMS) dataset, achieving an accuracy of 97.5%, sensitivity of 99%, specificity of 92% and AUC-value as 0.99. To test the robustness against medical traits based on ethnicity and to achieve optimization, a locally developed dataset has also been used for experiments and remarkable results with accuracy (96.5%), sensitivity (98%), specificity (92%) and AUC-value (0.97) were achieved. Comparison with state-of-the art methods proved the overall efficacy of the proposed method.

In third step of the thesis, a method has been proposed to classify brain MRI image into brain related disease groups and further tumor types. The proposed method employed Gabor texture followed by a set of more distinguished statistical features. These features are then used by SVM to classify the brain disorder. K-fold strategy has been adapted for cross validation of the results to enhance generalization of SVM. Experiments have been performed to classify brain MRI images as normal or belonging to either of the common diseases, such as cerebrovascular, degenerative, inflammatory, and neoplastic. Neoplastic disease is further classified into glioma, meningioma, metastatic adenocarcinoma, metastatic bronchogenic carcinoma, or sarcoma. Standard quantitative evaluation measures, i.e., accuracy, specificity, sensitivity, and AUC-value have been used to test

performance of the developed system. The proposed system has been trained on complete dataset of HMS, so the trained model has the ability to deal with a wide range of brain abnormalities. Further, to achieve robustness, a locally developed dataset has also been used for experiments. Remarkable results on different orientations, sequences of both of these datasets as per accuracy (up-to 99.6%), sensitivity (up-to 100%), specificity (up-to 100%), precision (up-to 100%) and AUC-value (up-to 1.0) have been achieved. The proposed method classifies the brain MRI slices into defined abnormality groups. It can also classify the abnormal slices into tumorous or non-tumorous one. The major achievement of the developed system is its auto classification of tumorous slices into the slices having primary tumor or secondary tumor and their further types, which possibly could not be determined without biopsy.

In fourth step of the thesis, results achieved through the proposed method of brain tumor classification have been validated on cross data set. The drive of this research activity is to verify the robustness of the reported approach. For this, the model has been trained completely on one data set, while tested completely on another one. A benchmarked dataset HMS and a locally developed dataset BVHB dataset has been used for this purpose. To ensure its robustness, complete HMS dataset was used to train the model and BVHB was used to test the trained model and vice versa. Standard evaluation measures, i.e., accuracy, specificity, sensitivity, precision and AUC-value have been used to evaluate the system. It has been established that the proposed method deals with multiformity and variability of brain MRI data. Overall, suppositions regarding robustness of the proposed method were attained with maximum measures as per accuracy as 92%, specificity as 92%, sensitivity as 93%, precision as 92%, and AUC-value as 0.93.

The overall results achieved through the proposed method, manifests that it is robust, efficient and reliable. It has been trained on a large volume of multi-orientations, multi-sequences belonging to multi-datasets to deal with multiformity and to face variability.

# TABLE OF CONTENTS

# LIST OF FIGURES

# LIST OF TABLES

# LIST OF ABBREVIATIONS

| | |
|---|---|
| ADF | Anisotropic Diffusion Filtering |
| AI | Artificial Intelligence |
| AMRI | Advance Magnetic Resonance Images |
| ANN | Artificial Neural Networks |
| BRATS | Brain Tumor Segmentation |
| BRINT | Binary Rotation Invariant and Noise Tolerant |
| BVH | Bahawal Victoria Hospital |
| BVHB | Bahawal Victoria Hospital, Bahawalpur |
| CNN | Convolution Neural Networks |
| CSF | Cerebrospinal Fluid |
| CT | Computed Tomography |
| DAE | Deep Auto Encoders |
| DBM | Deep Boltzmann Machines |
| DBN | Deep Belief Networks |
| DWT | Discrete Wavelet Transformations |
| EEG | Electro Encephalo Graphy |
| ELM | Extreme Learning Machine |
| FCM | Fuzzy C-Mean |
| FLAIR | Fluid Attenuated Inversion Recovery |
| fMRI | Functional Magnetic Resonance Images |
| FNR | False Negative Rate |
| FPR | False Positive Rate |
| GA | Genetic Algorithm |
| GLCM | Gray Level Co-occurrence Matrix (GLCM) |
| GM | Gray Matter |
| IBSR | Internet Brain Segmentation Repository |
| ICA | Independent Component Analysis |
| JC | Jaccard Coefficient |
| KNN | K-Nearest Neighbors |

| | |
|---|---|
| LBP | Local Binary Patterns |
| LDA | Linear Discriminative Analysis |
| LLB | Local Learning Based |
| LVQ | Learning Vector Quantization |
| MEG | Magneto Encephalo Graphy |
| MI | Mutual Information |
| MR | Magnetic Resonance |
| MR GAD | Gadolinium Contrast Medium |
| MRF | Markov Random Fields |
| MRI | Magnetic Resonance Images |
| MS | Multiple Sclerosis |
| NLM | Non Local Means |
| PCA | Principal Component Analysis |
| PDW | Proton Density-weighted |
| PET | Positron Emission Tomography |
| PNN | Probabilistic Neural Network |
| PSO | Particle Swarm Optimization |
| PVE | Partial Volume Effect |
| RLM | Run Length Matrix |
| ROI | Region of Interest |
| SIFT | Scale Invariant Feature Transform |
| SPECT | Single-Photon Emission Computed Tomography |
| SURF | Speeded Up Robust Features |
| SVM | Support Vector Machine |
| SVMs | Support Vector Machines |
| T1C | T1 with post contrast |
| T1W | T1 weighted |
| T2W | T2 weighted |
| TN | True Negative |
| TP | True Positive |
| UB | Urine Bile |

| | |
|---|---|
| WLD | Weber Law Descriptors |
| WM | White Matter |

# LIST OF PUBLICATIONS

1. **Gilanie G**, Bajwa UI, Waraich MM, Habib Z. "Computer aided diagnosis of brain abnormalities using texture analysis of MRI images", *International Journal of Imaging Systems and Technology*, (2019), 1–12, https://doi.org/10.1002/ima.22312, accepted article, (**IF:1.423**).

2. **Ghulam Gilanie**, Usama Ijaz Bajwa, Mustansar Mehmood Waraich, Zulfiqar Habib, Hafeez Ullah, Muhammad Nasir, "Classification of Normal and Abnormal Brain MRI Slices using Gabor Texture and Support Vector Machines", *Signal Image and Video Processing, (2018)*, 12(**3**), 479-487. (**IF:1.202**).

3. **Gilanie G.**, Ullah H., Mehmood Mustansar, Usama Ijaz, Habib Z., "Colored Representation of Brain Gray Scale MRI Images to potentially underscore the variability and sensitivity of images", *Current Medical Imaging Reviews, (2018)*, 14(**4**),555-560. (**IF:0.60**).

4. Usama Ijaz Bajwa, Abdullah Ali Shah, Muhammad Waqas, **Ghulam Gilanie**, Asma Ejaz Bajwa, "Computer-Aided Detection (CADe) System for Detection Of Malignant Lung Nodules In CT Slices – A Key For Early Lung Cancer Detection", *Current Medical Imaging Reviews, (2017)*, 13(**4**). (**IF:0.60**).

5. Asghar K, **Gilanie G.**, Saddique M., Habib Z, "Automatic Enhancement of Digital Images using Cubic Bézier Curve and Fourier Transformation", *Malaysian Journal of Computer Science (MJCS), (2017*), 30(**4**), 300-310. (**IF:0.405**).

6. **Ghulam Gilanie**, Usama Ijaz Bajwa, Mustansar Mehmood Waraich, Zulfiqar Habib, "Robust and automated brain disorders classification method validated Across datasets", *submitted article*.

# Chapter 1

# Introduction

## 1.1. Introduction

In human organs, a tumor is uncontrolled growth of abnormal cells [1]. Tumors belong to identical groups on the basis of their individualism. Clinically, these different disorders are healed with different methods. Brain tumors can originate inside the brain or invade to brain from else part of the human body. The brain tumors, which originate inside the brain and remain inside it are called primary tumors, while the brain tumors that originate in else parts of human body and travel toward human brain are called metastatic tumors [2]. World Health Organization (WHO) has issued a grading scheme for brain tumors, i.e., grade I to IV. Brain tumors of grade I-II are benign (low-grade), while brain tumors of grade III-IV (high-grade) are malignant. Clinically, if brain tumor of low-grade is not healed, possibly it will deteriorate to high-grade. Surgery, radiotherapy, chemotherapy and other treatment planning strictly depend upon the precision of brain tumor detection, classification and grading carried out by a radiologist, neuro-surgeon and radio oncologist [3].

With the advancement of imaging methods, medical imaging modalities are being used for the evaluation of subjects. Grayscale images of anatomical structures are usually obtained through medical imaging modalities, such as Ultrasonography, X-Ray, Computed Tomography (CT), Electro Encephalo Graphy (EEG), Magneto Encephalo Graphy (MEG), Positron Emission Tomography (PET), Single-Photon Emission Computed Tomography (SPECT) and Magnetic Resonance Imaging MRI [4]. They scan the human anatomical structures to exhibit their aspects. The targeted anatomical structures include liver, brain, prostate, kidney, heart, breast or abdominal structures [5]. Healthcare units, medical centers, hospitals, trauma centers, cancer diagnostic units and medical care units are using these imaging methods to scan the human anatomies and are generating terabytes of data in each moment [6].

Still, in this modern digital age, luminance values exhibiting anatomical structures are being interpreted through a naked eye by domain experts to determine the presence and level of aggressiveness of abnormal tissues. Manual analysis refers to the interpretation of medical data with necked aye using radiological & biological information and personal previous experience. The manual analysis for the evaluation of subjects enables the

clinicians and practitioners to study or to prepare treatment planning. With this massive volume of anatomical data, manual interpretation has become almost impossible [7]. Therefore, robust and efficient protocols, also called Computer Aided Diagnosis (CAD) systems always remained decisive in patient's treatment planning [8].

Although, thick bones of the skull have protected the brain, however, it is susceptible to many types of abnormalities, such as brain cerebrovascular diseases, degenerative diseases, inflammatory diseases and neoplastic (tumor) diseases [9]. The brain diseases that affect the blood vessels of the human brain are called cerebrovascular diseases. Some of the common diseases are subarachnoid hemorrhage, stroke and transient ischemic attack (mini-stroke). The brain disorders that are the result of a continuous process based on cell changes, affecting organs or tissues are called degenerative diseases. The brain disorders having a condition where the brain become inflamed are called inflammatory or infectious diseases. The examples of the diseases include irritation and swelling of brain tissue or blood vessels.

Being non-invasive medical examination, MRI is currently the best test for assessment of abnormalities present inside a brain. It has more contrast among soft tissues with a high spatial resolution that helps physicians in diagnosing and treating medical conditions. Brain disorders are quite extensive and complex. Therefore, these must be pictured well, so that a radiologist be assisted well in its accurate and definitive diagnosis procedure. MRI delivers important information about size, localization, and shape of brain tumors without revealing the subject to high ionization radiation [10]. Therefore, MRI has a central position in brain tumor evaluation process in a clinical atmosphere. Clinically, different sequences of MRI are utilized to diagnosis and delineate tumor spots [11, 12]. These sequences include T1-weighted (T1W), Gadolinium Contrast Medium (MR GAD), T1 with post contrast (T1C), Proton Density-weighted (PDW), T2-weighted (T2W) and Fluid Attenuated Inversion Recovery (FLAIR) [13] as shown in Figure 1.1 with direct views of the body in almost any orientation, i.e., coronal, sagittal and axial [14] as shown in Figure 1.2. These sequences and views enable tissues to be visualized well for their interpretation and analysis by a radiologist. These sequences have equal clinical importance regarding the anatomical detailed study, a better distinction between solid and

cystic structures and evaluation and monitoring of pathological changes etc. T1W sequence images are mostly used for the study of normal anatomy. However, necrotic, and active tumor areas can easily be recognized using this sequence after administration of intravenous contrast.

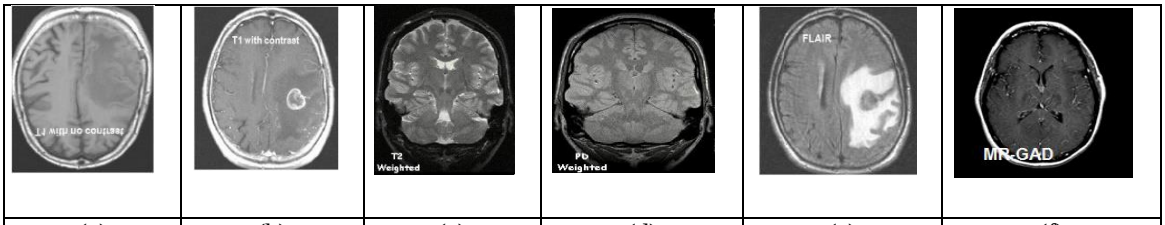


(a) (b) (c) (d) (e) (f)

Figure 1.1: MRI sequences (A) T1W (B) T1C (C) T2W (D) PDW (E) FLAIR and (F) MR-GAD

The surrounding areas of a brain tumor usually called edema are more easily distinguishable using T2W sequence images. FLAIR sequence images are mostly used to suppress the intraventricular CSF signals. This sequence is important in studying and separating the edema and CSF regions [15]. PDW is mostly used for the evaluation of MS lesions. These sequences as an individual or combination of these are used to differentiate any fatty deposit in the tumors. The presence of fat in the lesion determines its benign nature that is a differentiating point between neoplastic and non-neoplastic lesions.

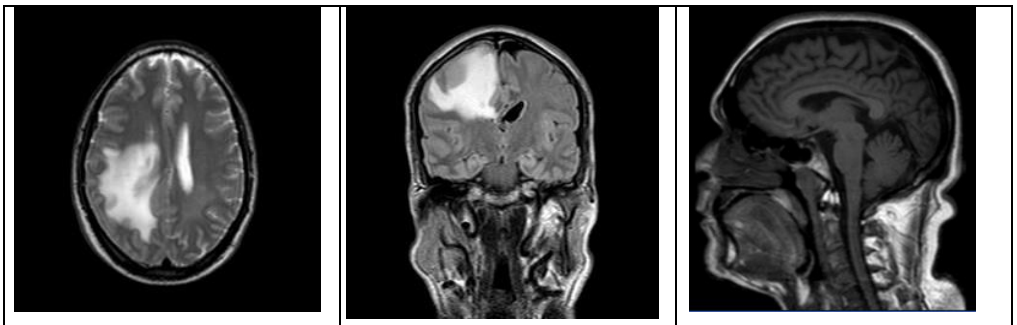

(a) (b) (c)

Figure 1.2: MRI orientations (a) Axial (b) Coronal (c) Sagittal

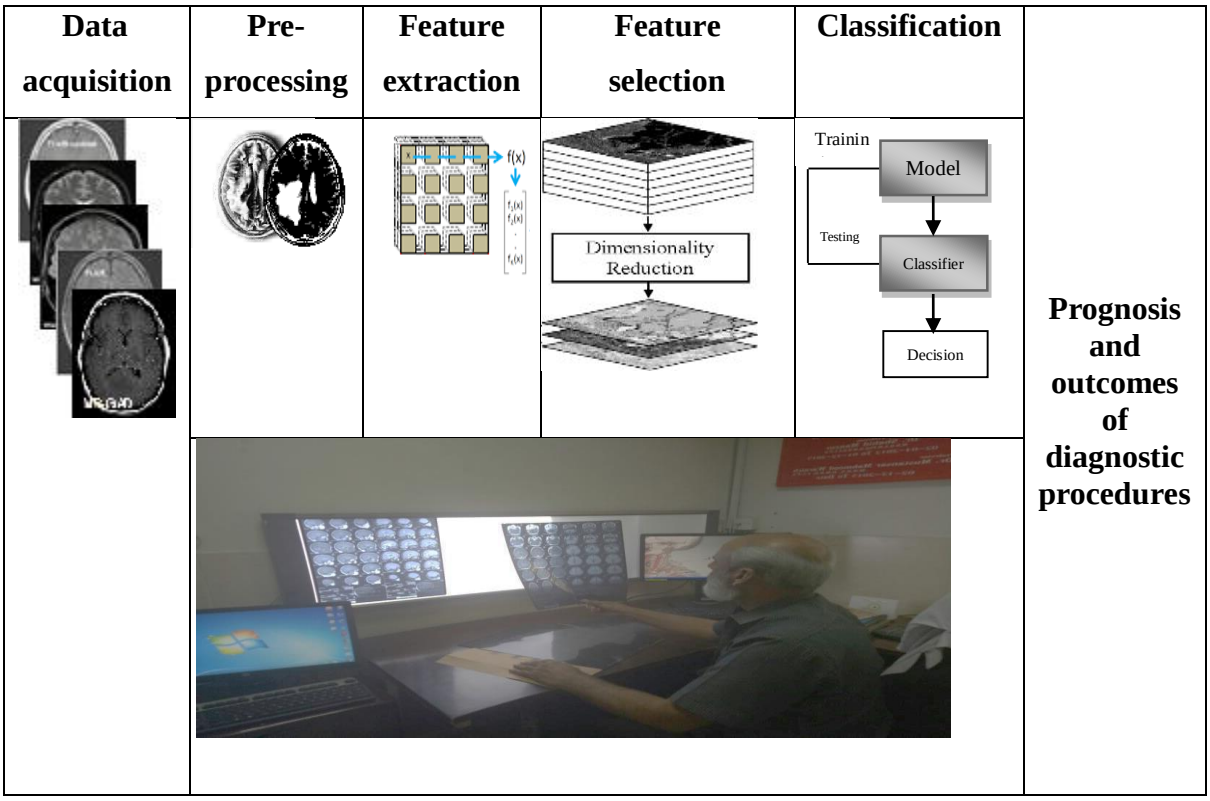


Figure 1.3: Typical computer aided diagnosis scheme and manual interpretation

Figure 1.3 shows the details of a typical CAD and manual system. In a CAD system, MRI slices are input to the system. If necessary, pre-processing is performed. In the next phase, suitable features are extracted. After having extracted features, classification algorithms are used. On the other hands, in a conventional clinical environment, a radiologist analyzes brain MR data through his/her naked eyes to determine an abnormality.

Brain tumor assessment and its cure depend upon the radiologist's opinion. Once, a brain tumor is medically suspected, its radiological assessment becomes necessary to decide its location, degree, and relationship to the neighboring tissues. Knowing these facts is vital in planning the way of its healing such as radiation, surgery and chemotherapy. Therefore, the evaluation of brain tumors using different medical imaging modalities is now one of the main issues of a radiology department in the routine health care environment.

In radiological environments, when a brain tumor is evaluated, radiologist manually outlines suspected areas on images, compares these regions on multiple MR (Magnetic

Resonance) series and marks the reference regions. This manual procedure is tiresome and difficult when irregular shapes are to outline, i.e., White Matter (WM) [16]. Due to a huge volume of brain data scanned by MRI scanners, manual interpretation and annotation of suspected areas compatible with the speed of generation of these scanners is almost impossible. Hence, automatic detection and classification has become inevitable. If gray scale brain MRI slices are mapped into their colored version, the radiologist or medical consultant will be assisted in interpretation for the lesions having both tumorous and non-tumorous cells such as necrotic core, active cells and edema from main brain regions, i.e., Gray Matter (GM), CSF and WM [17]. Automated brain tumor detection and classification methods to help health practitioners are extremely important. In general, most of abnormal brain tumor tissues may easily be detected by brain tumor segmentation methods but an accurate and definite type of malignant cells and their representation in colored version have not been solved all the way.

Most of the brain tumor classification methods for brain MRI images have been reviewed, but classification of brain tumor is still a big challenge. Therefore, further research is requisite to investigate more appropriate methods that could detect and localize brain tumor from MRI images with acceptable results in general so that classification of the tumor can be performed more precisely. The brain MRI slices colorization and automated analysis/interpretation has assists in monitoring of patients, diagnosis, treatment planning of patients, classification of brain tumor, clinical trials, localization of brain tumor, monitoring of therapy, examining effectiveness of radiation, pathological assessment of grows and disorder of soft tissues, automated surgical environment, clinical study of normal and abnormal tissues, volume estimation of normal and abnormal cells, radiation dose calculation, grading and staging of brain tumor [5, 8, 18].

Intensity inhomogeneity, partial volume effect (PVE), skull stripping, additive noise, radio frequency noise, slice overlapping, shading and etc. are the artifacts present in MRI slices directly effecting the classification process [7, 19]. Bias field correction is used to reduce the effect of intensity inhomogeneity. Fast and robust approach to estimate PVE has been reported in article [20]. Several robust skull stripping methods have been proposed by [21]. Analytically correction schemes, Markov Random Field (MRF), non-

local means (NLM), Anisotropic Diffusion Filtering (ADF) and wavelet models are used to de-noise the MR images. For MR image enhancement, median filter and its variants, low pass filter, Gaussian filters, gradient based methods, Prewitt edge-finding filters, etc. are mostly in practice [22].

In medical healthcare units, diagnosis of brain related disorders, mostly depends upon the texture analysis [23]. CAD systems performing automated analysis of brain cells can be more objective than traditional way of manually interpreting brain slices. Hence, for detection and auto classification of brain abnormalities, texture descriptors along with machine learning methods can be the best tools [19]. To analyze image texture, a number of image descriptors including Binary Rotation Invariant and Noise Tolerant (BRINT), Local Binary Pattern (LBP), Weber Law Descriptor (WLD), Gabor texture, Speeded Up Robust Features (SURF), Scale Invariant Feature Transform (SIFT), etc. are being used. Fuzzy C Mean (FCM), k-means, Naïve Bayes Classifiers, Artificial Neural Network (ANN), Support Vector Machine (SVM) and Atlas based methods are some of the examples of classification methods [5, 24]. SVM is the method to deal with the problems that are best solved in supervised manner. Therefore, it is being used commonly for classification of brain compartments [25]. The state-of-the-art methods of machine vision/learning enabled in the development of tools to perform auto classification. In healthcare units, these methods could assist in ease of computation and in reduction of operator's involvement. Resultantly, these methods allied with radiological information are assisting department of radiology and diagnostic images almost at every routine health care institute.

State-of-the-art methods do classify the brain MRI slices, but accurate, robust and optimized classification of brain slices is still a challenge in automated surgical environment. Therefore, further research is requisite to investigate more appropriate method of classification that could classify brain slices compatible to the image generation speed of these MR scanners. An efficient, and robust framework is presented in order to classify brain MRI slices. The reported approach consists of several steps executed in order to achieve the desired task. First of all, it colors the gray scale brain MRI slices using a novel proposed approach as a preprocessing. Texture of brain MRI images has been

exploited using Gabor filter and then Support Vector Machines (SVMs) are used to train a model in supervised fashion. Since, it was an objective of the proposed method to detect and classify brain tumor compatible to the speed of image acquisition modality from each slice. For this, several experiments have been performed to select more appropriate apartments for each of the phase including feature selection, representation, extraction and classification. Accuracy, specificity, sensitivity and AUC-values are the standard evaluation parameters used by the international community working of brain tumor detection and classification issue.

The proposed framework has been step wise evaluated for the classification of brain tumor and general brain disorders. Initially, the proposed novel method of colorization has been evaluated subjectively by a team of radiologists from BVHB, Pakistan. In the next step, evaluation of brain MRI slices as normal and abnormal has been performed. The achieved outcomes as per standard evaluation measures were ideal. In subsequent phase of the proposed framework, classification of brain general disorders (cerebrovascular, degenerative, inflammatory, and neoplastic) has been performed. Moreover, experiments regarding further classification of tumor types, i.e., glioma, sarcoma, meningioma, metastatic adenocarcinoma, metastatic bronchogenic carcinoma has also been performed. Additionally, to test the applicability of the reported approach regarding classification of neoplastic & non-neoplastic diseases and primary & metastatic brain tumor, experiments have also been performed in this segment. Conclusively, the proposed method achieved promising results. In the last phase, to check whether the proposed system deals with multiformity and variability present in MRI slices, experiments have also been conducted and evaluated with acceptable results. The experiments were carried out on a large set of brain MR images obtained from standard and bench marked datasets. To deal with medical and ethnic traits of a specific population, a dataset obtained from BVHB has also been used for research and experiments. Overall, results are appreciative in term of accuracy, specificity, sensitivity and AUC-value.

The proposed framework is a contribution in developing a reliable system to assist radiologists, neurosurgeons and healthcare practitioners to obtain another opinion regarding the presence and determining the type of brain related abnormality in MRI slices.

This framework can facilitate in further studies related to monitoring of therapy, examining efficacy of radiation, pathological assessment of the growth and disorder of soft tissues, automated surgical environment, clinical study of brain tissues, radiation dose calculation, grading or staging of brain tumor.

## 1.2. Motivation

Diagnosis related verdicts solely depend upon the tests such as CT-Scan, X-Ray, Ultrasound and MRI, which are based on luminance values emitted by human anatomies. In the age of inventions, still manual procedures are in practice to determine the presence of malignant tissues. Malignant tissues are the tissues having some sort of abnormality. When brain cells are suspected to be malignant through visual examinations, biopsy is seen as the last resort to determine their level of severity. Biopsy is an invasive surgical procedure in which a hollow needle is injected inside septic region of the tissues to resect infected cells. Then, through microscopic analysis, the type and grade of the tumor is determined. Overall, this procedure could outweigh the benefits especially in case of brain cells where edema is usually the outcome. Medically, the term edema is used for swelling of tissues. A non-invasive, optimized and robust protocol using image processing and machine learning methods is the only way that could be the alternate of biopsy procedures.

Automated analysis of brain MR images is a viable area in machine vision/learning domain. The state-of-the-art methods used for brain tumor detection, either classify brain MR slice as normal or abnormal with low classification rates or is unable to deal with multiformity and variability present in MR slices. In healthcare units, medical practitioners spend their time to manually analyze MR brain slices. Medical staff can be assisted by providing automated tools for the interpretation of brain MR images. This will improve accuracy in interpretation and save their time

Mostly, radiologists or any other medical practitioners are used to interpreting gray scale information embodied in MRI scans of human brain. However, if the information is presented in colored version, the variability and sensitivity of the information will be underscore. The aim of this research is to develop a robust technique/application to solve this problem. This application can be used by medical health care units as a standalone

protocol and/or can be integrated into their existing communications and image archival systems.

Automated, robust and optimized diagnostic systems could be the choice, if developed and integrated into the existing state-of-the-art scanners. The proposed system would be an indigenous solution being trained and tested on the medical traits of locals. MRI scanners are available in large hospitals of Pakistan which are producing large volume of data every moment. Software based solution for auto interpretation of this huge volume of medical data for pathological assessment of human anatomy would be a good indigenous solution. Hence, the proposed framework will be the only alternate to biopsy procedure which is currently in practice.

## 1.3. Problem statement

Automated diagnosis and classification of brain tumor from MRI images is most demanding in routine health care units. The state-of-the-art methods performing colorization of brain MRI images loss valuable information during their conversion process. Other state-of-the-art methods performing classification, do classify normal or abnormal MRI slices only, hence are unable to further classify brain disorders. Also the existing methods are not robust and efficient, further, are trained on small datasets. By exploiting texture of brain MRI images using supervised learning methods, a system can ultimately be applied to avoid invasive and hazardous procedures such as biopsy.

## 1.4. Research questions

Following are the research questions, which urged us to conduct this overall study;

- To what extent, a colorized versions of grayscale brain MRI images are helpful in diagnosis of brain tumor and its compartments?
- Does any protocol exist in the market that could automatically classify the brain tumor into its predefined type?
- How artificial intelligence allied with machine vision/learning be used for determination a type of brain tumor from MRI images to avoid/bypass a histopathological clinical procedures (biopsy)?

- To what extent, different MRI orientations, i.e., axial, coronal, and sagittal and different MRI sequences, i.e., T1W, T1C, T2W, FLAIR, PDW, MR-GAD as alone or combinations of any of these, have contributing patterns to auto classify brain disorders in general or further neoplastic types?
- Are systems completely trained on one brain MRI dataset, deployed on a remote location to deal with medical and ethnic traits of natives?

## 1.5. Research problem

A main challenge faced by the research community working in the domain of brain tumour detection and classification is that existing method either segment brain tumour or classify only a type of brain tumour. Another main issue faced by the community is that their brain tumour detection and classification approaches are not robust.

## 1.6. Research objectives & scope

Accurate and automated classification of brain abnormalities from MRI is needed in medical health care units. Much work has been done to assist medical practitioners during recent years, but still accuracy, robustness and optimization are issues to address.

The measurable objectives of the study with expected results are as under;

- To develop a complete, fledge automated tool, which is capable of assisting in auto image interpretation. Auto determination of tumor types, primary and secondary, benign and malignant, etc. are main objectives of the proposed system.
- The developed protocol can ultimately be integrated into existing MR scanners available in almost every national level hospital.
- This product can also be available as a standalone application for the medical units where MR scanners are not available but their patients have been scanned on other sites and treatment planning related verdicts are executed in same medical unit.
- To achieve self-sufficiency in the development of indigenous automated tools and its provision to different stake holders in this field, having MR scanners. This will save a lot of financial resources for these medical health care units.

- To independently evaluate all the recent algorithms for brain tumor detection and classification.

The drive of this study is to develop a robust and efficient system that could deal with medical traits of locals. Hence, a method has been proposed to classify brain MRI image into brain related disease groups and tumor types. To achieve the goal, MATLAB ® has been used. Results of the proposed method have been obtained using own developed software named as "MDIPT". The scope of the research is summarized as following;

- Since the proposed framework will replace ordinary biopsy procedure, therefore patients will be the main beneficiaries through this expeditious and non- invasive diagnostic protocol.
- Radiologist will directly be facilitated with another expeditious, more accurate and definitive assistance/opinion.
- The existing state-of -the-art MRI scanners will be integrated with indigenous and low cost software based solution to compete with the latest western technology.

Since the develop framework is a trustworthy, cost-effective and robust solution, practitioners will be assisted in classification, segmentation, monitoring and prognosis of brain tumor. The additional benefits of the developed system will be as;

- The proposed system will be the only pain free alternate to brain biopsy, which is an invasive way to determine the type and level of severity of the brain tumor.
- Development of an automated tool will speed-up the diagnosis procedure because biopsy is invasive and time taking.
- To monitor pre and post-surgical environments.

## 1.7. Challenges and issues

Manual interpretation of huge volume of medical data by experts in reasonable time is almost impossible. Several researchers addressed this issue and suggested solutions, which perform automated detection, segmentation and classification of brain tumor. However, still following challenges are faced by the personnel working in the domain of automated brain tumor diagnosis and classification.

1. Standard evaluation measures based on accuracy, precision, recall, true positive rate, etc. of the solutions are not up to the mark.
2. Provided solutions are not robust to different apartments
3. Provided solutions are trained on small datasets

Other challenges faced the international community working on the same domain include;

a) Artifacts such as intensity inhomogeneity, PVE, skull stripping, additive noise, radio frequency noise, slice overlapping, shading and etc. present in MRI images are main influence in the development of an automated system. How these artifacts will automatically be removed is a big challenge.

b) Automated ROI selection is another challenge faced by international researcher's community.

c) Unavailability of temporal MRI data is also a main challenge.

d) Investigation of proper set of distinguished texture features (extracted using texture exploitation methods) that could contribute in auto tumor grading, type determination and classification.

e) Investigation of novel feature representation model that could help in cell level information preserving and processing, cell level pattern recognition and classification to determine contributing pattern with the aim of auto tumor detection, type & grade identification.

f) Selection of more suitable machine learning method, i.e., supervised or unsupervised that could facilitate to achieve the target of brain tumor classification as well as selection of an appropriate classifier or clustering model (that best fits to exhibit trends, behavior and patterns of brain MRI data) to train and test the proposed expert system.

g) Robustness, accuracy and optimization in steps (d-f).

h) Modelling and development of optimized and robust protocols that might be deployed in real environments, assisting radiologists, neuro-surgeons and radio-oncologists performing the targeted goals, hence an alternate of biopsy.

## 1.8. Outline of the dissertation report

Chapter 1 of the dissertation presents significance of the selected research oriented issue, its introduction, motivational-factor, necessary guidelines, research directions, challenges and issues identified by previous research works. This chapter also contains research questions, aims and objectives, scope of the research and introduction to the sequence of the steps performed during experimental work with their research outcomes. Literature review of various brain tumor classification methods and brain anatomy is discussed in Chapter 2. Colorization, which is helpful in interpretation of different brain regions is provided in Chapter 3. After necessary interpretation of brain MRI slices, to achieve the dissertation's target, a method has been provided in Chapter 4, which classifies brain MRI slices as normal or abnormal. Chapter 5 deals with theoretical analysis of the proposed framework, which is the foundation of this dissertation. In this chapter, multiclass brain disorders classification problem has been addressed. To achieve the target of robustness, Chapter 6, presents the outcomes obtained through the proposed methodology on cross datasets, so that robustness of the proposed method be verified. Each of these chapters except Chapter 1 includes experimental results obtained through the developed MDIPT software with their detailed discussions on the basis of standard quantitative evaluation measures. Finally, conclusions are positioned in Chapter 7 along with recommendations for future extension.

# Chapter 2

# Literature Review and Brain Anatomy

In chapter 1, introduction to research work, problem statement, research objectives, research questions, scope, challenges, issues and dissertation outline was discussed. Here in chapter 2, literature reviewed in connection with datasets, features representation/extraction, classification and standard evaluation measures used for the evaluation of brain tumor classification and brain anatomy has been discussed in detail. Section 2.1, contains literature review, while in section 2.2 brain anatomy pertaining to biological & radiological information has been presented.

## 2.1. Literature review

In human organs, tumor is uncontrolled increase of cancerous cells [4]. Tumors belong to identical groups on the basis of their characteristics and are healed accordingly. Brain tumors are either primary or metastatic. Medical imaging protocols including CT, X-Ray, Ultrasonography, EEG, MEG, PET, SPECT and MRI are clinically in practice to evaluate the subjects. They are used to scan the human anatomical structures to exhibit their aspects and enable the clinician to study or to prepare their treatment planning. The targeted anatomical structures include liver, brain, prostate, kidney, heart, breasts or abdominal structures [26]. MRI is a non-invasive medical examination with more contrast among the soft tissues that helps physicians in diagnosing and treating medical conditions. It is frequently used to scan subjects having brain related injuries. Clinically, the images of different MRI sequences are used for identification and interpretation of tumor regions. These sequences include T1W, T1C, T2W, PDW and FLAIR. These medical imaging modalities are being used to scan human anatomies regarding their malignancy in a manual way. It is also pertinent to mention here that the proposed system would be an indigenous solution depending upon medical and ethnic traits of natives.

In radiological environments, when brain tumor is evaluated, radiologist manually outlines suspected areas on images, compares these regions on multiple MR (Magnetic Resonance) series and marks the reference regions. This manual procedure is tiresome, time consuming and becomes difficult when irregular shapes are to outline, i.e., White Matter (WM). Due to huge volume of brain data scanned by MRI scanners, manual interpretation and annotation of suspected areas compatible to the speed of generation of these scanners is almost impossible. Hence, automated detection and localization of brain

tumor has become inevitable. Brain tumor localization is to outline cancerous tissues belonging to main brain components, i.e., WM, GM and CSF [13]. At present, classification and clustering based machine learning methods have made significant progress in analysis of brain MRI data. Hence, brain tumor identification and its classification to assistance a radiologist is particularly demanding. The brain tumor localization and segmentation has impact on monitoring, diagnosis, treatment planning, and clinical trials of patients. Therefore, this research focuses on MRI based brain tumor detection and classification.

Researchers established several methods to segment and classify medical images. Classification and clustering based segmentation methods are the best methods for segmentation and classification of brain soft tissues from MRI images [5, 16, 27]. Intensity inhomogeneity, partial volume effect, skull stripping, and additive noise are the main factors directly effecting the automated brain tumor analysis process and results. A study [28] has proposed an automated method to enhance the images including medical images by using cubic Bezier curve and processing in frequency domain. ADF, wavelets, NLM and ICA are also some of the methods used for de-noising. Skull stripping, an essential step for brain data analysis, is for removal or delineation of non-cerebral tissues. The examples of non-cerebral tissues (of brain) are scalp, skull and meninges. Several robust methods have been reported in literature for skull stripping [5]. Bias field correction is used to reduce the effect of intensity inhomogeneity.

Classification based methods are representative methods of supervised machine learning algorithms, while clustering based methods are representative methods of unsupervised machine learning algorithms [29]. FCM (a clustering based segmentation method) divides data into clusters and is used frequently in pattern recognition. Although, FCM yields promising results, but due to its iterative nature it is computationally complex [30]. Atlas based segmentation methods are classification methods that uses prior information. Precise atlas is the key to the atlas based methods of segmentation [5].

SVM is a kernel based method. It deals with supervised classification problems and is used widely for classification of brain MR images [31]. SVM kernel learns by training examples. A multi-kernel based SVM integrated with a feature selection and a fusion

process has been proposed to segment the brain tumor from multi-sequence MRI image [32]. SVM owns great ability to deal with the problem of binary and multi class classification [32]. Parametric and geometric deformable methods are also used for segmentation of brain data [5].

In biomedical environments, still delineation is a manual procedure [16]. These manual procedures are tiresome and are not efficient. Due to huge volume of brain data scanned through MRI scanners, manual segmentation and annotation of suspected areas compatible to the speed of image generation of these scanners is almost impossible. Hence, automatic analysis for identification and classification of brain tumor has become inevitable. Brain tumor segmentation is to extract out cancerous tissues including edema and necrotic core from normal brain tissues such as WM, GM and CSF [17]. At present, classification and clustering based machine learning methods have shown noteworthy progress in classification of brain tumor. Therefore, tumor extraction and classification methods to help health practitioners are extremely important. The main objective of this research is to execute expeditious, robust and efficient protocol in non-invasive way. It will provide an automated way to analyze the brain data compatible to the speed of generation of the data, scanned through MR scanners. Hence, the proposed project will only be the alternate of biopsy procedure which is currently in practice to detect, determine the type and grade of brain tumor. Biopsy is dangerous procedure in case of brain, where edema is usually the outcome.

The open sources tools, which use start-of-the-art image processing algorithms are available worldwide and are able to perform auto detection, segmentation and visualization of brain tumor only. None of them is able to determine further types of brain tumor like, glioma, sarcoma, metastatic bronchogenic carcinoma, metastatic adeno carcinoma, meningioma etc. Moreover, determination of the tumor's severity according to WHO grades (I-IV), i.e., grades of tumor, is also an issue that is not addressed by these available open source tools. Despite of all these available tools, currently biopsy-a surgical process, is in practice to determine the further type and grade of tumor lesions, which is an invasive and dangerous clinical procedure.

The proposed framework, using image processing, machine vision and machine learning methods would be able to not only detect the cancerous tissues but their further types will also be auto determined from MRI slices directly with less computational expenditures. Hence, no need of biopsy. Several techniques for brain tumor detection and brain abnormalities classification have been discussed in the literature. Some of the proposed methods only detect tumor from brain MRI slices, while some also recognize the type of tumor. A few of the reported methods classify the general brain abnormalities.

The investigators [33] suggested an automated method for brain tumor detection using Fuzzy C-Means clustering algorithm and Hierarchical Self Organizing Map (HSOM). They used local dataset of KMC Hospital in Coimbatore, India. The suggested technique only detects brain tumor and does not classify further type of brain tumor. The researchers [34], proposed an automated method for brain tumor detection using modified Probabilistic Neural Network (PNN) model. The authors designed their PNN using learning vector quantization (LVQ) methodology. The authors used accuracy as standard evaluation measures for the evaluation of their proposed algorithm. A customized local dataset has been used for experiments with 100 % accuracy. The use of local dataset does not ensure the robustness of the proposed method. Authors [35], have reported methodology for the classification of brain tumor though MRI images using SVM and Co-occurrence matrix. A custom dataset obtained from Holy Family Hospital, Rawalpindi and benchmarked dataset of HMS has been used for the evaluation of reported methodology. Classification rates as per accuracy remained 99%, which was appreciative. However, the proposed method does not further classify neoplastic types.

Discrete Wavelet Transformations (DWT) and Artificial Neural Network (ANN) based method for MRI image classification as normal and abnormal method has been published by [7]. HMS dataset has been used for research and experimental purpose. They performed experiments on 101 T2W axial slices only. However, their achieved accuracy i.e. 99% was appreciative. Again 101 MR slices could not have enough variability and multiformity. The study only deals with MRI slice classification as normal and abnormal and does not classify brain related disorder, nor the proposed scheme classify types of tumor. Scholars [24], have reported an automated method for brain tumor classification

using SOM and KNN technique. Self-organising map neural networks have been used for features extracted from discrete wavelet transformation. KNN classifier has been used for classification of MR slices as normal or abnormal.

Researchers [36], reported an automated method for Alzheimer's disease detection from MRI images using Support Vector Machines (SVM). They performed experiments on local dataset obtained from Wellcome Trust Centre for Neuroimaging, Institute of Neurology, UCL, London and claimed the accuracy (96.4%), sensitivity (95.6%) and specificity (92.5%). Only Alzheimer disease has been detected in this study, rest of the diseases are neither detected nor classified, as well experiments have been performed and validated on local data set only. Another method for the identification and classification of primary glioma and grading of metastasis gliomas has been proposed by [19]. SVM, Linear Discriminant Analysis (LDA) and K-Nearest Neighbor (KNN) for classification of primary glioma and grading of brain tumors, has been utilized. A local dataset (MAGNETOM Trio Tim System, Siemens Medical Systems, Erlangen, Germany) has been used for the evaluation of developed algorithm. The proposed methodology achieved the accuracy for SVM (91.2%), KNN (89.8%, for k=3), and LDA (85.5%). Standard evaluation measures achieved, were not up to the mark, results are also validated on local dataset, which could not have robustness. Authors [37], have reported an automated method for brain tissue categorization using custom Genetic Algorithm (GA), Gray Level Co-occurrence Matrix (GLCM), Extreme Learning Machine (ELM) and Particle Swarm Optimization (PSO). Experiments have been performed on customized dataset (PSG IMSR & Hospital, T1 images). The performance evaluation measures for sensitivity, specificity and accuracy remained 95.9%, 98.88% and 98.05% respectively. The results have only been validated on T1C images obtained from local dataset. However, the results for glioma, meningioma and metastasis tissues classification are quite reasonable. [9] published research for automated classification of MRI slices using discrete wavelet transforms (DWT), Spider Web Plots and Probabilistic Neural Networks (PNN). On Randomly selected 75 T2W axial slices from HMS dataset, they claimed accuracy, specificity and sensitivity of 100%, 100% and 100% respectively. The learned model, trained on small axial and T2W dataset, could not have enough multiformity, variability, robustness and optimization. Neural network based training models always remained computationally complex [38].

A fully automated method of primary brain tissues components, i.e., GM, WM, CSF and CSF has been reported by Su Ruan et al. [12] using 3D partial volume modelling technique in unsupervised fashion of implementation. To demonstrate the stability and robustness of the reported algorithm, the results have been evaluated both on real and simulated MR images obtained from publically available benchmarked dataset BrainWeb. However, the study deals only T1W images. Another automated method for brain tumor segmentation has been investigated by Jason J. Corso et al. [17] using Integrated Bayesian Model that detects and segments brain tumor and edema from multichannel magnetic resonance volumes. They have performed experiments on a locally obtained dataset from Henry E. Singleton Brain Cancer Research Program, University of California, Los Angeles, CA 90095 USA. For the evaluation of their outcomes, they used Jaccard Coefficient (JC), precision and recall, which are 0.88, 0.96 and 0.92 respectively. The proposed method deals only segmentation of brain tumor; further classification of abnormal brain soft tissue has not been addressed by the researchers.

The researchers Arnaldo Mayer et al. [10] have suggested a method of brain tumor segmentation using adaptive Mean-Shift clustering approach, which classifies brain voxels into main brain tissue types, i.e., WM, GM and CSF. They have used BrainWeb, Internet Brain Segmentation Repository (IBSR) and a custom dataset obtained from Sheba Medical Center in Tel-Hashomer, Israel. The results have been evaluated on JC as standard evaluation parameter, which includes results 0.96 for GM and 0.97 for WM. However, their proposed method is not robust to noise and performs segmentation only and lacks classification of malignant tissues. The scholars Hassan Kotanlou et al. 2009 [39] have presented a technique of Brain tumor segmentation in MRI using Fuzzy Classification (applicable hyper-intense tumors), Symmetry Plane Analysis(applies to any type of tumor) and Spatially Constrained Deformable Models .They have experimented on Custom Dataset (Lariboisiere Hospital, Paris, France and Salpetriere Hospital, Paris, France) and IBSR. They used deformable models constrained by spatial relations for brain primary components extraction. The results have been evaluated as per True Positive (TP) =0.93, False Positive (FP) =7.58, Similarity Index (SI) =93 and Hausdorff Distance (HD) =4.39. Problem of brain tumor classification and its grading has not been addressed in this study.

The researchers [40] have suggested an approach for computer aided brain tumor identification and segmentation using global thresholding technique. The purposed method detects the tumor by reducing the noise, enhancing the image and then segments it. They used custom dataset in which 100 MRI images containing brain tumor of different shape, size and intensity. The results are evaluated as per accuracy, which has been obtained as 97%. But the method only performs detection and segmentation of brain tumor. A study conducted by M. Attique et al. [41] has reported a method for the segmentation of brain primary components using clustering algorithm, which uses prior anatomical knowledge for seed selection from histogram technique. They have performed experiments on custom dataset obtained from Bahawal Victoria Hospital, Bahawalpur, Pakistan and BrainWeb. The results have been evaluated as per JC as standard evaluation parameter, which includes 0.029 for GM, 0.026 for WM and 0.052 for CSF. The study did not address the problem of brain tumor classification.

The scholars M. Kanimozhi et al. [42] have suggested a novel method of brain segmentation from MR images using wavelet transformation and unsupervised self-organizing map. They have performed experiments on a dataset obtained from IBSR. The results are evaluated as per Quantization error (q) =0.63 and Topological error (t) =0.15. The investigators J. Sachdeva et al. 2013 [43] have reported a method of brain tumor classification using ANN and PCA techniques. They have been performed experiments on custom dataset obtained from department of radio diagnosis, Postgraduate Institute of Medical Education and Research (PGIMER), Chandigarh, India. The dataset has been split into 50% for both training and testing of the reported method. The results are evaluated as per accuracy which is obtained as 91%. Both of these studies lack addressing the classification issue.

A study [44] conducted using multilevel thresholding by histogram filtration method has extracted brain primary regions, i.e., GM, WM and CSF. Experiments have been performed on a custom dataset obtained from Bahawal Victoria Hospital, Pakistan and a publically available benchmarked dataset BrainWeb. JC has been used as a standard evaluation measure, which yield results 0.002 for GM, 0.012 for WM and 0.018 for CSF. The investigators Shunfeng Wang et al. [45] have presented a method of MRI image

segmentation using fuzzy c-means model and spatial structural information technique, which when applied on synthetic brain images gives perfect results. They have performed experiments on custom dataset obtained from McConnell Brain Imaging Center at the Montreal Neurological Institute, McGill University, QC H3A 2B4, Canada. The results have been evaluated as per Jaccard Similarity Coefficients (JSC). Both of these studies lacks addressing of further brain tumor classification issues.

The scholars Kang Han Oh et al. [13] have published a novel approach of tumor detection from brain MR images using regional features (mean and variance) and non-linear SVM with RBF kernel techniques. They have performed experiments on a custom dataset obtained from Seoul National University, Korea. The results have been evaluated as per precision, recall and f-measure, which are 0.96, 0.92 and 0.85 respectively. Another study conducted by Ines Njeh et al. [18] have investigated a novel method of 3D multimodal MRI brain glioma tumor and edema segmentation using graph cut distribution matching approach, which yields competitive performance in case of tumor and complete edema segmentation. They have performed experiments on a BraTS 2012 dataset. The results have been evaluated as per mean dice, which is for real cases (0.77) and for simulated cases (0.88). But, the study has a limitation as it only addressed the problem of glioma and edema segmentation. Further, the reported study is unable to address the problem of tumor classification and auto grade calculation.

The scholars Pawel Szwarc at el. [46] have proposed an automated way to detect brain tumor and neovasculature assessment from multi-series MRI using Regional Cerebral Blood Volume (RCBV) perfusion maps. They applied this technique on a custom dataset obtained from Radiodiagnostics Department of the Maria Sklodowska Curie Memorial Cancer Centre and Institute of Oncology, Gliwice Branch, Poland. They concluded that by applying this method, they achieved 0.94 as DSC but study has a limitation that it does not addressed classification problem. An automated approach of glioma segmentation using Deep Convolutional Networks has been reported by the authors Dennis Sangberg at el. [47]. They applied this technique on a dataset obtained from BraTS and results have been evaluated as per sensitivity, which is 98%. The main theme of proposed work is to improve the discrimination ability for segmentation and also helps the segmentation interpretation.

The reported study has appreciatively segmented glioma tumor, but lacks a feature of metastatic tumor segmentation and classification.

The investigators Sonali B.G. et al. [48] have presented a novel method of brain tumor classification using PCA and PNN techniques for feature extraction and classification problem respectively. They have performed experiments on custom datasets obtained from Government hospital of Aurangabad, Sahyadri Hospital of Pune, Maharashtra India. The dataset consists of 70 training samples and 35 testing samples for the classification of tumor as normal, malignant or benign and also contains 20 testing and 24 training samples for meningioma and glioma type classification. The results are evaluated as per accuracy which is obtained 97.14% and 100% with spread value $10^7$ and $10^6$ respectively. However, the study has a few of limitations as local datasets are used for evaluation and the proposed method can only diagnose two types of tumor. A novel method of brain tumor classification using Tolerance Rough Set and Firefly based Quick Reduct (STRSFF-QR) technique is presented by Jothi G. at el. [49], which gives better solutions in diagnostic problems than already proposed approaches. They performed experiments on dataset obtained from National Cancer Institute, United States, which contains 200 MR images taken from 20 different patients. The study has concluded that their reported algorithm can be used effectively for the analysis of real time medical images due to its consistency, simplicity and robustness. The reported algorithm can be applied on multimodal data obtained from mammography, ultrasound, PET and CT.

A multi modal framework of brain tumor glioblastomas classification using Local Binary Patterns (LBP), Binary Robust Independent Elementary Features (BRIEF), Histogram Of Oriented Gradients (HOG) and Auto-Encoders (AE) techniques is presented by Esther Alberts at el. [50]. They have concluded results by performing experiments on dataset obtained from The Cancer Imaging Archive (TCIA) database. They have performed experiments against 116 patients of brain tumor as training set composed of 92 images and a testing set of 24 images. The results are evaluated as per accuracy, which is obtained as 0.83. But, the study has limitations as the evaluation measures are not up to mark. The authors [23] have presented a method of classification of brain tumor using multi-modality images using Wavelet and Random Forest techniques. They have performed experiments

on a MICCAI BraTS dataset. The results have been evaluated as per DSC (0.95 ± 0.03), JC (0.91 ± 0.06), Specificity (0.89 ± 0.12) and Sensitivity (0.95 ± 0.03) as their maximum achievements. However, the study has few limitations as quantitative measures are not up to mark and only segmentation of tumor has been performed.

The review regarding all above mentioned studies, methods used, dataset used, evaluation measures and limitations of state-of-the-art methods used for detection, segmentation and classification of brain tumor is appended as Annexure-A.

In the light of reviewed literature, it is accomplished that some of the methods classify brain MRI slice as normal or abnormal, while some of them only determine the grades of glioma tumor. The state-of-the-art methods don't perform well in general to determine the type of brain abnormality. Still, it's a challenge to investigate computational paradigms that could perform robust and efficient brain disorders classification. The proposed robust and efficient system is trained and tested on multi-datasets, having multi-orientations and multi-sequence MRI slices. So that the developed system would be able to deal medical traits of natives. The proposed methodology will only be the alternate of biopsy procedure which is currently in practice in almost every medical health care unit.

## 2.2. Outcomes revealed from the reviewed literature

Following are the conclusions, revealed through the reviewed literature.

- The methods converting grayscale brain MRI data into colored versions, loss valuable information during their conversion process.
- Some of the methods do classify brain MRI slice as normal or abnormal only
- The state-of-the-art methods are trained on small datasets
- The state-of-the-art methods are not robust

## 2.3. Brain anatomy

Human brain is the most complex organ of human body. It works as control room for whole of the human body. Bing a complex organ of the human, the brain is the major research area of the current decades. The hypothetical image of the brain is show in Figure 2.1. Human brain is enriched with five senses including smell, sight, touch, hearing and

taste. These senses enable it to collect signals alongside. It decides how human have to deal with different situations [31].

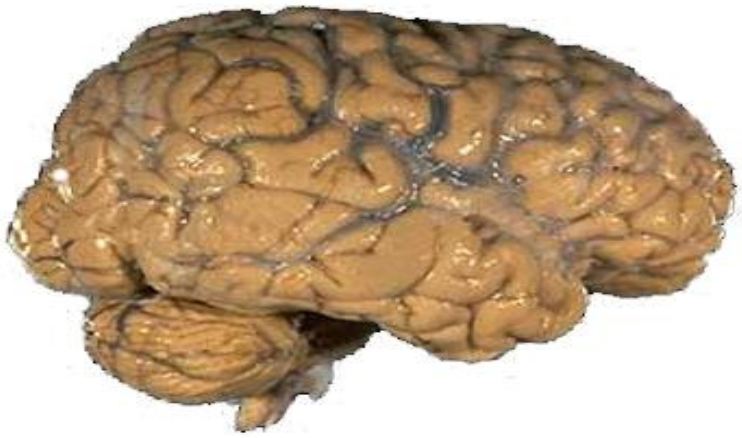

Figure 2.1: Human brain

Human brain contains about 86 billion nerve cells, the neurons or the gray matter and billions of nerve fibers, the axons and dendrites or the white matter. Glial cells surround neurons and provide them support. They are further categorized as astrocytes, oligodendrocytes, ependymal cells, microglia, Schwann cells and satellite cells. Astrocytes are star-shaped glial cells. Studies found that the astrocyte ranges from 20% to 40% of all glia [51].

### 2.3.1. Central nervous system

Human brain and spinal cord are the part of human central nervous system (CNS). Clinically, some brain related disorders are diagnoses from spinal cord [52].

### 2.3.2. Brain components and tumor types

“Oma” is a Greek word representing cancers, added to the name of the affected body cells like astrocytoma, the tumor that develop from astrocytes. Astrocytoma are primary intracranial tumors. Intracranial are the tumors inside the brain skull, while extra-cranial are the tumors outside of the skull. The main parts of human brain are forebrain, midbrain and hindbrain. Cerebrum, brain stem and cerebellum are primary components of brain as shown in Figure 2.2.

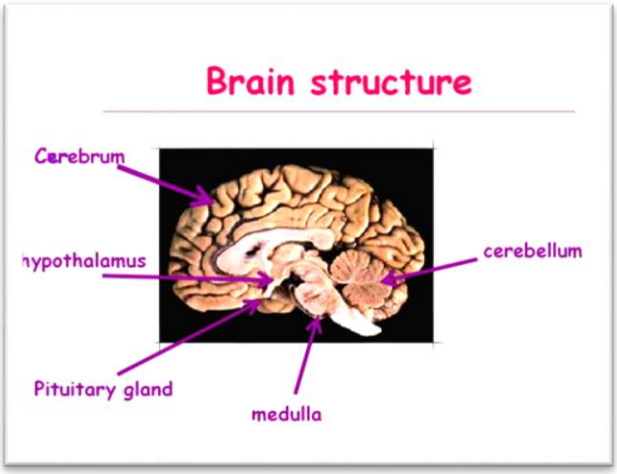


Figure 2.2: Primary brain components

- **Cerebrum** – Cerebrum is the largest organ of human brain. It is also called cortex. Its main functions include thoughts and their actions. It has two sides called right and left hemispheres. Basic roles of cerebrum include initiation and coordination of movements, judgment, temperature, touch, vision, hearing, reasoning, emotions, problem solving and learning. If any of brain related disorder is present inside cerebrum, one or more of these functionalities of human can be disturbed. The cerebrum is shown in Figure 2.3.

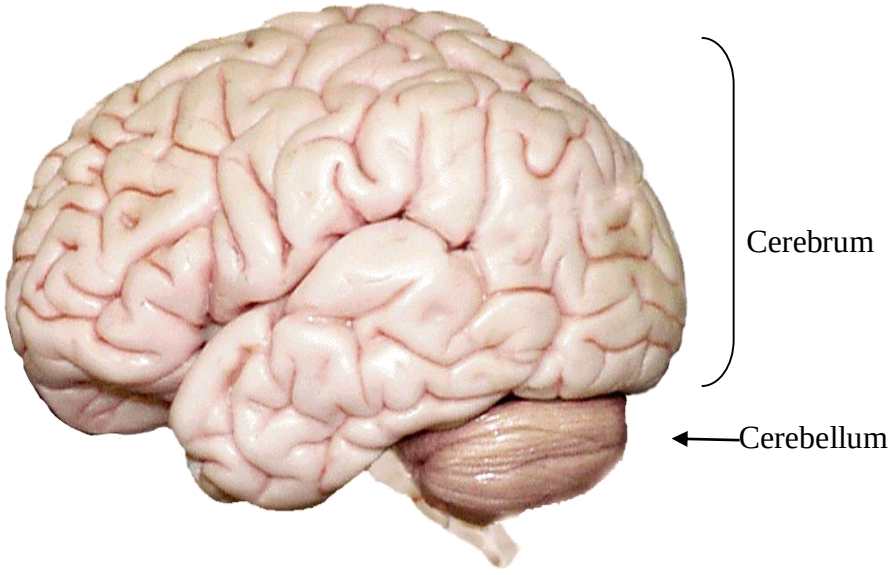


Figure 2.3: Cerebrum part of the brain

Both left and right sides of hemisphere are symmetrical. Medically, it has been documented that both of the sides have somewhat different functions. Both sides of the

hemispheres are connected through corpus callosum, which consists of several axons. The neocortex resides in the cerebrum's mass. The cerebral cortex is shown in Figure 2.4.

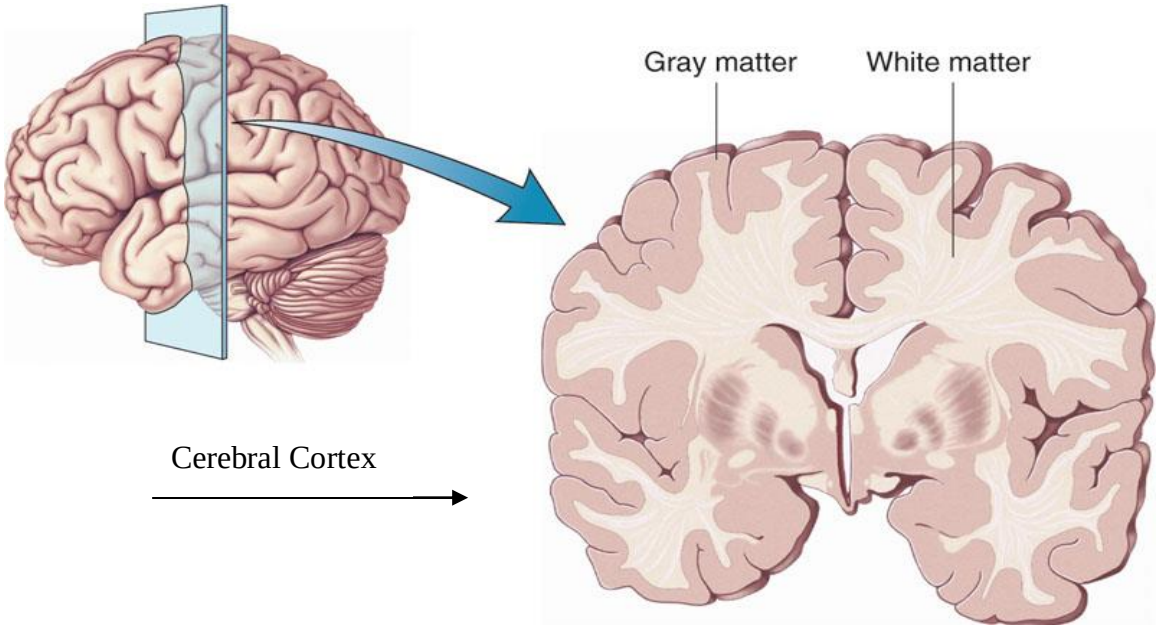


Figure 2.4: Slice of cerebral cortex

The cerebral cortex shown in Figure 2.5 is divided into four sections called lobes, i.e., parietal lobe, frontal lobe, temporal lobe and occipital lobe.

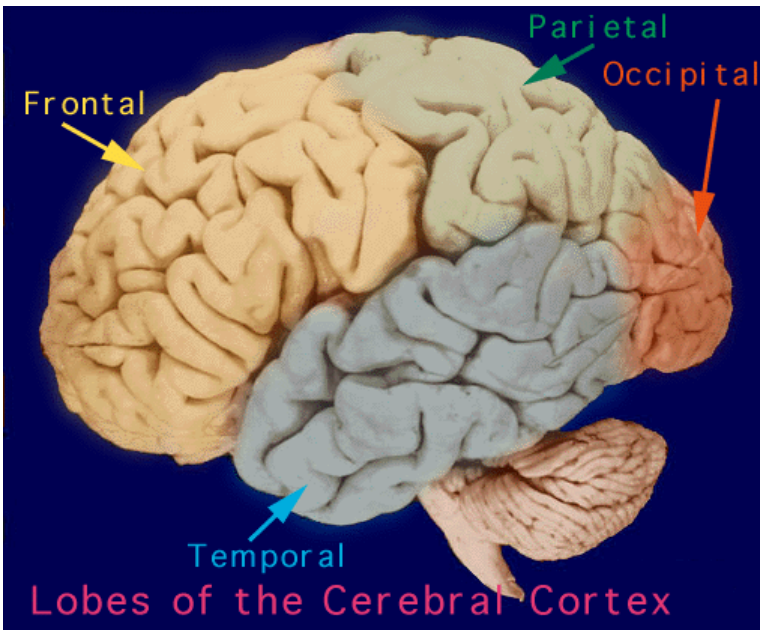


Figure 2.5: Lobes and their parts

## 2.4. Some major phases involved in the conducted study

There are four bold steps as shown in Figure 2.6, involved in the conducted research as following;

- Image input
- Preprocessing
- Feature extraction
- Classification

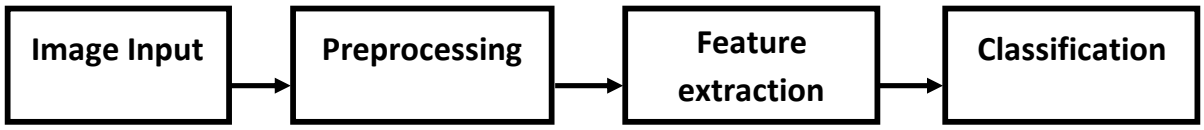


Figure 2.6: Major steps involved in the conducted research

### 2.4.1. Image input

In a first step of the conducted research, the dataset (consisting brain MRI images) is input through the provided interface.

### 2.4.2. Preprocessing

Preprocessing consists of numerous operations applied on brain MRI slices before further analysis. The preprocessing step in this research involves color adjustment by colorization of gray scale brain MRI slices and their enhancement. Preprocessing methods basically fall into two domains; frequency and spatial domain, but we have performed all of the process related to preprocessing in spatial domain.

### 2.4.3. Feature extraction

In this conducted research, we used Gabor filter and co-occurrence matrix as texture representation methods, then used texture features for the training and testing of the proposed method to achieve the desired results.

### 2.4.4. Classification

Recently, classification is most demanding target of image processing area. In this research work classification has been performed using SVM. The detail of the proposed method has been provided in chapter-3, chapter-4 and chapter 5.

## 2.5. Applications of automated systems in medical units

CAD systems plays vital role in healthcare units by automating detection of malignant regions, colorization of different regions so that their malignant tissues be interpret well, defining regions of interest.

## 2.6. Problems in auto classification of brain tumor

Following are the problems faced by the international community working in the domain of automated brain tumor detection, classification and grading;

- Wide variety of medical image modalities
- Biologic variability and multiformity
- Variation in image quality
- Radio Frequency noise in medical images
- Object shapes
- Artifacts present in medical data

# Chapter 3

# Colorization of Brain MRI Images

In chapter 2, literature regarding colorization of grayscale brain MRI slices, feature representation and extraction techniques, general image classification techniques, standard evaluation measures used the community working in the domain of brain tumor classification was reviewed. Moreover, radiological information related to human brain anatomy, which is a key clue in auto-classification of brain disorders was also presented in chapter 2. Here in chapter 3, to assist the radiologist or radio oncologist and even the classification methods, a novel method of colorization to convert grayscale brain MRI information into colored version has been presented. The presented approach has a central position in the proposed framework, which has also been deployed in Department of Radiology and Diagnostic Images, BVHB, Pakistan and is being used by the Chief Consultant/Radiologist in the assessment process of the patients. Section 3.2 contains introduction of colorization approach, while section 3.3 presents related work. Image acquisition has been positioned in section 3.4. The proposed methodology has been outlined in section 3.5. Results and discussions have been presented in section 3.6, while the lesson learned has been positioned in section 3.7.

## 3.1. Summary of this research activity

The drive of this research activity is to report a colorization method to enhance the visualization, cell characterization and interpretation of brain. The high dimensional brain data scanned through MRI embodied in gray scale, if converted, represented, mapped and/or visualized in colored versions, irrefutably, more definitive and more accurate the pathological assessment process will be. Several methods have been reported to represent brain MRI data in color with the cost of computational complexity. In this research activity, an efficient method of colorization using frequencies from visible range of color spectrum, has been proposed to embody the variations and sensitivity of the brain MRI images. Side by side visual comparison based on multiple MRI sequences of identical subjects, by domain experts, proved adequate success and fruitfulness of the story.

## 3.2. Introduction of this research activity

Since, in the age of inventions, electromagnetic signals, transmitted by human anatomies, listen through emerging medical imaging modalities are systematized to embody gray scale images. This medical imageries data is then visually inspected for the

evaluation of subjects and enables the clinician to study or to prepare its treatment planning. The targeted anatomical structures include liver, brain, prostate, kidney, heart, breasts or abdominal structures [5, 26]. Accurate and definitive radiological assessment has become decisive for subject's therapy such as surgery, radiation, and chemotherapy. Therefore, visualization of this medical data holding information of biological tissues for the evaluation and assessment is now one of the key issues of radiology departments in routine health care environments [46, 53].

Since MRI is the medical examination which is non-invasive, has more contrast among soft tissues and has high spatial resolution. The image quality and sensitivity of MRI scanners made this modality, the best, to evaluate brain abnormalities. Brain disorders are complex, therefore, radiologist be assisted through better visualization of anatomical structures for accurate and definitive diagnostic procedures. MRI delivers important information about shape, size, and localization of brain soft tissues without revealing the subject to high ionization radiation [11, 12]. Therefore, it has central position in brain tissues evaluation process in clinical atmosphere. In routine healthcare units, a number of MRI sequences are embodied. These sequences include T1W, T1C, T2W, PDW and FLAIR [13] with direct views of the body in almost any orientation i.e. coronal, sagittal and axial. These sequences enable tissues to be visualize well. T1C shows better anatomical details and enough distinction between cystic and solid structures, while PDW highlights pathological changes better than others [19]. Although, brain is protected by thick bones of skull, however, it is susceptible to many types of damages and diseases. The most common are neoplastic diseases, degenerative diseases, cerebrovascular diseases, inflammatory diseases, which can be diagnosed through MRI scanners. However, if following issues are addressed at manufacturing level by MRI machines venders, fully automate diagnostic procedures be facilitated in well.

1. Improvement in magnet technologies to create permanent homogeneity of magnetic field (i.e. there should be no loss /deterioration of field homogeneity with the passage of time) and magnet strength for clinical/human uses should be standardized and limited in MRI machines. Currently, all manufacturers design

their own choices of magnet strength. This results in varying quality images of same person`s same region examination at different machines.

2. Imaging protocols are not standardized for (say 1.5 T) all similar strength machines manufactured by different firms.
3. The detector designs need modifications to create smaller in size, more in number and more powerful sensors to avoid primary data loss at that level.
4. Instantaneous data-piling facilities needs to be added to computers in diagnostics to create almost real-time 3 Dimension (D)/4D, see-through and colour images in one go.

The identification of brain infarct in MR gray scale images is difficult due to the natural appearance of the infarct tissues isointense to the normal tissues in the brain MR images. In general, scanned anatomical data requires further processing to underscore veiled information. It is obvious that colored representations can enhance the visibility of signal intensity variations of this scanned data. However, radiologists are today trained mostly in reading such grey scale images. Representation of brain MRI images into colored version may help them to identify abnormal regions better. Colorization of brain MRI images may also assist in mapping of surface, classification of tissue and delineation of region of interest [41]. Hence, colored representation of both normal abnormal tissues including active cells and necrotic core became inevitable to underscore the variability and sensitivity of images [54]. It is established from the literature that current progress is shifting the MRI field slowly towards quantitative images such as T2stir, ADC, etc. for which colored representations with fixed scaling are becoming more customary & useful. The existing methods of colorization, color the soft tissues but efficient and definitive colorization of soft tissues is still a big challenge. Therefore, further research is requisite to investigate more appropriate methods of colorization that could color MRI images with acceptable results in general so that interpretation and classification of the lesions can be performed more precisely. To assist the radiologist in diagnosis, an efficient colorization method is presented in order to enhance the visualization and interpretation of brain MR images. This process can also be used to convert the gray scale medical images acquired through other medical scanners to their colorized version, as color increases the visual

appeal of an image. The reported approach uses color spectrum to colorize brain MR grey images. The results are promising according to the opinion of the radiologist.

## 3.3. Related work

Researchers established several methods to color human soft tissues acquired through medical imaging devices including brain MRI images. Each of the methods has its own pros and cons. Almost, all of these methods produce color images based upon estimated colors. Attique et al., [41] calculate luminance of each MRI image pixel and converts into CIELab using XYZ and then converges the color mapping process. There is an extra overhead of conversion from RGB to CIE lab and vice versa in this proposed method of colorization and is computationally not efficient. For grayscale images and videos V. G. Jacob and S. Gupta [55] proposed a semiautomatic approach to color. The algorithm requires position and color of the marker then few reference frames are manually selected to colorize using these markers and their chrominance information is then transferred to the other frames of the video. Operator involvement is the main drawback with this approach. The Luminance along-with texture has been used to find best matching source pixel. Then its chromaticity is assigned to target pixel by retaining its luminance value by [56]. Although, an automated approach for colorization has been proposed, but construction of such large image database along with parameters is an additional overhead. C. Sauvaget et al. [57] suggested an automatic gray image colorization approach in which user defines color from chromatic hue wheel. Bochko V et al. [58] suggested medical image colorization using support vector machine as a learning method to learn from set of images. They applied their method of colorization on dental and skin images wounded images, hence data set to learn is the requirement of the proposed medical image colorization. Holland GN and Bottomley PA [59] proposed color display technique for NMR images. MATLAB also colors the gray images and supports different types of color-maps (hot, summer and etc.). User is allowed to define his own color-map and color ranges; then linear mapping is used to assign colors to a gray image. Minimum and maximum values are calculated from source grayscale image and defined color-map. After calculation of these maximum and minimum values, the minimum gray value of the source image is replaced by calculated minimum color value while maximum gray value of the source

image is replaced by calculated maximum color value. The values of gray scale image that are in between minimum and maximum are linearly replaced by the middle colors from color-map colors [60]. Colorization methods based on multi-parametric MRI images have also been reported. Different sequences of same anatomical position have been utilized during colorization procedure, in such a way that T1w sequence is assigned red channel, T2w sequence is assigned blue channel, while FLAIR sequence is assigned green channel. After these primary channel assignments to individual sequences, these images are fused, resultantly a color image is embodied by Weiss, Kenneth L et al. [61]. Weiss KL et al. [62] has also reported multi-parametric based colorization solution for gray scale images. Two MRI images of same anatomical position scanned with different pulse sequence are used. Hue and luminance of corresponding pixels of both images is calculated to generate colored one. Similar nature of work based on multi-sequence has also been reported by Hernández, Maria del C Valdés et al. [63]. Thus, there is a need to investigate more efficient methods of colorization. Because, colored representation of same grayscale image enhances visual appeal. If such tools are matured, the assessment process on monochrome data will be more accurate and definitive [64-66].

In the proposed method of brain MRI colorization, MRI image is colorized in easy and efficient way. The overheads present in the reported techniques [61, 63] has been reduced. As there is no separate process to color each sequence, allied with fusion process to obtain colored image. The colorization process based on these multi phases is generally a costly solution in term of computational complexity. Since, change in gray value of any pixel can cause of artifacts. Therefore, the proposed method of colorization pertains original gray value of each while colorization procedure. The methods provide by MATLAB to color gray scale images don't retain original luminosity [60]. Major gain of using an image colorization is that it also colors the images acquired through other modalities such as OCT, X-Ray, CT, etc. OCT, X-Ray, CT, etc. have single selection of parameters available for image acquisition. In this study, a colorization method to convert brain gray scale MRI images into their colored version has been reported. The proposed method has enhanced the visual perception of brain MRI images. It has enabled the clinicians in more interpretation and precise tissue discrimination. This research would be contribution for modeling and designing reliable systems to assist radiologist,

neurosurgeon, and healthcare practitioner for better analysis pertaining classification of brain tumor, localization of brain tumor, monitoring of therapy, treatment planning, pathological assessment of grows and disorders of brain soft tissues.

## 3.4. Image acquisition

Brain MRI images have been scanned from a total of 49 patients (35 males, 14 females, 35 normal, 14 abnormal) of average 39 years old patients having hemorrhage. stroke, multiple sclerosis and tumors. Amongst these, a total of 29 patients (22 males, 07 females, 21 normal, 08 abnormal) have been used to derive a criterion for novel colorization method as shown in Table 3.1. Rest of the 20 patients (13 males, 07 females, 14 normal, 06 abnormal) have been used to derive a threshold. The images of all patients have been used to in verification of the proposed method of colorization. The colorization model as a flow diagram has been elaborated in Figure 3.1. Author [67] was consulted to obtain expert opinion and validation of the outcomes.

## 3.5. The proposed method

To convert gray scale brain MRI images into colored ones, a colorization method has been proposed. A gray scale brain MRI slices has only an intensity value *I*. this is also called a luminance value. This value represents a pixel and has values ranging from 0 to 255. In a color image, if represented in RGB color space, will have red, green and blue components. Human eye cannot identify two contiguous colors of visible spectrum, unless, there is significant change in saturation. Starting from 400nm to 700nm, there are total 301 unique colors. Since, each two contiguous colors are not human perceivable. Empirically, to derive the criterion (*C*) for colorization process, we made experiments on data set of 29 subjects that describes how many consecutive color pixels are to drop to select next pixel from color spectrum. This criterion best matches to give appropriate and considerable variations among tissues. Next derivable is the threshold (*T*), that determines the successfulness of the comparison using Euclidean Distance. The minimum value of *T* can be 1 (one), but if the value of *T* is adjusted at 1, the number of colors that are assigned is reduced, resultantly, inhomogeneities in color pixels are observed. Experiment results and their visual assessment by the domain experts established that these derivations are

adequate to have better brain soft tissues colorization. Table 3.1, shows the detail of the subjects used to derive both *C* and *T*.

Table 3.1: Subjects examined for the selection of *C* and *T*

| **Criteria** | **Total Subjects** | **Imaging Sequences** | **Normal/Abnormal** | **Male/Female** |
|---|---|---|---|---|
| **Color Gap (*C*)** | 29 | T1W,T2W, PDW, FLAIR,T1C | 21/08 | 22/07 |
| **Threshold (*T*)** | 20 | T1W,T2W, PDW, FLAIR,T1C | 14/06 | 13/07 |

The steps of the proposed algorithm used for brain soft tissues colorization process utilizing the visible spectrum ranging from 400nm to 700nm frequencies are represented in Algorithm 3.1. The top down approach this proposed paradigm is depicted in Figure 3.1. To know an efficiency, memory requirements, computational complexity or execution time of the proposed colorization algorithm, it has been tested on core2 duo processor and found it en efficient, requiring less memory and less computational complexity. Because colorization process does not require further conversion into any model, so has reasonable time for its execution.

Algorithm 3.1: Steps of the proposed colorization algorithm

Steps

1. Input gray scale brain MRI image ($I_g$).
2. Input linear vector ($I_c$) containing visible color spectrum ranging from 400nm to 700nm frequencies.
3. Input *C* and *T* calculated after analysis of subjects as shown in Table 1.
4. Repeat: read individual pixels ($P_i$) of $I_g$
5. Calculate Intensity (*I*) of *Pi*
    a. Repeat: read pixel ($P_c$) from $I_c$
    b. Calculate intensity (*i*) of $P_c$
    c. If (ABS(*I*-*i*)<=*T*) Then
        i. Replace $P_i$ with $P_c$
        ii. Goto step 4
    d. Else
        i. Skip no. of pixels from $I_c$, equal to *C*
        ii. Goto step 5 (a)
    e. End If
    f. End Repeat
6. End Repeat

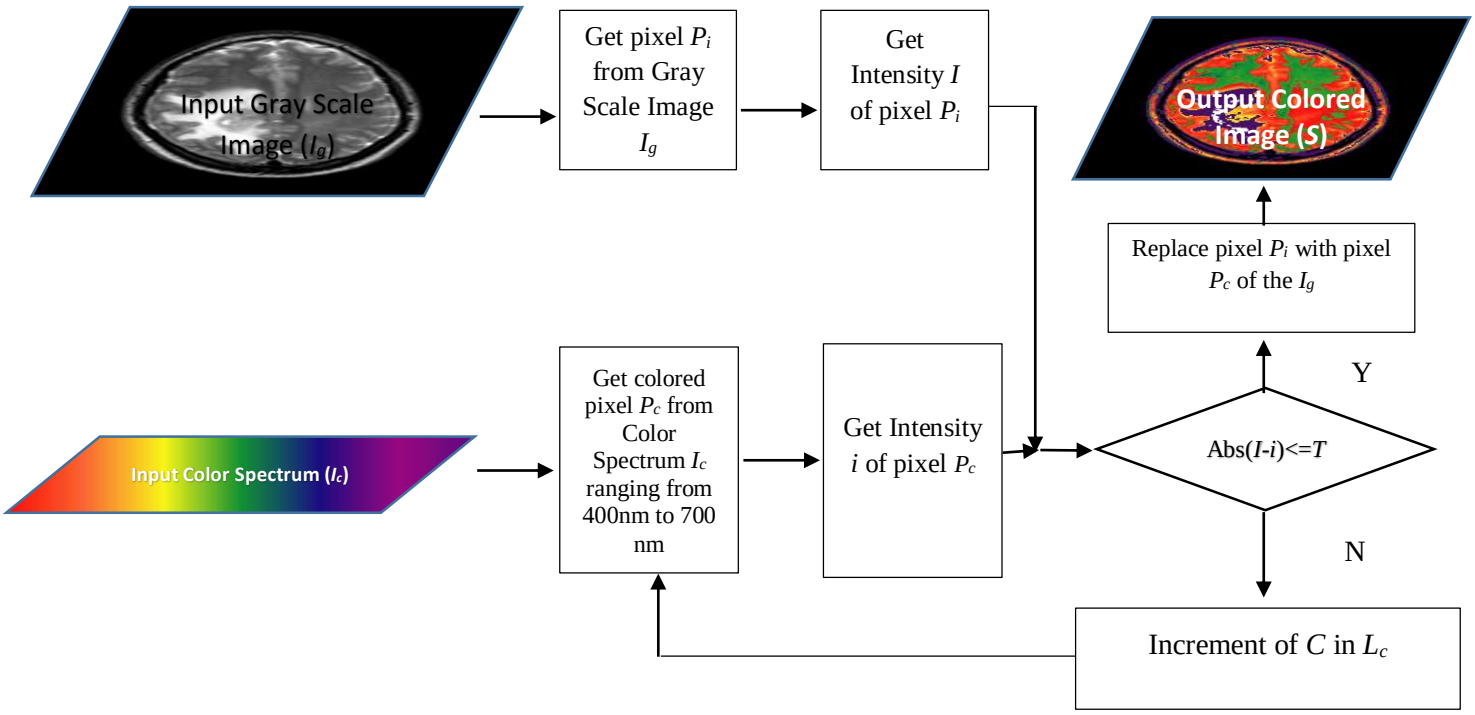


Figure 3.1: Top down approach for colorization of brain soft tissues using visible color spectrum ranging from 400nm to 700nm

## 3.6. Results and discussions

As the basic purpose of this system is to provide ease to the radiologist in identifying the MR images with more accuracy. So, we have tried colorization of brain tissues and obtained the results shown in Figure 3.2 (First column shows the gray scale MR image, second column shows colored image using 400 to 700 nm visible spectrum, and third column shows colored images using visible spectrum in reverse order i.e. 700 to 400 nm). Medical colored images are evaluated subjectively due to non-availability of their actual colored versions. Therefore, the outcomes have been visually evaluated from the radiologist.

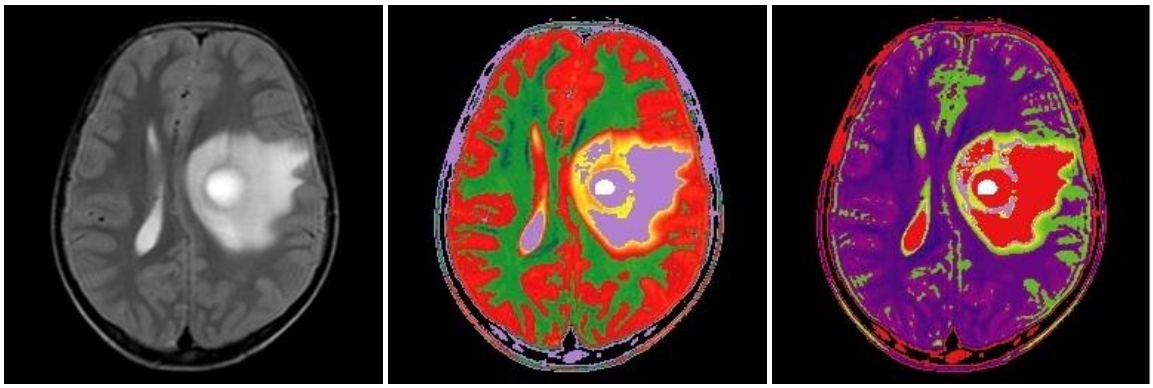

(a) (b) (c)

Figure 3.2: Results obtained through proposed method of colorization (a) T2W axial brain MRI image with dimension 256X256 (b) Colored version of (a) using 400 to 700 nm visible spectrum (c) Colored version of (a) using visible spectrum from 700nm to 400 nm

The results obtained through the proposed method of colorization were evaluated from the radiologist subjectively. The comments pertaining views and assessment regarding results shown in Figure 3.2 (b) re-structured from image Figure 3.2 (a) after color-rendering in 400nm to700nm range are as under;

1. Much better overall recognition of grey and white matters in the normal brain tissue. Grey scale image interpretation is only through rods in the human retina. Human eye/retina has separate receptors for color objects; hence color rendering will lead to much better perception of the same image as has already been scientifically proved.
2. The presence of fluid is clearly depicted by assigning light violet portion of color spectrum, thus a selection of specific signal levels can be more easily and readily recognized than in image Figure 3.2 (a).
3. There is a gradual transition of color spectrum between fluid (light-violet) → semisolid (yellowish) → denser organization tissues (whitish).
4. This has resulted in an effortless interpretation of entire image to differentiate between normal and abnormal image components even without proceeding to segmentation mode in color image.

5. The point discussed in para 4 above is one of major breakthrough in the interpretation of diagnostic images by different specialist doctors. This color rendering mode will lead to almost standardized and uniform description of the same image by all readers – thus minimizing the chances of human error factor in diagnostic modalities. At least all readers of this image will agree regarding the findings in the image. The final image analysis can still vary depending upon the individual knowledge and experience of the reader- but this will constitute a minor component of overall patient management.

6. Colorization of image Figure 3.2 (c), using 700nm-400nm mode has not resulted in any remarkable overall improvement in the image quality, details or interpretation level (as compared with image Figure 3.2 (c) using 400nm-700nm spectrum range). However, outer margin details of the abnormal area in the image Figure 3.2 (c) is much better as compared with other colorization modes.

7. Grey matter is a type of neural tissues, composed primarily of cell bodies, along with their dendrites. White matter, by contrast, is made from axons of nerve cells and full of myelin, which is a whitish fatty material. Examination of the CSF may diagnose a number of diseases. If the CSF is cloudy, meningitis (inflammation of the central nervous system lining) may be present. The results obtained from proposed colorization process are very helpful in examining CSF because variability in the CSF pixels and sensitivity of the images is pertained.

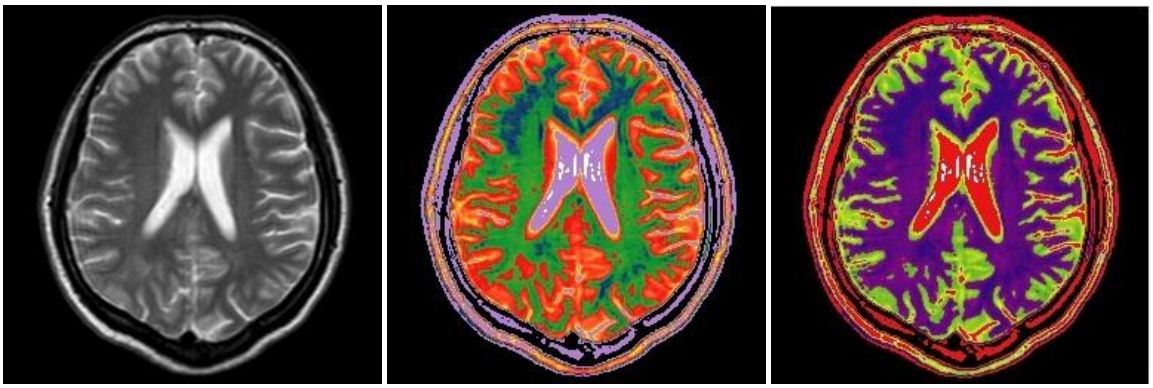

(a) (b) (c)

Figure 3.3: Results obtained through the proposed method of colorization (a) T2W axial brain MRI image with dimension 256X256 (b) Colored version of (a) using 400nm to 700nm visible spectrum (c) Colored version of (a) using visible spectrum from 400nm to 700nm

The results shown in Figure 3.3 (a) represent the normal brain image with a little brain atrophy. The detail of soft tissues is more clearly visible because of colorization. Images Figure 3.3 (b) and Figure 3.3 (c) shows the detail of the skin, scalp and meninges can be easily made out, if there is any abnormality in these structures that will be more easily picked up by human eye because of color rendering.

Improvement in diagnostic imaging modalities is rapidly taking place. Starting with above basics, every type of modifications can be generated to cope with newer developments. Since radiologists are trained in interpretation of grey scale images. They are assisted through coloured representation of the same grey data, so, that they may have another opinion in evaluation of suspicious or enhanced regions. In general, the reported method is appreciative. However, in some subtle pathological cases, a radiologist may have to evaluate both grey scale and coloured version for a definite decision.

## 3.7. Lesson learned

The colorization method has been presented, which colours brain grey scale MR images. The proposed method of colorization enhances visual perception, discrimination, variability and sensitivity of brain MRI images. The results obtained through the proposed

method of colorization have ability to unveil hidden information of brain MRI data, which could not be observe with naked eye, otherwise.

# Chapter 4

# Classification of Normal and Abnormal Brain MRI Slices

In chapter 3, to assist the radiologist or radio oncologist and even the classification methods, a novel method of colorization to convert gray scale brain MRI information into colored version was presented. Here in this chapter, an automated method of brain MRI slices classification as normal or abnormal has been presented. The reported approach has utilized Gabor filter as feature representation and SVM as a classifier to train and test the reported approach. In section 4.1, summary of this research activity has been outlined, section 4.2 represents introduction of this research activity. Section 4.3 contains material and methods, in section 4.4 results and their discussions have been positioned. In section 4.5 lesson learned has been discussed.

## 4.1. Summary of this research activity

In routine health care units, MR scanners are being used to generate a massive number of brain slices, underlying the anatomical details. Pathological assessment from this medical data is being carried out manually by the radiologists or neuro-oncologists. Due to huge volume of brain anatomical data produced by MRI scanners, it is almost impossible to manually analyze every slice. Conclusively, if automated protocols are executed for auto-interpretation; not only the radiologist will be assisted but also a better pathological assessment process would be expected. Several methods have been suggested to address the issue of auto classification of brain MRI slices as normal and abnormal, but accuracy, robustness and optimization is still an open issue. The proposed method, using Gabor filter and SVM, classifies brain MRI slices as normal or abnormal. Accuracy, sensitivity, specificity and AUC-value have been adopted as standard quantitative measures to evaluate the proposed algorithm. To the best of our knowledge, this is first study in which experiments have been performed on HMS dataset, achieving an accuracy of 97.5%, sensitivity of 99%, specificity of 92% and AUC-value as 0.99. To test the robustness against medical traits based on ethnicity and to achieve optimization, a locally developed dataset has also been used for experiments and remarkable results with accuracy (96.5%), sensitivity (98%), specificity (92%) and AUC-value (0.97) were achieved. Comparison with state-of-the art methods proved the overall efficacy of the proposed method.

## 4.2. Introduction of this research activity

In the age of inventions, electromagnetic signals transmitted by human anatomies and listened through emerging medical imaging modalities are systematized to represent image or clinically known as slice. These modalities include X-Ray, Ultrasonography, CT, MEG, EEG, PET, SPECT, and MRI [44], which are producing terabytes of anatomical data every moment. The targeted anatomical structures include liver, brain, prostate, kidney, heart, breast or abdominal structures. This medical imagery data is manually analyzed for the evaluation of subjects that enables the clinician to study or to prepare their treatment planning. With this massive volume of anatomical data, manual interpretation has become almost impossible [7]. Therefore, an automated, expeditious and robust radiological assessment protocols, generally called Computer Aided Diagnosis (CAD) systems always remained decisive to make subject's therapy planning [8].

MRI is a non-invasive medical examination with more contrast among the soft tissues and high spatial resolution. Because of the image quality and sensitivity, it is currently the best test to evaluate any abnormalities or severity of certain injuries within the brain. The diagnosis can be further correlated with the signs and health symptoms of a patient to determine the treatment. MRI delivers important information about shape, size, and localization of brain soft tissues without revealing the subject to high ionizing radiation. Therefore, it has a central position in brain tissues evaluation process in clinical atmosphere. Clinically, the images of different MRI sequences are used for diagnosis of tumor. These sequences include T1W, T1C, MR-GAD, T2W, PDW and FLAIR [13] as shown in Figure 1.1 with direct views of the body in almost any orientation, i.e., coronal, sagittal and axial as shown in Figure 1.2. These sequences enable tissues to be visualized well. T1C shows better anatomical details and enough distinction between cystic and solid structures, while PDW highlights pathological changes better than others. Although, thick bones of the skull have protected the brain, however, it is susceptible to many types of tumors, such as strokes, multiple sclerosis, seizures, dementia and aneurysms.

The diagnosis of brain diseases, mostly depends upon the texture analysis and CAD systems performing automated analysis of brain cells are more objective than traditional way of manually interpreting the slices. Hence, for auto classification of normal and

abnormal brain MRI slices, texture descriptors along with machine learning methods are the best tool [19]. The existing binary classification methods, do classify the slices, but accurate, robust and optimized classification of brain slices is still a challenge. Therefore, further research is requisite to investigate more appropriate methods of two class classification that could classify brain slices compatible to the image generation speed of these MR scanners. A robust and efficient method is presented in order to classify brain MRI slices. The reported approach exploits texture of brain MRI images using Gabor filter and then SVMs are used to train a model in supervised fashion. Overall, results are promising in term of accuracy, specificity, sensitivity and AUC-curve.

Researchers, established and used several methods to classify brain MRI slices as normal and abnormal [7]. Intensity inhomogeneity, PVE, skull stripping, additive noise, radio frequency noise, slice overlapping, shading and etc. are the artifacts directly effecting the classification process [7, 19]. Bias field correction is used to reduce the effect of intensity inhomogeneity [68]. Fast and robust approach to estimate PVE has been reported in article [20]. Several robust skull stripping methods have been proposed by [21]. Analytically correction schemes, MRF, anisotropic diffusion filtering, non-local means and wavelet models are used to de-noise the MR images. For MR image enhancement median filter and its variants, low pass filter, Gaussian filters, gradient based methods, Prewitt edge-finding filters, etc. are mostly in practice [22]. FCM, k-means, Naïve Bayes Classifiers, SVM, ANN and Atlas based methods are some of the examples of classification methods [5, 24].

Machine learning can be through supervised fashion, called classification, through unsupervised way, called clustering and through semi-supervised [29]. FCM [69], a clustering based method, divides data into clusters. Although, FCM yields promising results, but due to its iterative nature it is computationally complex [30]. Atlas based classification methods use prior information, another overhead in terms of precise atlas, which is key to the atlas based methods of classification [5]. SVM is the method to deal with the problems that are best solved in supervised manner. In clinical units, huge volume of annotated brain MRI data is available. Therefore, SVM is being used commonly for classification of brain compartments [25].

Several brain MRI slice classification methods have been reported in literature and have been reviewed, but still robust classification of normal and abnormal slices is an issue. Therefore, further research is requisite to investigate more appropriate methods of classification for brain MRI images with acceptable results in general. This study is a contribution towards a reliable system to assist radiologists, neurosurgeons and healthcare practitioners to obtain another opinion regarding normal or abnormal brain MRI slices. The proposed study can facilitate in further studies related to localization of brain tumor and determining the type of tumor, artifact or pathological, level of severity or aggressiveness of brain tumor, monitoring of therapy, examining efficacy of radiation, pathological assessment of the growth and disorder of soft tissues, automated surgical environment, clinical study and volume estimation of normal and abnormal tissues, radiation dose calculation, grading and staging of brain tumor [63].

## 4.3. Material and methods

### 4.3.1. Image acquisition

For research and experimental purposes, multiple datasets of brain MRI were used which consist of multiple sequences and multiple orientations. As shown in Table 4.1, HMS is among the open access and large benchmarked dataset, which have been used by most of the related studies for algorithm evaluations. HMS contains MRI, CT and SPECT/PET anatomical scans of both normal and abnormal subjects represented in 2 Dimension (D)/3D. To enable the learned model to deal with medical traits based on ethnicity, BVHB, a locally developed dataset has also been used. The subjects were randomly selected for training and testing of the proposed system. The aim of training and testing the proposed system on local dataset was to evaluate the robustness and efficiency of the proposed system. The data set consists of images belonging to both genders and comprising of normal and abnormal cases from volunteers and patients. The local dataset was obtained through a Philips Achieva 1.5 Tesla MRI, with twenty 0.5 mm thick slices. The experimental work was performed under institutional laws of BVH, Bahawalpur, Pakistan. The results were acquired from the "*m*-DIPT" project developed in collaborative work with the department of radiology and diagnostic images, BVH, Bahawalpur, Pakistan. Images from these two datasets relating to neoplastic disease, cerebrovascular disease,

inflammatory diseases and degenerative disease groups have been classified as abnormal images.

Table 4.1: Datasets used for experimental purposes

| # | Dataset | Sequences used for experiments | Orientations used for experiments | Total Slices used in experiments | |
|---|---|---|---|---|---|
| | | | | **Normal** | **Abnormal** |
| 1 | HMS [70] | T1W,T2W,MR GAD, PDW | Axial | 257 | 2319 |
| 2 | BVHB [41] | T1W,T2W, T1C, PDW, FLAIR | Axial, Coronal and Sagittal | 267 | 1746 |

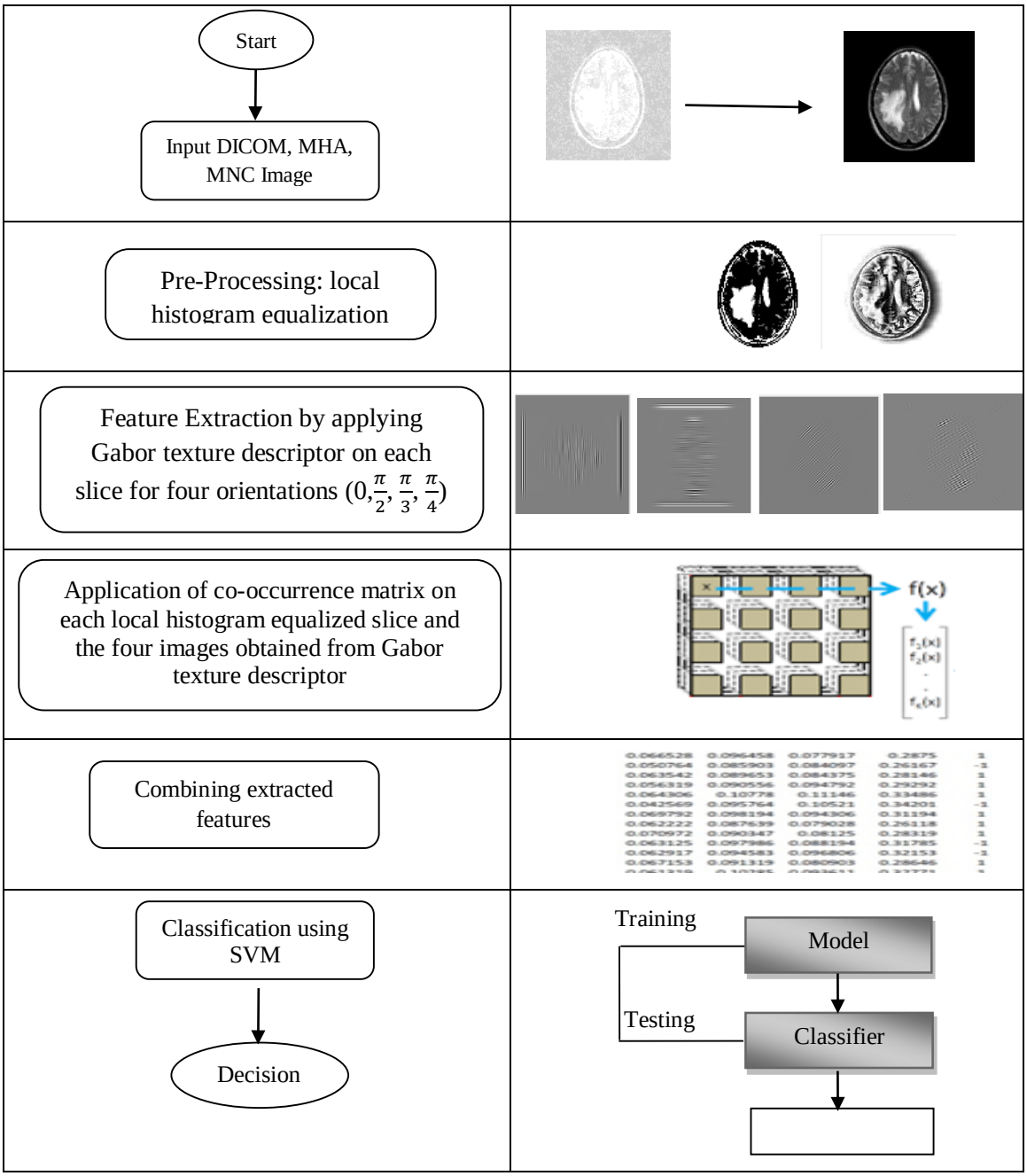


Figure 4.1: Top down approach of the proposed method of two class classification (normal and abnormal brain MRI slices)

### 4.3.2. The proposed method

In this research work, a method for auto classification of normal and abnormal brain MRI slices has been proposed. The research is initiated by investigating and exploring the texture parameters to represent brain MRI slices and it is found that Gabor filter is more suitable to exploit textural information [71]. Therefore, Gabor filter has been used to extract

texture features of both normal and abnormal brain MR slices. These features include Contrast, Smoothness, Mean, Kurtosis, Entropy and Homogeneity. Texture features of image $I(x, y)$ were calculated from each brain MRI by convoluting it with 2D Gabor filters [72]. The top down approach provided in Figure 4.1 shows the units of the proposed paradigm that are executed in order.

#### 4.3.2.1. Pre-processing

Pre-processing refers to a number of operations on an image. Primarily, the images of the datasets listed in Table 4.1 were converted from DICOM format to JPEG. JPEG is more appropriate image format in connection with exploitation of texture information regarding feature extraction and classification [73]. Although, MRI generates scans of high resolution and quality, however, artifacts present in MRI scans are still open challenges to address. Gaussian filter [74] has been used to remove noise and local histogram equalization [75] has been used to improve the contrast.

#### 4.3.2.2. Feature extraction

Feature extraction mean specific representation of the information present inside an image. The information to represent not only pertains pixels but their relationship too. Thus, exploitation, modelling and representation of texture information for brain images was a major challenge faced by the proposed system. The strength of magnetic field in an MRI machine determines the resolution of images. Therefore, same MRI brain image acquisition protocol of having images from MRI machines with magnetic field strength of 1.5 Tesla was followed for both training and testing of the classifier.

Texture descriptors are widely used in medical field to decompose slices acquired through medical scanners. Popular texture descriptors include LBP [76], BRINT [77], WLD [78] and Gabor [72] etc. Texture decomposition methods allied with co-occurrence matrix is also in practice [79]. LBP operator is widely used to extract features due to its discriminative computational power, however, it is a noise sensitive [80]. BRINT is robust to noise and does not require tuning of parameters but it is computationally expensive [77]. WLD is based on physiological law, it simulates human like sensing ability of surroundings, while extracting features from an image and is robust to noise. However, it is computationally complex due to calculation of orientations and differential excitation

[81, 82]. Gabor [72] texture descriptor is more significant among the texture descriptors where uniform patterns are observed in the image data. In medical images, texture holds its energy in narrow bands of frequency and orientation. Gabor filter can encode texture of image into several ways with narrow frequencies and orientations. So, it can be a better choice among texture descriptors for the analysis of brain MR data. Moreover, it can better deal with structural changes, occurring in images due to cancerous cells. Generally, Gabor filter requires five parameters, i.e. (1) *Wavelength* ($\lambda$) (2) *Orientation* ($\theta$) (3) *Phase offset* ($\varphi$) (4) *Sigma* ($\sigma$) and (5) *Gamma* ($\gamma$).

The selection of these parameters was central to this study and empirically the values of $\lambda$, $\varphi$, $\sigma$ and $\gamma$ were set to 3.5, 0, 2.8 and 0.3 respectively, where $\theta \in \{0, \frac{\pi}{2}, \frac{\pi}{3}, \frac{\pi}{4}\}$ resulting in four images at these orientations. The 2D Gabor filter is mathematically described in Equation 4.1.

$$g\lambda, \theta, \varphi, \sigma, \gamma(x, y) = \exp\left(-\frac{x' + \gamma^2 y'}{2\sigma^2}\right) \cos\left(2\pi \frac{x'}{\lambda} + \varphi\right), \quad (4.1)$$

where $x'$ and $y'$ have been calculated using Equation 4.2 and Equation 4.3 respectively.

$$x' = x\cos\theta + y\sin\theta \quad (4.2)$$

$$y' = y\cos\theta - x\sin\theta \quad (4.3)$$

Most of the studies related to classification, extract features from the output of texture descriptors (Gabor, Wavelet etc.) and input these annotated features to the classifiers for their learning. Co-occurrence matrix has been employed for this purpose, which has the ability of measuring texture of an image, considering the variations and dimensions of tonal values as repeating patterns [79]. Co-occurrence matrix has been used on the histogram equalized slice and on four images obtained after convoluting Gabor texture filter.

Since, statistical are being used mostly to represent image texture [79, 83]. They deal best for the delineation of abnormal regions and their surroundings in particular, when applied on medical images. The proposed method has used Smoothness, Kurtosis, Entropy,

Contrast, Mean and Homogeneity [43, 79, 83], on outputs of five co-occurrence matrices. Thus, system yielded a total of 30 features per brain MRI slice.

#### 4.3.2.3. Classification of brain slices

Assigning an incident to one of its class is classification. SVM, ANN, Deep learning, Naïve Bayes frameworks, Decision Trees, etc. are common classifiers for image classification. ANN based systems are mostly computational complexity. Literature indicates that SVM has relatively better performance for binary classification problems [84]. SVM with cubic kernel has been used as a classifier. As shown in Table 4.2, a total of 4589 slices (524 normal, 4065 abnormal) were used for training and testing of the proposed system. Out of these, total of 3029 slices (346 normal, 2683 abnormal) were used for training and total of 1560 slices (178 normal, 1382 abnormal) were used for testing of the proposed model.

Table 4.2: No. of slices used for training and testing of the proposed method of normal or abnormal brain MRI slices classification

| **Total No. of Slices** | | **No. of Training Slices** | | **No. of Testing Slices** | |
|---|---|---|---|---|---|
| Normal | Abnormal | Normal | Abnormal | Normal | Abnormal |
| 524 | 4065 | 346 | 2683 | 178 | 1382 |

## 4.4 Results and discussions

To achieve the goals of performance, robustness and effectiveness of the proposed approach, a large number of experiments were performed using multiple orientations (axial, coronal and sagittal) and multiple sequences (T1W, T2W, T1C, PDW, MR GAD and FLAIR). These experiments were performed on each individual dataset and a combination of the two datasets shown in Table 4.1.

Most of the related studies [7, 9, 19, 43, 85-87] have used accuracy, sensitivity, specificity and AUC-value as standard evaluation measures for the evaluation of their

classification algorithms. Therefore, the results obtained through the proposed method have been evaluated against these standard quantitative parameters.

For the sake of completion and to avoid confusion, the results and discussions have been grouped based on comparison with the state-of-the-art, datasets, abnormalities, sequences, orientations and most importantly the capability of the proposed system to deal with multiformity and variability.

### 4.4.1. Based on the comparison with state-of-the-art

In Table 4.3, a comparison between the proposed method and state-of-the-art methods, reported in recent years has been presented. From Table 4.3, it is observed that El-Sayed Ahmed El-Dahshan et al. obtained an accuracy of 99%, sensitivity of 100%, specificity of 92.8% and AUC of 0.98. However, their experiments were performed on a small randomly selected subset of HMS dataset consisting of axial T2-weighted 101 slices only. When the proposed method was applied on randomly selected same number of T2W slices belonging to the same dataset, it yielded perfect accuracy of 100%, sensitivity of 100%, specificity of 100% and AUC-value of 1.0, which is the best that can be achieved. Saritha et al. have claimed the accuracy of 100%, sensitivity of 100% and specificity of 100% on HMS dataset by randomly selecting a limited subset comprising of 75 images (15 normal and 60 abnormal) that could not possess enough variability. Again, the proposed method on the same dataset consisting of randomly selected 75 images (15 normal and 60 abnormal) scored maximum measuring values. Another comparison with an earlier study El-Sayed Ahmed El-Dahshan et al. presents the superiority of the proposed system on a subset of 70 images (10 normal and 60 abnormal). In a nutshell, the comparison between the reported method and other recent state of the art methods as shown in Table 4.3, proves the effectiveness of the reported method.

Table 4.3: Comparison between the proposed approach and state-of-the-art methods

| **Reported Approaches** | **Dataset used for experiments** | **No. of slices, sequence(s) and orientation used for training and testing** | **Accuracy (%)** | **TP Rate /Sensitivity** | **TN Rate/Specificity** | **AUC-value** |
|---|---|---|---|---|---|---|
| DWT+FPCNN+PCA (El-Sayed A. El-Dahshan et al., 2014 [7]) | Harvard Medical School | 101 (14 Normal and 87 Abnormal)-T2W-Axial | 99 | 100 | 92.8 | 0.98 |
| DWT + spider web plot + PNN (M. Saritha et al., 2013 [9]) | Harvard Medical School | 75 (15 Normal and 60 Abnormal)-T2W-Axial | 100 | 100 | 100 | - |
| PCC + SVM (F. G. Zöllner et al., 2012 [87]) | Gadovist, Bayer Schering Pharma, Berlin, German | 101 subjects | 85 | 89 | 84 | - |
| DWT + PCA + K-NN (El-Dahshan et al., 2010 [86]) | Harvard Medical School | 70 (10 Normal and 60 Abnormal) | 98 | 96 | 97 | - |
| **Proposed Method** | Harvard Medical School | 101 (14 Normal and 87 Abnormal)-T2W-Axial | **100** | **100** | **100** | **1.0** |

| | | | | | | |
|---|---|---|---|---|---|---|
| | | 75 (15 Normal and 60 Abnormal)-T2W-Axial | **100** | **100** | **100** | **1.0** |
| | | 70 (10 Normal and 60 Abnormal)-T2W-Axial | **100** | **100** | **100** | **1.0** |

To test the robustness of the system and for the sake of optimization, a large volume of multi-dataset consisting of multi-sequence and multi-orientation brain slices, have been used to train and evaluate the proposed model and the results are presented in Table 4.4.

### 4.4.2. Based on datasets

Since HMS is the most frequently used and publicly available benchmarked dataset. To the best of our knowledge, no study has so far presented results on the complete HMS dataset which contains slices from multiple sequences belonging to a large number of brain abnormalities. In this study, all of its normal and abnormal slices have been used for training and testing of the proposed system. Experiments have been performed on a total of 2576 axial slices (257 normal and 2319 abnormal) with 839 T1W (110 normal and 729 abnormal), 995 T2W (109 normal and 886 abnormal), 428 PDW (38 normal and 390 abnormal) and 314 MR-GAD (all 314 abnormal). The details against individual sequences and abnormalities belonging to this dataset have been presented in Table 4.4. The proposed system has achieved a quite decent overall classification rate on the HMS dataset with respect to accuracy, sensitivity, specificity and AUC which in turn are 97.5%, 99%, 92% and 0.99 respectively, as shown in Table 4.4 (S#6).

To deal with medical traits based on ethnicity, the proposed system was also trained and test on BVHB dataset. This dataset consists of images belonging to both normal and abnormal subjects having neoplastic disease, cerebrovascular disease, inflammatory disease or degenerative disease. A total of 2013 slices (267 normal and 1746 abnormal)

with 671 (89 normal and 582 abnormal) slices of each axial, coronal and sagittal orientations were used during training and testing of reported method. The proposed system achieved remarkable results of classification in terms of accuracy as 97.9%, sensitivity as 98%, specificity as 99% and AUC as 0.98, as shown in Table 4.4 (S#33).

Increasing the number of training examples, has a direct impact on the system's performance. In case of testing against HMS dataset, when large volume of instances was used to evaluate the learning model, the relative performance was lower as compared to what was achieved against BVHB which have comparatively lesser images. Hence having more variability in training and test data provides a better chance to assess the performance of a classification system, which served as a reason to employ the complete HMS dataset in the study.

### 4.4.3. Based on abnormalities

The reported system has an overall accuracy of 97.5%, sensitivity of 99%, specificity of 92% and AUC-value of 0.99 on complete HMS dataset as shown in Table 4.4 (S#6), against all abnormalities belonging to cerebrovascular disease, neoplastic disease, degenerative disease or inflammatory diseases. During radiological procedures, identification and classification of metastatic type of abnormality (also known as secondary tumor) from the brain MRI slices is a very tedious task [88]. Therefore, to check the performance of developed system against such type of abnormalities, metastatic adenocarcinoma and metastatic bronchogenic carcinoma slices were used from HMS dataset and remarkable results were achieved with accuracy (95.1%), sensitivity (94%), specificity (100%) and AUC-value (0.98) as shown in Table 4.4 (S#4). When the proposed system was tested against non-metastatic abnormalities, the results were notable with significant improved performance as accuracy (97.9%), sensitivity (99%), specificity (94%) and AUC-value (0.99), as shown Table (S#5).

With similar aims, when the reported system was used to train and test on the basis of abnormality type, on BVHB dataset, the results obtained were impressive on metastatic type of brain abnormalities as per accuracy (95.2%), sensitivity (96%), specificity (98%) and AUC-value (.97) as shown in Table 4.4 (S#31). When slices from same dataset, having non-metastatic type of abnormalities were used to evaluate the proposed system, the

measures remained excellent, 99.2%, 99%, 100% and 1.0 respectively as per performance measures as shown in Table 4.4 (S#32). Overall, for the classification against all abnormalities, the system's performance remained reasonable i.e. 97.9%, 98%, 99% and 0.98 respectively as shown in Table 4.4 (S#33).

In could be concluded from the experiments that slices having metastatic type of abnormality are relatively harder to classify as abnormal irrespective of the orientation, sequence and dataset, while brain MRI slices having non-metastatic type of abnormalities are easier to be classified as abnormal.

### 4.4.4. Based on slice sequences

Slice sequences play a vital role in radiological decisions. Therefore, experiments were conducted to measure the performance of the proposed system against slices from different sequences. Initially, experiments were performed on T1W axial slices of HMS dataset for the classification of normal or abnormal slices, measures obtained were 95.3%, 97%, 91% and 0.96 respectively, as shown in Table 4.4 (S#2). Similarly, for the classification of T2W slices, the results were 97.5%, 96%, 94% and 0.98 respectively, as shown in Table 4.4 (S#1).

Most of the times, radiologists use PDW axial slices to confirm about an abnormality [89]. Therefore, from HMS dataset, PDW axial slices were also taken under consideration for experimental purposes. Both normal and the abnormal slices having diseases earlier were used. The results achieved were ideal i.e. 100%, 100%, 100% and 1.0 respectively on a total of 428 slices (38 normal and 390 abnormal), as shown in Table 4.4 (S#3).

When experiments were performed on T1W, T2W and PDW axial slices from BVHB dataset, the achieved efficacy was excellent, but for T1C and FLAIR axial slices of the same dataset, the performance was slightly lower than what was achieved on T1W, T2W and PDW as shown in Table 4.4 (S#7-11). Similarly, while experimenting with coronal slices belonging to BVHB dataset, T1W, T1C and PDW slices achieved greater classification rate as compared to T2W and FLAIR slices of the same dataset as shown in Table 4.4 (S#15-19). On experiments against PDW sagittal slices from the same dataset, the classification rate remained noteworthy as per accuracy (100%), sensitivity (100%),

specificity (100%) and AUC (1.0) as shown in Table 4.4 (S#27). While performance against other sequences, i.e., T1W, T2W, T1C and FLAIR was slightly lower than what was achieved on PDW as shown in Table 4.4 (S#23-26).

It is established from the experiments that PDW slices have more contributing patterns than other sequences. Therefore, their classification rate remained noteworthy, irrespective of the orientation and type of abnormality they have.

### 4.4.5. Based on slice orientations

In clinical environment, analyzing different orientation slices of a subject enables a radiologist to detect an abnormality which might not be evident in a single orientation. Therefore, in this study, experiments were conducted to study the impact of slice orientation on the accuracy of classification.

The proposed study was tested on a total of 2576 (257 normal and 2319 abnormal) axial slices from the HMS dataset. Overall, the proposed methodology obtained promising results on these slices as per accuracy, sensitivity, specificity and AUC-value, i.e. 97.5%, 99%, 92% and 0.99 respectively as shown in Table 4.4 (S#6).

During experiments on axial slices belonging to BVHB dataset, the proposed system achieved significant accuracy (99.4%), sensitivity (99%), specificity (100%) and AUC-value (1.0) as shown in Table 4.4 (S#14). While performing experiments on same dataset, the results remained ideal for coronal slices as per accuracy (99.8%), sensitivity (100), specificity (100) and AUC-value (1.0), as shown in Table 4.4 (S#22). The results obtained against sagittal slices belonging to same dataset, the results were quite admirable as per accuracy (98.8%), sensitivity (99%), specificity (100%) and AUC-value (0.99), as shown in Table 4.4 (S#30).

When all datasets were combined to evaluate the performance of the proposed system against different orientations, results were slightly better against the coronal orientation as evident from Table 4.4 (S#35). However, it can be concluded that any orientation alone cannot guarantee better classification as it does not possess all the information regarding an abnormality, therefore for achieving better results, combining the outcomes against different orientations might result in a better overall accuracy.

### 4.4.6. Based on the capability of the proposed system to deal with multiformity and variability

To test the robustness of the reported system and to deal with variability of different MRI scanners, all datasets were combined to train and test the system, the results proved the adequate success of the proposed paradigm. The system was trained and tested on a total volume of 4589 (524 normal and 4065 abnormal) slices, and the values of quantitative parameters attained an accuracy of 96.5%, sensitivity of 98%, specificity of 92% and AUC-value 0.97 as shown in Table 4.4 (S#36).

The overall performance of the proposed method, manifests that it is robust, efficient and more definitive as compared to the state-of-the-art methods. The proposed paradigm does not require complex training phase, rather it just calculates Gabor texture parameters. It has already been trained on a large volume of training examples of multi-orientations, multi-sequences belonging to multi-datasets to deal with multiformity and to face variability.

## 4.5. Lesson learned

Increasing the number of training examples, has a direct impact on the system's performance. Hence having more variability in training and test data provides a better chance to assess the performance of a classification system. Slices having metastatic type of abnormalities are relatively harder to be classified as abnormal in comparison to brain MRI slices having non-metastatic type of abnormalities, irrespective of the orientation, sequence and dataset. PDW slices have more contributing patterns than other sequences. Classification rates are slightly higher against coronal orientation slices as compared to the slices belonging to other orientations. However, any orientation alone cannot guarantee better classification as it does not possess all the information regarding an abnormality. Overall, accuracy, sensitivity, specificity and AUC-value based standard evaluation measures proved adequate success of the proposed methodology.

Table 4.4: Dataset-wise, orientation wise, sequence wise and combined results of experiments

| S# | Dataset | Orientation | Sequences | No. of slices used for experiments | | | | Accuracy (%) | Sensitivity (%) | Specificity (%) | AUC-value |
|---|---|---|---|---|---|---|---|---|---|---|---|
| | | | | Total | Normal | Abnormal | Abnormalities | | | | |
| 1 | HMS | Axial | T2W | 995 | 109 | 886 | Cerebrovascular disease<br>Neoplastic disease<br>Degenerative disease<br>Inflammatory diseases | 97.5 | 96 | 94 | 0.98 |
| 2 | | | T1W | 839 | 110 | 729 | | 95.3 | 97 | 91 | 0.96 |
| 3 | | | PDW | 428 | 38 | 390 | | 100 | 100 | 100 | 1 |
| 4 | | | T1W, T2W, MR GAD,PDW | 259 | 120 | 139 | Neoplastic disease (Metastatic adenocarcinoma and Metastatic bronchogenic) | 95.1 | 94 | 100 | 0.98 |
| 5 | | | T1W, T2W, MR GAD,PDW | 2437 | 257 | 2180 | Cerebrovascular disease<br>Neoplastic disease | 97.9 | 99 | 94 | 0.99 |

| | | | | | | | | | | | |
|---|---|---|---|---|---|---|---|---|---|---|---|
| 6 | | | T1W, T2W, MR GAD,PDW | 2576 | 257 | 2319 | Degenerative disease Inflammatory diseases | 97.5 | 99 | 92 | 0.99 |
| 7 | BVHB | Axial | T1W | 133 | 14 | 119 | | 100 | 100 | 100 | 1 |
| 8 | | | T2W | 181 | 28 | 153 | | 100 | 100 | 100 | 1 |
| 9 | | | T1C | 133 | 14 | 119 | | 99.1 | 99 | 98 | 0.99 |
| 10 | | | FLAIR | 101 | 12 | 89 | | 99.5 | 100 | 99 | 1 |
| 11 | | | PDW | 123 | 21 | 102 | | 100 | 100 | 100 | 1 |
| 12 | | | T1W, T2W, T1C, PDW, FLAIR | 105 | 19 | 86 | Neoplastic disease (Metastatic adenocarcinoma and Metastatic bronchogenic) | 96.1 | 95 | 100 | 0.98 |
| 13 | | | T1W, T2W, T1C, | 566 | 70 | 496 | Cerebrovascular disease | 99.1 | 99 | 100 | 1 |

| | | | | | | | | | | | |
|---|---|---|---|---|---|---|---|---|---|---|---|
| | | | PDW, FLAIR | | | | Neoplastic disease Degenerative disease Inflammatory diseases | | | | |
| 14 | | | T1W, T2W, T1C, PDW, FLAIR | 671 | 89 | 582 | | 98.7 | 99 | 100 | 1 |
| 15 | | Coronal | T1W | 133 | 14 | 119 | | 100 | 99 | 100 | 1 |
| 16 | | | T2W | 181 | 28 | 153 | | 99 | 100 | 99 | 1 |
| 17 | | | T1C | 133 | 14 | 119 | | 100 | 99 | 98 | 1 |
| 18 | | | FLAIR | 101 | 12 | 89 | | 99.5 | 98 | 99 | 0.99 |
| 19 | | | PDW | 123 | 21 | 102 | | 100 | 100 | 100 | 1 |
| 20 | | | T1W, T2W, T1C, PDW, FLAIR | 105 | 19 | 86 | Neoplastic disease (Metastatic adenocarcinoma and Metastatic bronchogenic) | 96.5 | 96 | 99 | 0.99 |

| | | | | | | | | | | | |
|---|---|---|---|---|---|---|---|---|---|---|---|
| 21 | | | T1W, T2W, T1C, PDW, FLAIR | 566 | 70 | 496 | | 99.1 | 100 | 100 | 1 |
| 22 | | | T1W, T2W, T1C, PDW, FLAIR | 671 | 89 | 582 | Cerebrovascular disease Neoplastic disease Degenerative disease Inflammatory diseases | 99.8 | 100 | 100 | 1 |
| 23 | | Sagittal | T1W | 133 | 14 | 119 | | 98 | 99 | 97 | 0.98 |
| 24 | | | T2W | 181 | 28 | 153 | | 97 | 99 | 97 | 0.98 |
| 25 | | | T1C | 133 | 14 | 119 | | 97.8 | 99 | 99 | 0.99 |
| 26 | | | FLAIR | 101 | 12 | 89 | | 99.5 | 98 | 99 | 1 |
| 27 | | | PDW | 123 | 21 | 102 | | 100 | 100 | 100 | 1 |
| 28 | | | T1W, T2W, T1C, | 105 | 19 | 86 | Neoplastic disease (Metastatic adenocarcinoma and | 95.9 | 95 | 99 | 0.97 |

| | | | | | | | | | | | |
|---|---|---|---|---|---|---|---|---|---|---|---|
| | | | PDW, FLAIR | | | | Metastatic bronchogenic) | | | | |
| 29 | | | T1W, T2W, T1C, PDW, FLAIR | 566 | 70 | 496 | Cerebrovascular disease Neoplastic disease Degenerative disease Inflammatory diseases | 98.4 | 99 | 98 | 0.98 |
| 30 | | | T1W, T2W, T1C, PDW, FLAIR | 671 | 89 | 582 | | 98.8 | 99 | 100 | 0.99 |
| 31 | | Combined (Axial, Coronal and Sagittal) | T1W, T2W, T1C, PDW, FLAIR | 305 | 47 | 258 | Neoplastic disease (Metastatic adenocarcinoma and Metastatic bronchogenic) | 95.2 | 96 | 98 | 0.97 |
| 32 | | | | 1708 | 220 | 1488 | Cerebrovascular disease Neoplastic disease | 99.2 | 99 | 100 | 1 |
| 33 | | | | 2013 | 267 | 1746 | | 97.9 | 98 | 99 | 0.98 |

| | | | | | | | | | | | |
|---|---|---|---|---|---|---|---|---|---|---|---|
| 34 | Combined (Harvard Medical School and Bahawal Victoria Hospital, Bahawalpur) | Axial | T1W, T2W, PDW, MR GAD, FLAIR | 3247 | 346 | 2901 | Degenerative disease Inflammatory diseases | 97.3 | 98 | 95 | 0.98 |
| 35 | | Coronal | T1W, T2W, PDW, MR GAD, FLAIR | 671 | 89 | 582 | | 99.4 | 99 | 100 | 1 |
| 36 | | Combined (Axial, Coronal and Sagittal) | T1W, T2W, T1C, PDW, MR GAD, FLAIR | 4589 | 524 | 4065 | | 96.5 | 98 | 92 | 0.97 |

# Chapter 5

# Multiclass Classification of Brain Tumor

In chapter 4, an automated method of brain MRI slices classification as normal or abnormal was presented. The method achieved remarkable results. Here in this chapter, further classification of brain tumor, i.e., glioma, sarcoma, meningioma, metastatic has been performed. Section 5.1 has summary of this research activity, section 5.2 contains introduction. Materials and methods have been organized in section 5.3. In section 5.4, results and discussion has been presented, while in section 5.5, lesson learned is outlined.

## 5.1. Summary of this research activity

Accurate and automated classification of brain abnormalities from Magnetic Resonance Images (MRI) is needed in routine medical health care units. To assist medical practitioners, some work has been reported in literature but accuracy and optimization is still needed. The drive of this study is to develop a robust and an efficient system that could deal with medical traits based on ethnicity. Hence, a method to classify brain MRI image into brain related disease groups and tumor types has been proposed. The proposed method employed Gabor texture followed by a set of distinguished statistical features. These features are then used by Support Vector Machine (SVM) to classify the brain disorder. Experiments have been performed to classify brain MRI images as normal or diseases including cerebrovascular, degenerative, inflammatory, and neoplastic. Neoplastic disease is further classified into meningioma, glioma, metastatic bronchogenic carcinoma, metastatic adenocarcinoma or sarcoma. Standard evaluation measures, i.e., accuracy, specificity, sensitivity, and AUC-value have been used to test performance of the developed system. The proposed system has been trained on complete dataset of HMS. Further, to achieve robustness, a dataset developed locally has been used. Extraordinary results on different orientations, sequences of both of these datasets as per accuracy (up-to 99.6%), sensitivity (up-to 100%), specificity (up-to 100%), precision (up-to 100%) and AUC-value (up-to 1.0) have been achieved. The proposed method classifies the brain MRI slices into defined abnormality groups. It can also classify the abnormal slices into tumorous or non-tumorous one. The major achievement of the developed system is its auto classification of tumorous slices into the slices having primary tumor or secondary tumor as well as their further types as Glioma, Sarcoma, Meningioma, Bronchogenic carcinoma, and Adenocarcinoma, which could not be possible to determine without biopsy, otherwise.

## 5.2. Introduction of this research activity

Still in this modern digital age, luminance values exhibiting anatomical structures are interpreted through naked eye by domain experts to determine the presence and extent of abnormal region's severity. Anatomical structures are usually obtained through medical imaging modalities including MRI [44, 90]. Human anatomy including brain are used to scan with these medical imaging modalities [41]. This scanned data is analyzed manually for the treatment planning of the patients. Due to large volume of this medical data, manual interpretation is rarely possible. Therefore, robust and efficient protocols, also called Computer Aided Diagnosis (CAD) systems are necessary in patient's treatment planning [8].

Human brain is susceptible to several abnormalities including cerebrovascular diseases, degenerative diseases, inflammatory diseases and neoplastic (tumor) diseases [9]. Being non-invasive medical examination, MRI is currently the best examination for assessment of brain disorders. It produces images with different sequences including, T2-weighted (T2W), T1-weighted (T1W), T1 with contrast (T1C), Fluid Attenuated Inversion Recovery (FLAIR), Proton Density-weighted (PDW) and Gadolinium Contrast Medium (MR GAD) as shown in Figure 1.1. It can scan the subject from sagittal, coronal, and axial [14, 23] orientation as shown in Figure 1.2. These sequences and views enable tissues to be visualized well for their interpretation and analysis by a radiologist. These sequences have equal clinical importance regarding anatomical detailed study, evaluation and monitoring of pathological changes etc. T1W sequence images are mostly used for the study of normal anatomy. However, necrotic, and active tumor areas can easily be recognized using this sequence after administration of intravenous contrast. The surrounding areas of a brain tumor usually called edema are more easily distinguishable using T2W sequence images. FLAIR sequence images are mostly used to suppress the intraventricular CSF signals. This sequence is important in studying and separating the edema and Cerebrospinal Fluid (CSF) regions [15]. PDW is mostly used for the evaluation of Multiple Sclerosis (MS) lesions. These sequences as an individual or combination of these are used to differentiate any fatty deposit in the tumors. The presence of fat in the lesion determines its benign nature that is a differentiating point between neoplastic and non-neoplastic lesions.

Several methods of brain disorders classification in general and tumor types in specific have been reported in literature, but robust, accurate and efficient classification is still challenging. As per our best knowledge, it is a first study, in which brain disorders along with further tumor types has been classified. The proposed method has exploited brain MRI texture using Gabor filter. Then SVMs have been used to train a model. The reported method has obtained remarkable results as per standard evaluation measures.

This study is a contribution in developing a reliable system to assist radiologists, neurosurgeons, and healthcare practitioners to obtain another opinion regarding presence or determining a type of brain related abnormality in MRI slices. The proposed study can facilitate in further studies related to monitoring of therapy, examining efficacy of radiation, pathological assessment of the growth and disorder of soft tissues, automated surgical environment, clinical study of brain tissues, radiation dose calculation, grading or staging of brain tumor.

Several techniques for brain tumor detection and brain abnormalities classification have been discussed in the literature. Some of the proposed methods only detect tumor from brain MRI slices, while some also recognize the type of tumor. A few of the reported methods classify the brain general abnormalities.

The investigators [33] suggested an automated method for brain tumor detection using Fuzzy C-Means clustering algorithm and Hierarchical Self Organizing Map (HSOM). They used local dataset of KMC Hospital in Coimbatore, India. The suggested technique only detects brain tumor and does not classify further type of brain tumor. The researchers [34], proposed an automated method for brain tumor detection using modified Probabilistic Neural Network (PNN). The authors used accuracy as standard evaluation, measures for the evaluation of their proposed algorithm. A customized local dataset has been used for experiments with 100 % accuracy. The use of local dataset does not ensure the robustness of the proposed method. Authors [35], have reported methodology the classification of brain tumor though MRI images using SVM and Co-occurrence matrix. A locally collected dataset and a benchmark dataset of HMS were used for the evaluation of reported methodology. Classification rates as per accuracy remained 99%, which was appreciative but did not further classify the neoplastic types. Our proposed study has been conducted in continuation to the earlier work [4] in which, an automated approach for brain MRI

slices classification using Gabor Texture and Support Vector Machines was reported. The results were appreciative, however, the reported method was limited to classify the brain MRI slices as normal or abnormal. It did not further classify the type of brain abnormality.

Discrete Wavelet Transformations (DWT) and ANN based method for MRI image classification as normal and abnormal method has been published by [7]. HMS dataset has been used for research and experiments purpose. They performed experiments on 101 T2W axial slices only. However, their achieved accuracy i.e. 99% was appreciative. Again 101 MR slices could not have enough variability and multiformity. The study only deals with MRI slice classification as normal and abnormal and does not classify brain related disorder, nor the proposed scheme classify types of tumor. Scholars [24], have reported an automated method for brain tumor classification using SOM and KNN technique. Self-organising map neural networks have been used for features extracted from discrete wavelet transformation. KNN classifier has been used for classification of MR slices as normal or abnormal.

Researchers [36], reported an automated method for Alzheimer's disease detection from MRI images using SVM. They performed experiments on local dataset obtained from Wellcome Trust Centre for Neuroimaging, Institute of Neurology, UCL, London and claimed the accuracy (96.4%), sensitivity (95.6%) and specificity (92.5%). Only Alzheimer disease has been detected in this study, rest of the diseases are neither detected nor classified, as well experiments have been performed and validated on local data set only. Another method for the identification and classification of primary glioma and grading of metastasis gliomas has been proposed by [19]. SVM, Linear Discriminant Analysis (LDA) and K-Nearest Neighbor for classification of primary glioma and grading of brain tumors, has been utilized. A local dataset (MAGNETOM Trio Tim System, Siemens Medical Systems, Erlangen, Germany) has been used for the evaluation of developed algorithm. The proposed methodology achieved the accuracy for SVM (91.2%), KNN (89.8%, for k=3), and LDA (85.5%). Standard evaluation measures achieved, were not up to the mark, results are also validated on local dataset, which could not have robustness. Authors [37], have reported an automated method for brain tissue categorization using custom Genetic Algorithm (GA), Gray Level Co-occurrence Matrix (GLCM), Extreme Learning Machine (ELM) and Particle Swarm Optimization (PSO). Experiments have been performed on customized dataset (PSG IMSR & Hospital, T1 images). The performance evaluation measured for sensitivity,

specificity and accuracy remained 95.9%, 98.88% and 98.05% respectively. The results have only been validated on T1C images obtained from local dataset. However, the results for glioma, meningioma and metastasis tissues classification are quite reasonable. [9] published research for automated classification of MRI slices using discrete wavelet transforms (DWT), Spider Web Plots and Probabilistic Neural Networks (PNN). On randomly selected 75 T2W axial slices from HMS dataset, they claimed accuracy, specificity, and sensitivity of 100%, 100% and 100% respectively. The learned model, trained on small axial and T2W dataset, could not have enough multiformity, variability, and robustness. Neural network based training models, always remained computationally complex [38].

In the light of reviewed literature, it is accomplished that some of the methods do classify brain MRI slice as normal or abnormal, while some of them only determine the grades of glioma tumor. The state-of-the-art methods don't perform well in general to determine the type of brain abnormality. Still, it's a challenge to investigate computational paradigms that could perform robust and efficient brain disorders classification. The proposed robust and efficient system is trained and tested on multi-datasets, having multi-orientations and multi-sequence MRI slices. So that the developed system would be able to deal medical and ethnic traits of local vicinity. The proposed methodology will only be the alternate of biopsy procedure which is currently in practice in almost every medical health care unit.

## 5.3. Materials and methods

### 5.3.1. Image acquisition

For research and experiments purposes, multiple datasets of brain MRI have been used, which consist of multiple sequences and multiple orientations. As shown in Table 5.1, HMS is among the open access and large benchmarked datasets, which have been used by most of the related studies for algorithm evaluations. HMS contains MRI, CT and SPECT/PET anatomical scans of both normal and abnormal subjects represented in 2D/3D. To enable the learned model to deal with medical traits based on ethnicity, BVHB, a locally developed dataset has also been used. The subjects were randomly selected for training and testing of the proposed system. The aim of training and testing the proposed system on local dataset was to evaluate the robustness of the proposed system. The data set consists of images belonging to both genders and comprising of

normal and abnormal cases from volunteers and patients. The collection of abnormal images from these two datasets relating to different brain diseases has been grouped into four main brain disease groups as shown in Table 5.2.

Table 5.1: Datasets used for experiments of brain tumor classification

| S# | Dataset | Sequences used for experiments | Orientations used for experiments | Classes and no. of slices used for training and testing | |
|---|---|---|---|---|---|
| | | | | Class | No. of slices |
| 1 | HMS [70] | T1W, T2W, MR GAD, PDW | Axial | Normal | 309 |
| | | | | Cerebrovascular disease | 737 |
| | | | | Degenerative disease | 307 |
| | | | | Inflammatory disease | 473 |
| | | | | Neoplastic disease | 648 |
| 2 | BVHB [41, 44] | T1W, T2W, T1C, PDW, FLAIR | Axial, Coronal and Sagittal | Normal | 3750 |
| | | | | Cerebrovascular disease | 3750 |
| | | | | Degenerative disease | 3750 |
| | | | | Inflammatory disease | 3750 |
| | | | | Neoplastic disease | 3750 |

Table 5.2: Brain diseases classified as abnormalities

| S# | Brain disease group | Abnormalities |
|---|---|---|
| 1 | Cerebrovascular disease | – Multiple embolic infarction<br>– Diffusion<br>– Acute stroke<br>– Sub-acute stroke<br>– Chronic subdural hematoma<br>– Cavernous angioma<br>– Arteriovenous malformation<br>– Vascular dementia<br>– Hypertensive encephalopathy<br>– Multiple embolic infarction<br>– Fatal stroke<br>– Cerebral hemorrhage |
| 2 | Neoplastic disease (brain tumor) | – Glioma<br>– Metastatic adenocarcinoma<br>– Metastatic bronchogenic carcinoma<br>– Meningioma<br>– Sarcoma |
| 3 | Degenerative disease | – Alzheimer's disease<br>– Huntington's disease<br>– Motor neuron disease<br>– Cerebral calcinosis<br>– Pick's disease |
| 4 | Inflammatory or infectious disease | – Multiple sclerosis<br>– AIDS dementia |

| | | |
|---|---|---|
| | | – Lyme encephalopathy<br>– Herpes encephalitis<br>– Creutzfeld-Jakob disease<br>– Cerebral Toxoplasmosis |

### 5.3.2. The proposed method

In this research work, a method is proposed to classify the brain MRI slices into multiple classes has been proposed. The research is initiated by investigating and exploring the texture parameters to represent brain MRI slices and it is found that Gabor filter is more suitable to exploit textural information [71]. Therefore, Gabor filter has been used to extract texture features of brain MR slices having abnormalities shown in Table 5.2. Texture features were calculated from each brain MRI by convoluting it with 2D Gabor filter [72]. The top down approach provided in Figure 5.1 shows the units of the proposed paradigm that are executed in order.

#### 5.3.2.1. Pre-processing

Although, MRI generates scans of high resolution and quality, but, artifacts are also observed in the scans, which need to address investigators. To remove the noise present in MR slices used in both training and testing, Gaussian filter [74] has been used to remove MR noise present in the brain MRI data and local histogram equalization [75] has been used to improve the contrast.

#### 5.3.2.2. Feature extraction

Feature extraction refers a particular representation of the texture based information. Thus, modeling and representation of features was main challenge faced by the proposed system. The strength of magnetic field in an MRI machine determines the resolution of images. Therefore, same MRI brain image acquisition protocol with magnetic field strength of 1.5 Tesla was followed for both training and testing of the classifier.

Since brain MRI contains spatially dependent class characteristics, texture extraction methods have been commonly used to generate feature information for brain tumor classification [43, 91]. The most common texture feature extraction method for biomedical data is the application of co-occurrence matrix. This study has investigated the ability of co-occurrence matrix to classify

brain abnormalities. Texture features as shown in Table 5.3 were applied to the output of co-occurrence matrix.

Decomposing an image into meaningful components is known as feature extraction, which is challenging and important task. To decompose medical slices, acquired through medical scanners texture features are mostly used. Popular texture descriptors include LBP [76], BRINT [77], WLD [81] and Gabor [72] etc.

| | |
|---|---|
| Step1<br>Data acquisition and Pre- processing using Local Histogram Equalization | 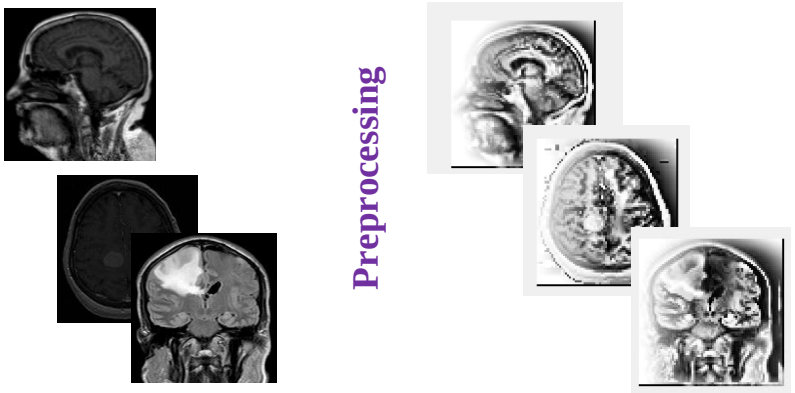 |
| Step2<br>Feature Extraction by applying Gabor filter on each slice for four orientations $(0,\frac{\pi}{2},\frac{\pi}{3},\frac{\pi}{4})$ | 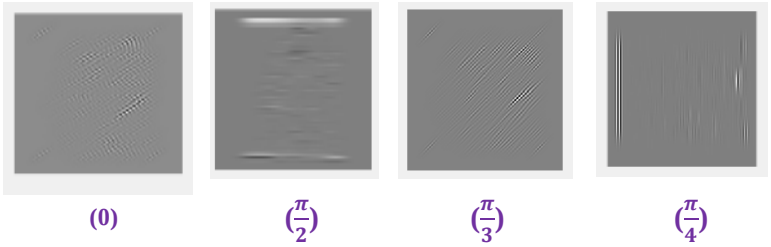 |
| Step3<br>Application of co-occurrence matrix on the four output images of step2 and the equalized image | 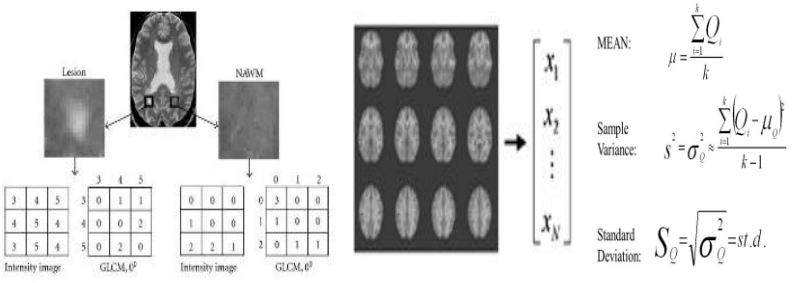 |

Step4

Combining extracted features

| contrast2 | mean_3_v | hom2_3_v | smoth_4_ | kurt_4_w | entrp_4_v | contrast2 | mean_4_v | hom2_4_v | Class |
|---|---|---|---|---|---|---|---|---|---|
| 25908 | -1.65228 | 0.46103 | 0.98654 | 45.8023 | 2.57318 | 18637.7 | -0.01135 | 0.49396 | Degenerative |
| 34483.7 | -1.19849 | 0.36321 | 0.9931 | 26.0494 | 2.63904 | 25088.1 | -0.01343 | 0.40612 | Degenerative |
| 35152 | -1.61487 | 0.36044 | 0.99342 | 21.2461 | 2.61114 | 26789.2 | 0.02124 | 0.39236 | Degenerative |
| 34873.8 | -0.82294 | 0.35042 | 0.99285 | 24.8234 | 2.7496 | 24754 | -0.11078 | 0.39374 | Degenerative |
| 32000.9 | -1.60062 | 0.39864 | 0.99201 | 27.3684 | 2.5329 | 23279.4 | 0.00211 | 0.44262 | Inflamatory |
| 31133.2 | -0.92807 | 0.39281 | 0.99054 | 25.2923 | 2.66804 | 22261.6 | -0.0452 | 0.43572 | Inflamatory |
| 29521.2 | -1.51855 | 0.43871 | 0.99024 | 23.5912 | 2.37922 | 21308.3 | 0.04755 | 0.48489 | Inflamatory |
| 27753.7 | -1.92227 | 0.46635 | 0.9894 | 33.7564 | 2.28583 | 20044.8 | 0.01321 | 0.52068 | Neoplastic |
| 28807.6 | -1.314 | 0.41038 | 0.98842 | 41.9743 | 2.62802 | 19923.8 | -0.05954 | 0.46911 | Neoplastic |
| 24865.9 | -1.67908 | 0.50208 | 0.98411 | 38.3358 | 2.19027 | 17226.2 | -0.02643 | 0.56301 | Neoplastic |
| 28787.5 | -1.29697 | 0.41175 | 0.9887 | 39.7398 | 2.70207 | 20311.3 | -0.04593 | 0.45593 | Neoplastic |
| 30039 | -1.61411 | 0.40696 | 0.99062 | 27.809 | 2.66883 | 21901.4 | 0.0303 | 0.44207 | Cerebrovasular |
| 30848.5 | -1.5683 | 0.40093 | 0.99102 | 28.3286 | 2.62437 | 22063.5 | 0.06573 | 0.44657 | Cerebrovasular |
| 32198.6 | -1.31183 | 0.39303 | 0.99307 | 23.6374 | 2.50392 | 24196 | 0.04132 | 0.43393 | Cerebrovasular |
| 33356.3 | -1.54977 | 0.37148 | 0.99321 | 23.0063 | 2.59314 | 24235.1 | -0.06454 | 0.42279 | Cerebrovasular |

Step5

Classification using SVM
-Cerebrovascular disease, Degenerative disease, Inflammatory disease, Neoplastic disease
-Glioma, Meningioma, Adenocarcinoma, Bronchogenic carcinoma, Sarcoma
-Neoplastic, Non- neoplastic
-Primary tumor, Secondary tumor

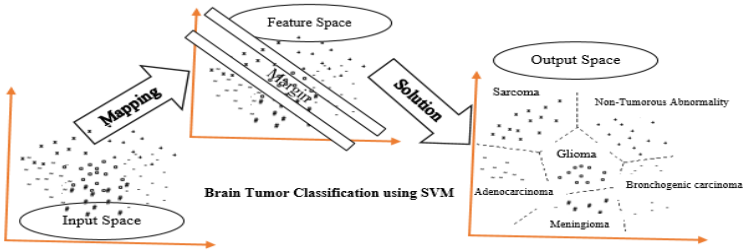


Step6

Evaluation of the Proposed System
Accuracy
Specificity
Sensitivity
ROC

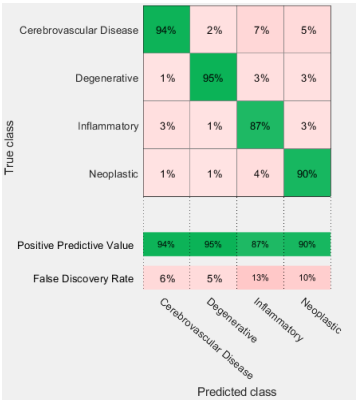


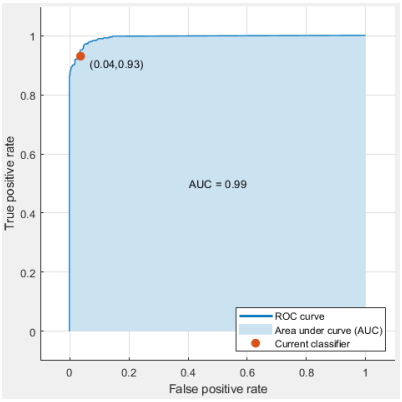


Figure 5.1: Top down approach of the proposed system for brain tumor classification

Table 5.3: Texture parameters used for classification of brain abnormalities

| S# | Texture Parameter | Purpose | Reference |
|---|---|---|---|
| 1 | Contrast | The measure of contrast or local intensity variation favors contributions of pattern to classify a region from other regions. | R. M. Haralick et al., [79] |
| | Energy | Energy is helpful in classification of abnormal regions by the extent of intensity variation in them. | |
| | Sum of squares | This feature also represents variance, it deals specifically with the dispersion around the mean of combinations of referenced normal and abnormal regions. | |
| | Variance | These features have been used to measure the roughness of both normal and abnormal regions. They have further played their role in determining more contributing patterns for neoplastic class classification. | |
| | Sum average | | |
| | Sum variance | | |
| | Difference variance | | |
| | Dissimilarity | | |
| | Correlation | These features have been used to measure linear dependencies between normal and abnormal regions as well as among the types of abnormalities present at the specified positions relative to each other. | |
| | Information measure of correlation | | |
| | Information measure of correlation2 | | |

| | | | |
|---|---|---|---|
| 2 | Autocorrelation | This feature has been utilized in classification of brain abnormalities especially neoplastic types. It is among the best texture parameters to measure correlation of set of pixels with themselves at different regions of the same slice. Experimentally, we found it the best representative measure for the identification of repeating patterns, such as the presence of a normal and abnormal set of pixels obscured by lesions. | L.-K. Soh and C. Tsatsoulis [92] |
| | Cluster prominence | These parameters have been used to measure asymmetry behavior of normal and abnormal regions and their contributions toward repeating patterns. | |
| | Cluster shade | | |
| | Entropy | These features have been used to identify a slice having amount of information and measure of randomness. The slices having greater value of entropy have more texture. | |
| | Sum entropy | | |
| | Homogeneity | This is an important feature for knowing the uniformity present in a substance or organ. A homogeneous brain MRI slice is uniform in composition and its characteristics based on its texture. | |
| | Maximum probability | This statistical feature is also important for classifying brain abnormalities, because a maximum entropy probability distribution has entropy that is at least as great as that of all other members of a specified class of probability distributions. | |
| 3 | Inverse difference moment | This parameter also measures slice homogeneity. It achieves its largest value when most of the occurrences in GLCM are concentrated near the main diagonal. | D. A. Clausi [93] |

| | | | |
|---|---|---|---|
| | Inverse difference normalized | Based on energy parameter calculated through PCA. This parameter has very small impact on classification. However, when these parameters are combined with the parameters at S#1, there is minor improvement in performance. | |
| | Inverse difference moment normalized | | |

Texture decomposition methods allied with co-occurrence matrix, run length matrix and difference matrix are also in practice to extract texture features [79].The LBP operator is widely used in research due to its discriminative computational power, however, it is noise sensitive [80]. BRINT is robust to noise and does not require tuning of parameters but it is computationally expensive [77]. WLD is based on physiological law, it simulates human like sensing ability of surroundings, while extracting features from an image. It is robust to noise and change in illumination and has better ability of feature representation. However, the calculation of orientation and differential excitation makes it computationally complex [81, 82]. Gabor [72] texture descriptor is more significant among the texture descriptors where uniform patterns are observed in the image data. In medical images, texture holds its energy in narrow bands of frequency and orientation. Gabor filter can encode texture of image into several ways with narrow frequencies and orientations. So, it can be a better choice among texture descriptors for the analysis of brain MR data. Moreover, it can better deal with structural changes, occurring in images due to cancerous cells. Generally, Gabor filter requires five parameters, i.e., (1) *Wavelength* ($\lambda$), (2) *Orientation* ($\theta$), (3) *Phase offset* ($\varphi$), (4) *Sigma* ($\sigma$), and (5) *Gamma* ($\gamma$).

The selection of these parameters is central to this study. Several experiments were performed using online simulation tool [94] to find out most suitable pattern of these parameters. Empirically, the values of $\lambda$, $\varphi$, $\sigma$ and $\gamma$ were tuned to 3.5, 0, 2.8 and 0.3, respectively, where $\theta \in \{0, \frac{\pi}{2}, \frac{\pi}{3}, \frac{\pi}{4}\}$, resulting in four images at these orientations.

Most of the studies related to classification, extract features from the output of texture descriptors (Gabor, Wavelet etc.) and input these annotated features to the classifiers for their learning. If features; extracted directly from source image, are combined with features obtained from the output of texture descriptors, more contributing patterns will be recognized. There will be better pattern identification from the annotated instances. Resultantly, strengthening the

learning model in terms of accuracy. The extraction of texture parameters from the histogram equalized image itself was a decisive factor in the overall performance of the proposed system.

As described above, features can be extracted from the output of texture descriptors using methods such as co-occurrence matrix, run length matrix and difference matrix. Co-occurrence matrix has been employed for this purpose, which has the ability of measuring texture of an image, considering the variations and dimensions of tonal values as repeating patterns [79]. Co-occurrence matrix was applied on the histogram equalized slice as well as on the four images obtained from Gabor texture descriptor.

Statistical parameters are the best representatives of image texture [79, 83]. In medical images, they are capable for delineating the abnormal regions and their surroundings in particular. To utilize the capabilities of these parameters, the proposed system has applied 21 texture parameters as shown in Table 5.3 [43, 79, 83], on the outputs of 5 co-occurrence matrices, hence, yielding total 105 features per slice.

#### 5.3.2.3. Classification of brain abnormalities

Classification refers to assigning an incident to one of the predefined classes. ANN, SVM, Deep learning and its variants, Naïve Bayes frameworks, Decision Trees etc. are among the most popular classifiers used for image classification. They have achieved noteworthy targets in Artificial Intelligence tasks such as object recognition. ANN naturally sorts the experimental knowledge. Systems that are built using ANN can detect all possibilities at the cost of computational complexity. SVM with Cubic kernel is a promising nonlinear and non-parametric classification technique [84], hence has been used as a classifier in this study. In clinical environment, sequence of radiological procedures to determine brain related disorder, is shown in Figure. As shown in Table 5.4, a total of 21224 slices (4059 Normal, 4487 Cerebrovascular diseases, 4057 Degenerative diseases, 4223 Inflammatory diseases and 4398 Neoplastic diseases) were used for training and testing of the proposed system. Out of these, total of 14008 slices (2679 Normal, 2961 Cerebrovascular disease, 2678 Degenerative disease, 2787 Inflammatory disease and 2903 Neoplastic disease) were used for training and a total of 7216 slices (1380 Normal, 1526 Cerebrovascular disease, 1379 Degenerative disease, 1436 Inflammatory disease and 1495 Neoplastic disease) were used for testing of the proposed model.

Table 5.4: No. of slices used for training and testing of the proposed system of brain tumor classification

| **Classification Type** | **Type of Class** | **No. of Training Slices** | **No. of Testing Slices** |
|---|---|---|---|
| Multiclass (Normal and brain general abnormalities group) Classification | Normal | 2679 | 1380 |
| | Cerebrovascular disease | 2961 | 1526 |
| | Degenerative disease | 2678 | 1379 |
| | Inflammatory disease | 2787 | 1436 |
| | Neoplastic disease | 2903 | 1495 |
| Multiclass (Neoplastic tumor types) Classification | Glioma | 581 | 299 |
| | Meningioma | 581 | 299 |
| | Adenocarcinoma | 580 | 299 |
| | Bronchogenic carcinoma | 580 | 299 |
| | Sarcoma | 581 | 299 |
| Two class (Neoplastic and Non-neoplastic) Classification | Neoplastic disease | 2903 | 1495 |
| | Non-neoplastic disease | 11105 | 5721 |
| Two class (Primary and Secondary tumor) Classification | Primary Tumor | 1742 | 898 |
| | Secondary tumor | 1160 | 598 |

## 5.4. Results and discussion

In medical environments, upon observation of suspicious tissues, a radiologist first subjectively decides to classify a slice as normal or abnormal with the help of available sequences and orientations. If slice is abnormal, it becomes obligatory to determine whether slice is neoplastic or non-neoplastic. Because not only tumor, other brain related diseases as shown in Table 5.2, may cause a slice to be abnormal. At this, it becomes important to diagnose, what type of abnormality is present in brain? For instance, if an abnormal slice is a tumorous one, it becomes essential to know whether a slice has a tumor which has originated inside the brain (primary tumor) or a tumor which has traveled towards brain from any other part of the body (secondary tumor). Moreover, this becomes equally mandatory to determine further type of brain tumor as Glioma, Metastatic adenocarcinoma, Metastatic bronchogenic carcinoma, Meningioma, and Sarcoma. Treatment planning is executed strictly after having confirmation about the type of abnormality. The possible sequence of these radiological procedures relating to the assessment of brain related abnormalities is shown in Figure 5.2.

Table 5.5: Dataset, orientation and sequence wise average results obtained through the proposed system of brain tumor classification

| Dataset | Orientation | Sequence | Classification Type | Accuracy (%) | Sensitivity (TPR/Recall/Probability of detection) (%) | Specificity(TNR) (%) | Precision (Positive Predictive Value) (%) | AUC-value |
|---|---|---|---|---|---|---|---|---|
| HMS | Axial | T1 | Five class (Normal, Cerebrovascular, Degenerative, Inflammatory, and Neoplastic) | 96.6 | 94.04 | 99.98 | 99.82 | 0.95 |
| | | T2 | | 96.2 | 94.66 | 99.98 | 97.94 | 0.96 |
| | | MR-GAD | | 98.1 | 98.23 | 99.97 | 99.40 | 0.98 |
| | | PDW | | 96.1 | 91.48 | 99.93 | 94.55 | 0.94 |
| | | T1 | Four class (Cerebrovascular, Degenerative, Inflammatory, and Neoplastic) | 96.3 | 93.43 | 99.98 | 97.28 | 0.96 |
| | | T2 | | 95.6 | 92.83 | 99.98 | 96.83 | 0.95 |
| | | PDW | | 97.1 | 93.60 | 99.97 | 96.77 | 0.95 |

| | | | | | | | | |
|---|---|---|---|---|---|---|---|---|
| | | T1 | Five class Neoplastic (Glioma, Meningioma, Metastatic Adenocarcinoma, Metastatic Bronchogenic carcinoma, and Sarcoma) | 99.7 | 100 | 100 | 100 | 1.00 |
| | | T2 | | 96.3 | 93.08 | 99.96 | 95.76 | 0.96 |
| | | MR-GAD | | 96.8 | 83.66 | 99.68 | 98.02 | 0.90 |
| | | PDW | | 98.2 | 93.55 | 99.98 | 96.08 | 0.96 |
| | | T2 | Two class (Primary Tumor and Secondary Tumor) | 99.6 | 100 | 100 | 100 | 1.00 |
| | | MR-GAD | | 98.6 | 95.75 | 99.95 | 99.25 | 0.96 |
| | | PDW | | 98.6 | 90.9 | 99.4 | 98.2 | 0.90 |
| | | T1 | Two class (Neoplastic and Non-neoplastic) | 97.9 | 97.85 | 99.95 | 98.95 | 0.98 |
| | | T2 | | 96.8 | 96.3 | 99.95 | 99.4 | 0.96 |
| | | MR-GAD | | 96.2 | 93.3 | 99.9 | 97.2 | 0.93 |
| | | PDW | | 96.2 | 98.85 | 99.95 | 99.65 | 0.99 |
| BVHB | | T1 | Five class Neoplastic (Glioma, Meningioma, Metastatic Adenocarcinoma, Metastatic Bronchogenic carcinoma, Sarcoma) | 95.1 | 90.2 | 93.34 | 93.4 | 0.98 |
| | | T2 | | 96.9 | 93.2 | 96.8 | 96.8 | 0.99 |
| | | T1C | | 95.2 | 93.4 | 92.86 | 92 | 0.98 |
| | | PDW | | 96.3 | 92.20 | 95.58 | 95.20 | 0.99 |
| | | FLAIR | | 94.3 | 92 | 91.56 | 90.2 | 0.97 |
| | Coronal | T1 | | 96.1 | 92.20 | 95.94 | 96.00 | 0.99 |
| | | T2 | | 96.8 | 93.20 | 95.12 | 95.40 | 0.99 |
| | | T1C | | 96.2 | 93.80 | 95.06 | 95.00 | 0.98 |
| | | PDW | | 95.4 | 89.80 | 97.28 | 97.00 | 0.98 |
| | | FLAIR | | 92.5 | 87.60 | 91.62 | 90.20 | 0.96 |

| | | | | | | | | |
|---|---|---|---|---|---|---|---|---|
| | Sagittal | T1 | | 94.2 | 86.80 | 93.60 | 93.20 | 0.97 |
| | | T2 | | 94.9 | 91.60 | 93.08 | 92.80 | 0.98 |
| | | T1C | | 96 | 93 | 94.76 | 95.4 | 0.98 |
| | | PDW | | 94.4 | 88.20 | 90.20 | 92.00 | 0.98 |
| | | FLAIR | | 95.1 | 91.20 | 94.04 | 93.40 | 0.99 |
| | Axial | T1 | Two class (Primary Tumor and Secondary Tumor) | 98.6 | 96 | 98.5 | 98.5 | 0.99 |
| | | T2 | | 98.5 | 96.5 | 95.5 | 97 | 0.97 |
| | | T1C | | 97.9 | 97.5 | 98 | 97.5 | 0.98 |
| | | PDW | | 98 | 91.5 | 96.5 | 97 | 0.96 |
| | | FLAIR | | 98.7 | 98.5 | 95 | 96.5 | 0.99 |
| | Coronal | T1 | | 98.8 | 97 | 97.5 | 97.5 | 0.99 |
| | | T2 | | 97.8 | 93.5 | 96 | 97 | 0.99 |
| | | T1C | | 95.8 | 94.5 | 94.5 | 94.5 | 1.00 |
| | | PDW | | 98.5 | 96.5 | 96.5 | 97 | 0.99 |
| | | FLAIR | | 98.7 | 94 | 96 | 99.5 | 0.98 |
| | Sagittal | T1 | | 98.8 | 97.5 | 96 | 97 | 0.99 |
| | | T2 | | 99.2 | 97.5 | 97.5 | 98.5 | 1.00 |
| | | T1C | | 95.8 | 96 | 94.5 | 94 | 0.99 |
| | | PDW | | 99.3 | 98.5 | 99 | 98.5 | 1.00 |
| | | FLAIR | | 97.7 | 93.5 | 95 | 94 | 0.97 |
| | Axial | T1 | Two class (Neoplastic and Non-neoplastic) | 99.2 | 98.5 | 99.5 | 99 | 1.00 |
| | | T2 | | 96.5 | 91 | 95 | 95 | 0.97 |
| | | T1C | | 97.3 | 91 | 96 | 97 | 0.99 |
| | | PDW | | 98.1 | 96.5 | 98 | 98 | 0.98 |

| | | | | | | | | |
|---|---|---|---|---|---|---|---|---|
| | | FLAIR | | 98.3 | 97 | 96.5 | 98.5 | 1.00 |
| | Coronal | T1 | | 99.7 | 99.5 | 98.5 | 99.5 | 1.00 |
| | | T2 | | 97.1 | 93.5 | 95 | 95.5 | 0.98 |
| | | T1C | | 97.1 | 91.5 | 96.5 | 95.5 | 0.99 |
| | | PDW | | 96.9 | 95.5 | 98.5 | 96 | 0.96 |
| | | FLAIR | | 98.7 | 97.5 | 98 | 98.5 | 1.00 |
| | Sagittal | T1 | | 99.2 | 99.5 | 98.5 | 99 | 1.00 |
| | | T2 | | 97.6 | 92.5 | 97.5 | 98 | 0.98 |
| | | T1C | | 96.9 | 90.5 | 96 | 96 | 0.97 |
| | | PDW | | 97.2 | 96.5 | 94.5 | 95.5 | 0.98 |
| | | FLAIR | | 99.2 | 98.5 | 98.5 | 99.5 | 0.99 |
| | Axial | T1 | Five class (Normal, Cerebrovascular diseases, Degenerative diseases, Inflammatory diseases, and Neoplastic diseases) | 97.8 | 96.4 | 96.8 | 97 | 0.99 |
| | | T2 | | 94.8 | 95 | 95.6 | 95.6 | 0.99 |
| | | T1C | | 97 | 97.2 | 97.6 | 97.2 | 0.99 |
| | | PDW | | 93.7 | 93.8 | 94.4 | 93.8 | 0.98 |
| | | FLAIR | | 98.2 | 98.4 | 97.9 | 97.4 | 0.99 |
| | Coronal | T1 | | 98.5 | 97.6 | 97 | 98.2 | 1.00 |
| | | T2 | | 95.2 | 95.6 | 95.8 | 95.8 | 0.99 |
| | | T1C | | 97.1 | 97.2 | 97.3 | 97.2 | 1.00 |
| | | PDW | | 96.9 | 97.4 | 97.8 | 97.6 | 0.99 |
| | | FLAIR | | 98.9 | 98.6 | 98.4 | 99.2 | 1.00 |
| | Sagittal | T1 | | 99.6 | 99.6 | 99.26 | 99.4 | 1.00 |
| | | T2 | | 95.9 | 96.2 | 96 | 96 | 0.99 |
| | | T1C | | 96.4 | 96 | 97.12 | 97.4 | 1.00 |

| | | | | | | | | |
|---|---|---|---|---|---|---|---|---|
| | | PDW | | 96.4 | 96.2 | 95.6 | 96.2 | 0.98 |
| | | FLAIR | | 97.8 | 97.8 | 96.8 | 97 | 0.99 |
| | Axial | T1 | Four class (Cerebrovascular, Degenerative, Inflammatory, and Neoplastic) | 98.8 | 98.25 | 97.5 | 98.75 | 1.00 |
| | | T2 | | 94.2 | 93.5 | 94.75 | 94.75 | 0.98 |
| | | T1C | | 96.3 | 96.5 | 96 | 96.5 | 0.99 |
| | | PDW | | 96 | 96.75 | 96 | 95.5 | 0.99 |
| | | FLAIR | | 97.1 | 95.75 | 97.5 | 97.5 | 0.98 |
| | Coronal | T1 | | 98.8 | 98.5 | 98.25 | 99.25 | 1.00 |
| | | T2 | | 94.6 | 94.5 | 94.75 | 94.75 | 0.98 |
| | | T1C | | 97.2 | 96.75 | 96 | 96.5 | 0.99 |
| | | PDW | | 96.2 | 97.25 | 95.75 | 95.75 | 0.98 |
| | | FLAIR | | 97.5 | 97 | 95.75 | 95.25 | 0.99 |
| | Sagittal | T1 | | 98.7 | 94.25 | 98.25 | 99.25 | 0.95 |
| | | T2 | | 92.9 | 93 | 93.5 | 92.5 | 0.98 |
| | | T1C | | 96.1 | 95.25 | 96.5 | 96.75 | 0.99 |
| | | PDW | | 95.3 | 91.5 | 92.5 | 91 | 0.90 |
| | | FLAIR | | 96.9 | 93.5 | 97.78 | 97.75 | 0.99 |

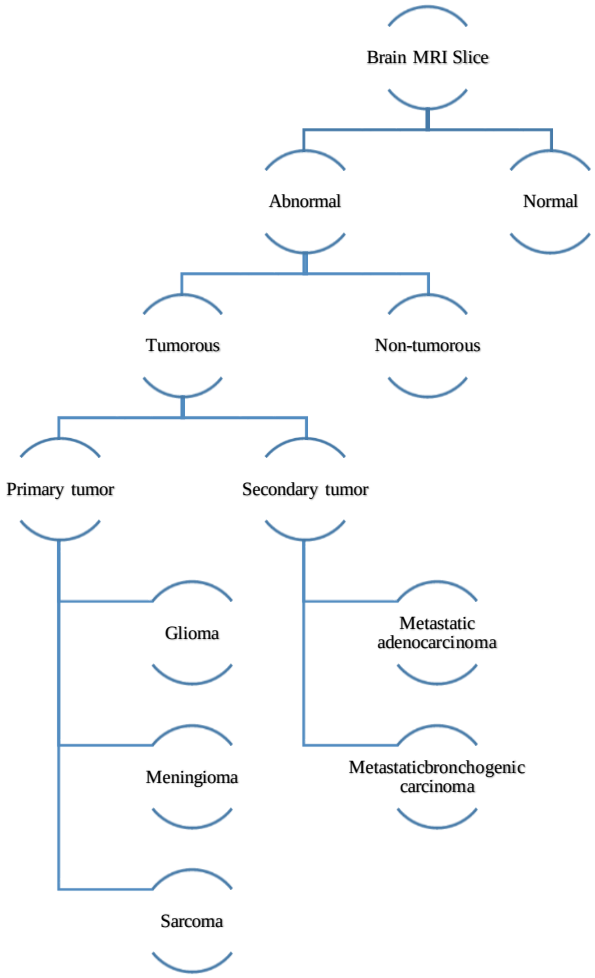


Figure 5.2: Sequence of radiological procedures executed to determine brain abnormalities

Most of the related studies [7, 9, 19, 43, 85-87] have used accuracy, sensitivity, specificity and AUC-value as the standard evaluation measures for the evaluation of their classification algorithms. Therefore, the results obtained through the proposed method have been evaluated against these standard quantitative measures. To prove adequate success of texture parameters shown in Table 5.3 and the proposed framework for classification of brain abnormalities as shown in Table 5.2, the results have been grouped based on datasets, abnormalities, sequences, orientations and the comparison with state-of-the-art. Table 5.5 presents the dataset, orientation and sequence wise results in average as per the standard evaluation parameters. The details of the results as per of these evaluation measures for each of the brain abnormality type has been provided in Appendix-B.

### 5.4.1. Based on datasets

HMS is the commonly used and publicly available benchmarked dataset. In this study, all its normal and abnormal slices having abnormalities shown in Table 5.2, have been used to test whether these texture parameters combined or their subsets are able to classify. Classifications regarding tumor types have also been performed on the complete dataset. It is hence conceded that these texture parameters on each axial sequence belonging to HMS dataset, obtained quite decent rate as per accuracy, sensitivity, specificity and AUC-value as shown in Table 5.5.

To deal with medical traits based on ethnicity, the developed system was also trained and tested on BVHB dataset. This dataset consists of images belonging to normal individuals and patients having abnormalities shown in Table 5.2. Endorsing the suppositions, the results remained remarkable on all axial, coronal, and sagittal orientation on each T1, T1C, T2W, PDW and FLAIR sequence as shown in Table 5.5.

Increasing the number of training examples, has a direct impact on the system's performance. In case of testing against HMS dataset, when a large volume of instances was used to evaluate the learning model, the relative performance was lower as compared to what was achieved against BVHB which has comparatively lesser images. Hence having more variability in training and test data provides a better chance to assess the performance of a classification system, which served as a reason to employ the complete HMS dataset in the study.

### 5.4.2. Based on abnormalities

To test the application of texture parameters, Gabor texture and applicability of SVM for the classification of brain related abnormalities, a large volume of brain slices having abnormalities shown in Table 5.2, have been used. To summarize their application using the proposed method, experimental results have been grouped into the following classes;

- Five class (Normal, Cerebrovascular, Degenerative, Inflammatory and Neoplastic)
- Four class (Cerebrovascular, Degenerative, Inflammatory and Neoplastic)
- Two class (Primary and Secondary tumors)
- Two class (Neoplastic and Non-neoplastic diseases)

- Five class Neoplastic (Meningioma, Glioma, Metastatic adenocarcinoma, Metastatic bronchogenic carcinoma and Sarcoma)

For five and four class brain abnormalities classification, the proposed system achieved remarkable results as shown in Table 5.5. During radiological procedures, identification and classification of metastatic type of abnormality (also known as secondary tumor) from the brain MRI slices is a very tedious task [88]. Therefore, to check the performance of developed system against such type of abnormalities, metastatic adenocarcinoma and metastatic bronchogenic carcinoma slices were used from HMS and BVHB dataset and appreciative results have been achieved as per accuracy, sensitivity, specificity and AUC-value as shown in Table 5.5. With similar aims, when the reported system was trained and tested to classify the brain abnormality as neoplastic and non-neoplastic, again the proposed methodology, obtained promising results as shown in Table 5.5. When slices from both datasets, having neoplastic diseases were used to evaluate the proposed system, the measures remained excellent and up to the mark as shown in Table 5.5.

Overall, for classification against all abnormalities, the system's performance remained reasonable. However, it could be concluded from the experiments that slices having metastatic type of abnormality are relatively harder to classify than other abnormal types, irrespective of the orientation, sequence, and dataset, while brain MRI slices having non-metastatic type of abnormalities are easier to be classified.

### 5.4.3. Based on sequence

Most of the times, radiologists analyze all available sequences to confirm about an abnormality [89]. Therefore, experiments have been performed on all sequences of both HMS and BVHB datasets. Experimental results revealed that T1 sequence for both axial and coronal orientations belonging to HMS and BVHB respectively, remained pioneer in classification as shown in Table 5.5. For HMS dataset, T1 axial slices obtained good classification rates for the classification of Glioma and Sarcoma as shown in Table 5.5, while the same sequence showed its supremacy in the classification of neoplastic and non-neoplastic diseases for BVHB coronal dataset as shown in Table 5.5. T1 sequence with sagittal orientation when used to classify brain general abnormalities, proved its contain-ship of contributing patterns as shown in Table 5.5. T2 axial slices belonging to HMS dataset, using the proposed system achieved significant results for

primary and secondary tumor classification, which are shown in Table 5.5. However, the results obtained from other sequences were also comparable to the discussed results.

It is established from the experiments that T1 axial and coronal and T2 axial sequences have more contributing patterns than others for the classification of Glioma and Sarcoma and primary and secondary tumors respectively. While T1 sagittal, is the best sequence for classifying between brain general disease groups.

### 5.4.4. Based on orientations

Slice sequences play a vital role in radiological decisions. In clinical environment, analyzing different orientation slices of a subject enables a radiologist to detect an abnormality which might not be evident in a single orientation. Therefore, in this study, experiments were conducted to study the impact of slice orientation on the accuracy of classification. There was only axial orientation available in HMS dataset. Experiments established that classification measures for axial orientation, remained notable for T1 slices, when classify neoplastic types i.e. Glioma and Sarcoma tumors, as shown in Table 5.5. Same orientation achieved remarkable outcomes for T2 slices when classify primary and secondary tumors as shown in Table 5.5. However, with the axial orientation for rest of sequences on same dataset, classification rates for other brain abnormalities classes were also acceptable.

To test the robustness of the reported system and to deal with variability of different MRI scanners, axial orientation of BVHB dataset on T2 slices for neoplastic and non-neoplastic quantitative parameters attained were noteworthy as shown in Table 5.5. On coronal orientation of same dataset, classification rate of T1 slices was top of the list for the classification of neoplastic and non-neoplastic diseases as shown in Table 5.5. Similarly, sagittal orientation with T1 sequence outperformed classification for brain general diseases classification as shown in Table 5.5. Although, experiments performed on both HMS and BVHB dataset on each available orientation to classify brain disorders using these texture parameters remained successful. However, performance evaluation analysis of the proposed system against different orientations yields that axial orientation of HMS and coronal of BVHB are slightly better than other orientations as evident from Table 5.5.

It is documented that any orientation alone cannot guarantee better classification as it does not possess all the information related to an abnormality, therefore for achieving better results, combining the outcomes against different orientations will result in a better overall accuracy.

### 5.4.5. Based on state-of-the-art

Most of the researchers working in the same domain have performed their experiments on HMS dataset and using T2W axial slices only. As shown in Table 5.6, in the methods presented by [9], [86], [95] and [96], experiments have been performed on a small subset of HMS dataset, consisting of axial T2W slices only. As per consultation with radiologists and neurosurgeons of BVHB, it is documented that for more accurate and definitive opinion, it is decisive that a subject be analyzed through each sequence and orientation. The training model, trained on limited number of slices of single sequence and orientation could not possess enough variability and multiformity. So, there is hardly any exaggeration in saying that a system trained on datasets having multiformity and variability will not be acceptable in real environment. Therefore, to achieve the goal of performance, robustness and effectiveness of the proposed approach, a large number of experiments have been performed using multiple orientations (axial, coronal and sagittal) and multiple sequences (T1W, T2W, T1C, PDW, MR-GAD and FLAIR) on multi-datasets described in Table 5.1. The efficacy of texture parameters explained in Table 5.3, allied with Gabor texture features and SVM as a classifier has been recognized and proves its superiority.

Table 5.6: Comparison of state-of-the-art methods for brain abnormalities/tumor classification

| **Approach & reported by** | **Dataset** | **Sequence** | **Orientation** | **No. of slices** | **Abnormality wise no. of slices** |
|---|---|---|---|---|---|
| SVM, LDA, KNN [19] | Custom Dataset (MAGNETOM Trio Tim System, Siemens Medical Systems, Erlangen, Germany) | T1 | Axial | 102 | 24-Metastasis<br>4-Meningiomas<br>22-Gliomas WHO grade 2<br>18-Gliomas WHO grade 3<br>34-Glioblastomas |
| | | T2 | Sagittal | | |
| | | T1 | FLAIR | | |

| | | | | | |
|---|---|---|---|---|---|
| DWT + PCA + ANN and k-NN [86] | HMS | T2 | Axial | 70 | 10-Normal<br>60-Abnormal of categories shown in Table 2. |
| DWT + PCA + ANN [95] | HMS | T2 | Axial | 66 | 18-Normal<br>48-Abnormal having diseases glioma, meningioma, Alzheimer, Alzheimer plus visual agnosia, Pick's disease, sarcoma, Huntington's disease |
| RT + PCA + SVM [96] | HMS | T2 | Axial | 66 | 18-Normal<br>48-Abnormal having diseases glioma, meningioma, Alzheimer's disease, Alzheimer's disease plus visual agnosia, Pick's dis-ease, sarcoma and Huntington's disease |
| | HMS | | | 160 | 20-Normal<br>140-Abnormal having diseases glioma, meningioma, Alzheimer's disease, Alzheimer's disease plus visual agnosia, Pick's dis-ease, |

| | | | | | |
|---|---|---|---|---|---|
| | | | | | sarcoma and Huntington's disease |
| | Custom-local dataset | | | 255 | 35-Normal<br>220-Abnormal with 10 slices of each of the following disease glioma, meningioma, Alzheimer's disease, Alzheimer's disease plus visual agnosia, Pick's dis-ease, sarcoma and Huntington's disease, chronic subdural hematoma, cerebral toxoplasmosis, herpes encephalitis and multiple sclerosis |
| DWT + spider web plot + PNN [9] | HMS | T2 | Axial | 75 | 15 slices for each of normal and abnormal categories shown in Table 2. |
| **Proposed Method** | HMS | T1, T1C, T2, MR-GAD | Axial | 1061 | 112-Normal<br>365-Cerebrovascular<br>233-Degenerative<br>207-Inflammatory<br>144-Neoplastic |

| | | | | | |
|---|---|---|---|---|---|
| | BVHB | T1, T1C, T2, FLAIR & PDW | Axial, Sagittal & Coronal | 1000 | 250-Normal<br>170-Cerebrovascular<br>160-Degenerative<br>170-Inflammatory<br>250-Neoplastic |

The overall performance of the proposed method, manifests that it is robust, efficient, and more definitive as compared to the state-of-the-art methods. The proposed paradigm does not require complex training phase, rather it just calculates Gabor texture parameters. It has already been trained on a large volume of training examples of multi-orientations, multi-sequences belonging to multi-datasets to deal with multiformity and to face variability.

## 5.5. Lesson learned

In this study, an automated method has been proposed, which classifies the brain MRI abnormal slices into one of the defined abnormality groups. Moreover, the reported approach is also able to auto classify the abnormal slices whether the slice is tumorous or non-tumorous. The major achievement of the developed scheme is its auto classification of tumorous slices into the slices having primary tumour or secondary tumour as well as their further types as Glioma, Sarcoma, Meningioma, Bronchogenic carcinoma, and Adenocarcinoma, which could not be possible to determine without biopsy, otherwise. The investigated framework has used local histogram equalization for pre-processing and Gabor filter for feature extraction. SVM with cubic kernel model has been used to train the learned model. The suggested technique has been tuned and verified on multi-sequence, and multi-orientation belonging to two datasets, i.e., HMS and locally developed BVHB.

Increasing the number of training examples, has a direct impact on the system's performance. Hence having more variability in training and testing data provides a better chance to assess the performance of a classification system. Slices having metastatic type of abnormalities are relatively harder to be classified as abnormal in comparison to brain MRI slices having non-metastatic type of abnormalities, irrespective of the orientation, sequence, and dataset. The sequence T1 with axial and coronal views and T2 with axial orientation have more contributing

patterns than others for the classification of Glioma and Sarcoma and primary and secondary tumors respectively. While sequence T1 with sagittal orientation, is the best for classifying between brain general disease groups. Conclusively, any orientation alone cannot guarantee better classification as it does not possess all the information related to an abnormality, therefore for achieving better results, combining the outcomes against different orientations results in a better overall accuracy. The overall performance of the proposed method, manifests that it is robust, efficient, and more definitive as compared to the state-of-the-art methods. The proposed paradigm does not require complex training phase.

# Chapter 6

# Validation of Outcomes Across Datasets

In chapter 5, multi class classification for different brain disorders including tumor types was performed. Here in this chapter, to check the robustness of the proposed method, outcomes have been validated across data sets. Summary of this research activity has been presented in section 6.1. Section 6.2 contains introduction of this research activity, section 6.3 has methodology. Results and their discussion has been positioned in section 6.4, while lesson learned has been outlined in section 6.5.

## 6.1. Summary of this research activity

In this research activity, results achieved through the proposed method of brain tumor classification have been validated across data set. The drive of this research activity is to check the robustness of the reported approach. For this purpose, the model has been trained on one data set, while tested on another dataset. A benchmarked dataset HMS and a locally developed dataset BVHB has been used for this purpose. To ensure its robustness, complete HMS dataset was used to train the model and BVHB was used to test the trained model and vice versa. Standard evaluation measures, i.e., accuracy, specificity, sensitivity, precision and AUC-value have been used to evaluate the system. It has been established that the proposed method deals with multiformity and variability of brain MRI data. Overall, suppositions regarding robustness of the proposed method were attained with highest values, i.e., accuracy as 92%, specificity as 92%, sensitivity as 93%, precision as 92% and AUC-value as 0.93.

## 6.2. Introduction of this research activity

Besides developments in the field of computation up to the extent of holography and virtual reality, still luminance values exhibited through medical imaging modalities are interpreted through naked eye by domain experts to determine the presence and level of severity of different abnormalities. Anatomical information is mostly embodied into images using different imaging modalities such as X-Ray, Ultrasonography, Computed Tomography (CT), Magneto Encephalo Graphy (MEG), Electro Encephalo Graphy (EEG), Positron Emission Tomography (PET), Single-Photon Emission Computed Tomography (SPECT), and MRI. The human body organs such as liver, brain, prostate, kidney, heart, breast or abdominal structures are scanned using these imaging modalities. Medical imaging data is manually analyzed for the evaluation of subjects that enables a clinician to study or to prepare decide/finalize their treatment planning. With this massive volume of anatomical data, manual interpretation has become almost impossible.

Being non-invasive medical examination, MRI is currently the best test for assessment of abnormalities present inside brain. It has more contrast among soft tissues and higher spatial resolution. MRI delivers important information about the shape, size, and localization of brain soft tissues without revealing the subject to high ionizing radiation. Clinically, the images of different MRI sequences are used for diagnosis of abnormalities. These sequences include T1-weighted (T1W), T1 with post contrast (T1C), Gadolinium Contrast Medium (MR GAD), T2-weighted (T2W), Proton Density-weighted (PDW) and Fluid Attenuated Inversion Recovery (FLAIR) as shown in Figure 1.1 with direct views of the body in almost any orientation, i.e., coronal, sagittal and axial as shown in Figure 1.2. These sequences and views enable tissues to be visualized well for their interpretation and analysis by a radiologist. These sequences have equal clinical importance regarding anatomical detailed study, better distinction between solid and cystic structures and evaluation and monitoring of pathological changes etc. T1W sequence images are mostly used for the study of normal anatomy. However, necrotic, and active tumor areas can easily be recognized using this sequence after administration of intravenous contrast. The surrounding areas of a brain tumor usually called edema are more easily distinguishable using T2W sequence images. FLAIR sequence images are mostly used to suppress the intraventricular CSF signals. This sequence is important in studying and separating the edema and CSF regions. PDW is mostly used for the evaluation of Multiple Sclerosis (MS) lesions. These sequences, individually or in combination are used to differentiate any fatty deposit in the tumors. The presence of fat in the lesion determines its benign nature that is a differentiating point between neoplastic and non-neoplastic lesions. It is radiologically documented that variation in age, weather, culture and ethnicity, results in change of medical traits of patients and is the source of variability and multiformity of medical data. Therefore, robust and efficient protocols are always decisive in subject's successful treatment planning. However, if CAD systems trained on one dataset are deployed at remote locations/sites, will not be able to address the issue of variability and multiformity.

In medical healthcare units, diagnosis of brain related disorders, mostly depends upon the texture analysis. CAD systems performing automated analysis of brain cells can be more objective than traditional way of manually interpreting brain slices. Hence, for detection and auto classification of brain abnormalities, texture descriptors along with machine learning methods are the best tool [19]. Fourier transformation, Local Binary Pattern (LBP), Statistical Moments, Binary

Ration Invariant and Noise Tolerant (BRINT), Weber Law Descriptor (WLD), Gray Level Co-occurrence Matrix, Haralick Texture features, Gabor Texture features, Discrete Wavelet Transform (DWT), Scale Invariant Feature Transform (SIFT), etc. are mostly used as feature representation/extraction techniques. Similarly, Support Vector Machine (SVM), K nearest neighbors (KNN), Artificial Neural Networks (ANN), Fuzzy C Mean (FCM), Self-Organising Maps (SOM), Gaussian Mixture Models (GMM), Hybrid techniques, Naïve Bayes framework, Random transform, etc. are the methods mostly used as a classifier. The state-of-the-art methods of machine vision/learning enabled in the development of tools to perform auto classification. In healthcare units, these methods could assist in ease of computation and in reduction of operator's involvement. Resultantly, these methods allied with radiological information are assisting department of radiology and diagnostic images almost at every routine health care institute.

The existing brain MRI slice classification methods, do classify the slices, but accurate, robust and optimized classification of brain slices is still a challenge. Therefore, further research is requisite to investigate more appropriate method of classification that could deal with variability and multiformity present in MRI data. This research activity has been conducted in continuation to our previous work [4], in which, an efficient method to classify brain MRI slices as normal or abnormal was presented. The reported approach exploited texture of brain MRI images using Gabor filter and then Support Vector Machines (SVMs) were used to train a model in supervised fashion. Overall, results were promising in term of accuracy, specificity, sensitivity and AUC-value.

The proposed method when applied for two class classification of brain MRI slices as normal or abnormal, achieved appreciative results as per accuracy, sensitivity, specificity and AUC-value. The measures obtained were accuracy of 97.5%, sensitivity of 99%, specificity of 92% and AUC-value as 0.99 on HMS dataset. The evaluation measures gained on BVHB data were accuracy (96.5%), sensitivity (98%), specificity (92%) and AUC-value (0.97). It was noticed that the standard evaluation measures were slightly lower in case of BVHB than what was gained against HMS dataset. Similarly, when the proposed model utilized texture parameters as shown in Table 5.3 for multi class classification of brain disorders, it acquired evenhanded outcomes. On average, the standard evaluation measures for HMS data set obtained were 97.3% as accuracy, 94.6% as sensitivity, 99.9% as specificity, 98.0 as precision and 0.96 as AUC-value. When BVHB

dataset was used to train and test the learned model, these measures remained 96.96% as accuracy, 94.95% as sensitivity, 96.0% as specificity, 96.3% as precision and 0.98 as AUC-value.

It has been noticed that there is minor difference in these evaluation measures, possibly due to local medical traits, variability and multiformity present in MR data. In both of these experimental segments, identical learned models were trained and tested on individual data sets, therefore, a difference of measures was observed. It became most necessary to inspect whether the learned model if deployed in third world countries will work or not? For this purpose, another research task has been performed, in which model has been trained on one dataset and tested on another dataset and vice versa. This research enthusiasm has been adopted deliberately to mark and verify the robustness of the proposed model of brain tumor detection and classification.

From the analysis of the outcomes, it has been established that the proposed model of brain disorder classification in general and tumor types in specific has enough ability to deal with multiformity and variability present in MRI data due to medical traits of local ethnicity.

## 6.3. Methodology

For these experiments, datasets shown in Table 6.1 have been used for both training and testing purpose. Methodology shown in Figure 6.1 has been executed in order to achieve the target of classification through training the proposed model. However, with the difference that when the model was trained on HMS dataset, it was tested on BVHB dataset and vice versa. Texture features shown in Table 5.3 have been utilized on each of the slice obtained through Gabor filter. The values of $\lambda$, $\varphi$, $\sigma$ and $\gamma$ were tuned to 3.5, 0, 2.8 and 0.3, respectively, where $\theta \in \{0, \frac{\pi}{2}, \frac{\pi}{3}, \frac{\pi}{4}\}$. Gabor filter has been described in Equation 4.1, Equation 4.2 and Equation 4.3 mathematically. For the selection of Gabor parameters, experiments were performed using online simulation tool [94]. No. of brain MRI slices containing brain disorders belonging to both HMS and BVHB dataset, used in this research activity, have been depicted in Table 6.1. A total of 16720 slices belonging to HMS dataset were used to train, while a total of 8712 slices belonging to BVHB dataset were used to test the proposed system. Similarly, when a total of 16911 slices belonging to BVHB dataset were used to train the model, then a total of 8638 slices belonging to HMS dataset were used to test the proposed learned model.

Table 6.1: No. of slices used for training and testing of the proposed system to check robustness

| **Classification Type** | **Type of Class** | **HMS dataset** | | **BVHB dataset** | |
|---|---|---|---|---|---|
| | | **No. of Training Slices** | **No. of Testing Slices** | **No. of Training Slices** | **No. of Testing Slices** |
| Multiclass (Normal and brain general abnormalities group) Classification | Normal | 1200 | 650 | 1340 | 690 |
| | Cerebrovascular disease | 1450 | 750 | 1481 | 763 |
| | Degenerative disease | 1330 | 670 | 1339 | 690 |
| | Inflammatory disease | 1390 | 710 | 1394 | 718 |
| | Neoplastic disease | 1450 | 750 | 1452 | 748 |
| Multiclass (Neoplastic tumor types) Classification | Glioma | 290 | 150 | 291 | 150 |
| | Meningioma | 290 | 150 | 291 | 150 |
| | Adenocarcinoma | 290 | 150 | 290 | 150 |
| | Bronchogenic carcinoma | 290 | 150 | 290 | 150 |
| | Sarcoma | 290 | 150 | 291 | 150 |

| | | | | | |
|---|---|---|---|---|---|
| Two class (Neoplastic and Non-neoplastic) Classification | Neoplastic disease | 1450 | 750 | 1452 | 748 |
| | Non-neoplastic disease | 5550 | 2860 | 5553 | 2861 |
| Two class (Primary and Secondary tumor) Classification | Primary Tumor | 870 | 450 | 871 | 449 |
| | Secondary tumor | 580 | 300 | 580 | 299 |
| Total | | 16720 | 8638 | 16911 | 8712 |

## 6.4. Results and discussions

Since, the drive of this research activity is to check the robustness of the proposed method of brain general abnormalities and tumors classification. So, separately each data set has been first used to train the model, while second one has been used to test the learned model and vice versa. The same standard evaluation measures, i.e., accuracy, sensitivity, specificity, precision and AUC-values have been used to evaluate the learning rates. It is noteworthy to mention here that both of the data sets have following distinctions, so robustness of the proposed model against these aspects could not be verified.

- HMS dataset has axial sequence only, while BVHB dataset has all of the three sequences.
- HMS data set has MR-GAD sequence, while BVHB dataset does not have this sequence.
- BVHB dataset has FLAIR sequence, while HMS dataset does not have this sequence.
- BVHB dataset has T1C sequence, while HMS dataset does not have this sequence.

Due to non-availability of these MRI protocols, the robustness could only be verified against axial orientation with T1W, T2W and PDW sequences belonging to both datasets. Table 6.2 shows the results (in average), when model was trained on the slices belonging to HMS dataset and tested on slices belonging to BVHB dataset. The model has been trained and tested on the following classes for the aim of classification.

- Five class (Normal, Cerebrovascular, Degenerative, Inflammatory and Neoplastic)

- Four class (Cerebrovascular, Degenerative, Inflammatory and Neoplastic)
- Two class (Primary and Secondary tumors)
- Two class (Neoplastic and Non-neoplastic diseases)
- Five class Neoplastic (Meningioma, Glioma, Metastatic adenocarcinoma, Metastatic bronchogenic carcinoma and Sarcoma)

Similarly, Table 6.3 shows the results (in average), when model was completely trained on the slices belonging to BVHB dataset and tested completely on the slices belonging to HMS dataset.

Table 6.2: Evaluation measures obtained when the proposed model has been trained on HMS and tested on BVHB dataset

| **Sequence** | **Classes used for classification** | **Accuracy (%)** | **Sensitivity (%)** | **Specificity (%)** | **Precision (%)** | **AUC-value** |
|---|---|---|---|---|---|---|
| T1W | Normal, Cerebrovascular, Degenerative, Inflammatory and Neoplastic | 89% | 91% | 88% | 90% | .91 |
| | Cerebrovascular, Degenerative, Inflammatory, and Neoplastic | 90% | 91% | 89% | 91% | .92 |
| | Primary and Secondary tumors | 91% | 90% | **92%** | 90% | .92 |
| | Neoplastic and Non-neoplastic diseases | **92%** | 89% | 90% | 91% | .92 |

| | | | | | | |
|---|---|---|---|---|---|---|
| | Meningioma, Glioma, Metastatic adenocarcinoma, Metastatic bronchogenic carcinoma, and Sarcoma | 86% | 87% | 88% | 90% | .89 |
| T2W | Normal, Cerebrovascular, Degenerative, Inflammatory and Neoplastic | 86% | 89% | 87% | 89% | .88 |
| | Cerebrovascular, Degenerative, Inflammatory, and Neoplastic | 89% | 90% | 88% | 90% | .89 |
| | Primary and Secondary tumors | 89% | 84% | 87% | 89% | .88 |
| | Neoplastic and Non-neoplastic diseases | 89% | 86% | 88% | 88% | .89 |
| | Meningioma, Glioma, Metastatic adenocarcinoma, Metastatic bronchogenic | 87% | 86% | 88% | 90% | .89 |

| | | | | | | |
|---|---|---|---|---|---|---|
| | carcinoma, and Sarcoma | | | | | |
| PDW | Normal, Cerebrovascular, Degenerative, Inflammatory and Neoplastic | 90% | **92%** | 89% | 90% | .92 |
| | Cerebrovascular, Degenerative, Inflammatory, and Neoplastic | 91% | **92%** | 89% | 91% | .92 |
| | Primary and Secondary tumors | 91% | 89% | **92%** | 90% | .92 |
| | Neoplastic and Non-neoplastic diseases | **92%** | 90% | 91% | 91% | .92 |
| | Meningioma, Glioma, Metastatic adenocarcinoma, Metastatic bronchogenic carcinoma, and Sarcoma | 89% | 90% | 89% | 91% | .91 |

Table 0.1: Evaluation measures obtained when the proposed model has been trained on BVHB and tested on HMS dataset

| **Sequence** | **Classes used for classification** | **Accuracy (%)** | **Sensitivity (%)** | **Specificity (%)** | **Precision (%)** | **AUC-value** |
|---|---|---|---|---|---|---|
| T1W | Normal, Cerebrovascular, Degenerative, Inflammatory and Neoplastic | 90% | 91% | 89% | 89% | .90 |
| | Cerebrovascular, Degenerative, Inflammatory, and Neoplastic | 89% | 91% | 90% | **92%** | .91 |
| | Primary and Secondary tumors | 91% | 91% | **93%** | 91% | .92 |
| | Neoplastic and Non-neoplastic diseases | 92% | 90% | 89% | 90% | .91 |
| | Meningioma, Glioma, Metastatic adenocarcinoma, Metastatic bronchogenic carcinoma, and Sarcoma | 85% | 86% | 89% | 89% | .88 |

| | | | | | | |
|---|---|---|---|---|---|---|
| T2W | Normal, Cerebrovascular, Degenerative, Inflammatory and Neoplastic | 85% | 89% | 86% | 88% | .87 |
| | Cerebrovascular, Degenerative, Inflammatory, and Neoplastic | 89% | 91% | 89% | 87% | .88 |
| | Primary and Secondary tumors | 88% | 85% | 88% | 88% | .88 |
| | Neoplastic and Non-neoplastic diseases | 89% | 88% | 87% | 88% | .89 |
| | Meningioma, Glioma, Metastatic adenocarcinoma, Metastatic bronchogenic carcinoma, and Sarcoma | 86% | 85% | 88% | 90% | .88 |
| PDW | Normal, Cerebrovascular, Degenerative, | 91% | 91% | 90% | **92%** | .92 |

| | | | | | | |
|---|---|---|---|---|---|---|
| | Inflammatory and Neoplastic | | | | | |
| | Cerebrovascular, Degenerative, Inflammatory, and Neoplastic | 90% | **92%** | 89% | 91% | .91 |
| | Primary and Secondary tumors | 91% | 89% | **93%** | 90% | .92 |
| | Neoplastic and Non-neoplastic diseases | **93%** | 89% | 92% | 91% | **.93** |
| | Meningioma, Glioma, Metastatic adenocarcinoma, Metastatic bronchogenic carcinoma, and Sarcoma | 91% | 89% | 90% | 91% | .92 |

To prove adequate success of the proposed method against robustness, discussions have been grouped based on datasets, sequences and abnormalities.

### 6.4.1. Based on datasets

When the proposed model was trained on HMS dataset and tested on BVHB dataset, the average classification rates as per accuracy, sensitivity, specificity, precision and AUC-value remained 89%, 89%, 89%, 90% and 91% respectively as shown in Table 6.2. Similarly, when the model was trained using BVHB dataset and tested on HMS dataset, the classification measures achieved in average were 89%, 89%, 89%, 90% and 90% as per evaluation measures respectively

as shown in Table 6.3**.** Regardless of sequence and abnormality, evaluation measures are slightly greater when trained on BVHB and tested on HMS dataset. The maximum measures are 93%, 92%, 93%, 92% and 0.93 respectively.

It could be established from the experiments and their outcomes that model trained on one dataset and tested on other dataset, endorsing the suppositions, does not have significant difference. Further, in continuation of the previous experiments, it could further be resulted that there is certainly some difference in medical traits. Due to which, evaluation measures are not so high, as these were up to the mark in case of normal or abnormal, brain disorders and tumor type classification. When a model was trained and tested on the same dataset, it yielded remarkable measures. On the other hands, when it was trained and tested on completely different ones, the evaluation measures remained round 90%, possibly due to difference in medical traits, variability and multiformity present in MRI data.

### 6.4.2. Based on sequences

The proposed method when trained and tested on completely different datasets, experiments and their results, yielded that T2W is the sequence that has minimum contribution patterns for the auto classification. On the other hands, in both of the cases, PDW is the sequence that has comparatively more contributing patterns, which could play its role for auto classification problems. As shown in Table 6.2 and Table 6.3, classification rates remained higher in case of PDW brain MRI slices, as compared to others.

Although, the evaluation measures obtained in case of T1W were slightly lower than what the system has achieved for PDW. However, T1W can also be used as an option with the aim of brain tumor classification as well.

### 6.4.3. Based on abnormalities

In the perspective of brain disorders, it is established from the results and experiments that primary and secondary tumors and neoplastic and non-neoplastic classification could be assured as compared to other brain disorders groups. In both of the cases, classification rates, measured against these two group of classification were high than other ones. Classification rates for all other disorders were close to each other, whether it was four class or five class classification problem.

It can be documented that primary and secondary tumor or neoplastic and non-neoplastic tumors classification could be ensured when model is learned on one dataset and tested on others.

## 6.5. Lesson learned

It has resulted that there is a slight difference in medical traits of both of datasets. PDW, is the sequence containing more contributing patterns, hence can be deployed to train the model with the aims of robustness. It has been documented that primary and secondary tumor or neoplastic and non-neoplastic tumors classification are the classes ensuring robustness when model is trained on one dataset and tested on others.

The overall results achieved through the proposed method, manifests that it is robust and efficient. It has been trained on a large volume of multi-orientations, multi-sequences belonging to multi-datasets to deal with multiformity and to face variability.

# Chapter 7

# Conclusion & Future Work

## 7.1. Conclusion

### 7.1.1. Conclusion of novel method of colorization

The colorization method has been presented to colorize the grey scale MR images to enhance the visual perception, variability, sensitivity and discrimination. The results obtained with the proposed method are excellently refined and clearly unveiling the hidden information that is difficult to observe with naked eye. The proposed colorization method as a colorization protocol has been deployed in the Department of Radiology and Diagnostic Images, BVHB, Pakistan and is being used by Chief Radiologist for decision making, which is a crystal clear and an adequate proof of the successfulness of the reported method.

### 7.1.2. Conclusion of classification methods

An efficient method has been proposed using these multidisciplinary approaches to classify brain MRI slices as normal or abnormal.

Increasing the number of training examples, has a direct impact on the system's performance. Hence having more variability in training and test data provides a better chance to assess the performance of a classification system. Slices having metastatic type of abnormalities are relatively harder to be classified as abnormal in comparison to brain MRI slices having non-metastatic type of abnormalities, irrespective of the orientation, sequence and dataset. PDW slices have more contributing patterns than other sequences. Classification rates are slightly higher against coronal orientation slices as compared to the slices belonging to other orientations. However, any orientation alone cannot guarantee better classification as it does not possess all the information regarding an abnormality.

For normal and abnormal brain MRI slices classification, overall, accuracy, sensitivity, specificity and AUC-value based standard evaluation measures proved adequate success of the proposed methodology.

Regarding multiclass brain disorders, increasing the number of training examples, has a direct impact on the system's performance. Hence having more variability in training and testing data provides a better chance to assess the performance of a classification system. Slices having metastatic type of abnormalities are relatively harder to be classified as abnormal in comparison to brain MRI slices having non-metastatic type of abnormalities, irrespective of the orientation,

sequence, and dataset. T1 axial and coronal and T2 axial sequences have more contributing patterns than others for the classification of Glioma and Sarcoma and primary and secondary tumors respectively. While T1 sagittal, is the best sequence for classifying between brain general disease groups.

The overall performance of the proposed method for multi class classification, manifests that it is an efficient and more definitive as compared to the state-of-the-art methods. The proposed paradigm does not require complex training phase.

It has been established that there is a slight difference in medical traits of both datasets. PDW, is the sequence containing more contributing patterns, hence can be deployed to train the model with the aim of robustness. It has been documented that primary and secondary tumor or neoplastic and non-neoplastic tumors classification are the classes ensuring robustness when model is trained on one dataset and tested on another.

The overall results achieved through the proposed method, manifests that it is robust, efficient, definitive, and reliable. It has been trained on a large volume of multi-orientations, multi-sequences belonging to multi-datasets to deal with multiformity and to face variability, variability and multiformity.

## 7.2. Future work

### 7.2.1. Future work of colorization method

As a future work, the colour rendering technologies can be developed that generate/assign true colours to acquired images through other medical imaging modalities including CT, X-Ray, Ultrasound, OCT, etc. For this purpose, computer can guide itself by self-recognition of anatomical region and organs being studied. Initially, it is suggested that acquired organ's image colours will be assigned and standardized as follows by software tools;

a. The main texture of a particular organ could be assigned its original colour e.g. reddish brown colour for liver, light-pink colour for lungs and so on.

b. The arteries could be painted red (recognize through speed of blood flow).

c. The veins could be painted blue (recognize through speed of blood flow).

d. Bile could be painted green (recognize through its location).

e. CSF, Urine in Urine Bile (UB) and other body fluids be painted lemon-yellow.

The colorization of the brain tissues in their natural color will be achieved when the MRI scanners would be so powerful to pick up the intensities at sub-molecular level.

### 7.2.2. Future work of classification method

The proposed method of classification (with few modifications) can also be employed to classify the normal and abnormal slices obtained through other medical imaging modalities such as CT, X-Ray, Ultrasound, OCT, etc. embodying brain or other anatomies. Still there are several open challenges related to auto classification, allied with brain MRI images that needs to be addressed such as; (1) the grading of malignant slices, as suggested by the World Health Organization (WHO) (2) localization of tumor within brain (3) volume calculation of the tumor compartments.

In future, one or more of these mentioned problems will be addressed with improved accuracy and less computational cost. Still there is enough space for investigators to replace surgical biopsy procedures in determining grade (I-IV), stage (initial-last) or level of aggressiveness or severity of a brain tumour. These developed protocols can be integrated into the existing state-of-the-art image retrieval and communication systems.

# Chapter 8

# References

[1] K. Ganesan, U. Acharya, C. K. Chua, L. C. Min, K. T. Abraham, and K. B. Ng, "Computer-aided breast cancer detection using mammograms: a review," *IEEE Reviews in Biomedical Engineering*, vol. 6, pp. 77-98, 2013.

[2] M. A. Balafar, A. R. Ramli, M. I. Saripan, and S. Mashohor, "Review of brain MRI image segmentation methods," *Artificial Intelligence Review*, vol. 33, pp. 261-274, 2010.

[3] G. Gilanie, U. I. Bajwa, M. M. Waraich, and Z. Habib, "Computer aided diagnosis of brain abnormalities using texture analysis of MRI images," *International Journal of Imaging Systems and Technology*, pp. 1-12, 2019.

[4] G. Gilanie, U. I. Bajwa, M. M. Waraich, Z. Habib, H. Ullah, and M. Nasir, "Classification of normal and abnormal brain MRI slices using Gabor texture and support vector machines," *Signal, Image and Video Processing*, vol. 12, pp. 479-487, 2018.

[5] J. Liu, M. Li, J. Wang, F. Wu, T. Liu, and Y. Pan, "A survey of MRI-based brain tumor segmentation methods," *Tsinghua Science and Technology*, vol. 19, pp. 578-595, 2014.

[6] B. H. Menze, A. Jakab, S. Bauer, J. Kalpathy-Cramer, K. Farahani, J. Kirby, *et al.*, "The multimodal brain tumor image segmentation benchmark (BRATS)," *IEEE transactions on medical imaging*, vol. 34, p. 1993, 2015.

[7] E.-S. A. El-Dahshan, H. M. Mohsen, K. Revett, and A.-B. M. Salem, "Computer-aided diagnosis of human brain tumor through MRI: A survey and a new algorithm," *Expert Systems with Applications*, vol. 41, pp. 5526-5545, 2014.

[8] P. Szwarc, J. Kawa, M. Rudzki, and E. Pietka, "Automatic brain tumour detection and neovasculature assessment with multiseries MRI analysis," *Computerized Medical Imaging and Graphics*, 2015.

[9] M. Saritha, K. P. Joseph, and A. T. Mathew, "Classification of MRI brain images using combined wavelet entropy based spider web plots and probabilistic neural network," *Pattern Recognition Letters*, vol. 34, pp. 2151-2156, 2013.

[10] A. Mayer and H. Greenspan, "An adaptive mean-shift framework for MRI brain segmentation," *IEEE Transactions on Medical Imaging*, vol. 28, pp. 1238-1250, 2009.

[11] K. Van Leemput, F. Maes, D. Vandermeulen, and P. Suetens, "Automated model-based tissue classification of MR images of the brain," *IEEE Transactions on Medical Imaging*, vol. 18, pp. 897-908, 1999.

[12] S. Ruan, C. Jaggi, J. Xue, J. Fadili, and D. Bloyet, "Brain tissue classification of magnetic resonance images using partial volume modeling," *IEEE Transactions on Medical Imaging*, vol. 19, pp. 1179-1187, 2000.

[13] K. H. Oh, S. H. Kim, and M. Lee, "Tumor detection on brain MR images using regional features: Method and preliminary results," in *Frontiers of Computer Vision (FCV), 2015 21st Korea-Japan Joint Workshop on*, 2015, pp. 1-4.

[14] M. Havaei, A. Davy, D. Warde-Farley, A. Biard, A. Courville, Y. Bengio, *et al.*, "Brain tumor segmentation with deep neural networks," *Medical image analysis*, vol. 35, pp. 18-31, 2017.

[15] S. Abbasi and F. Tajeripour, "Detection of brain tumor in 3D MRI images using local binary patterns and histogram orientation gradient," *Neurocomputing*, vol. 219, pp. 526-535, 2017.

[16] M. Sezgin, "Survey over image thresholding techniques and quantitative performance evaluation," *Journal of Electronic imaging*, vol. 13, pp. 146-168, 2004.

[17] J. J. Corso, E. Sharon, S. Dube, S. El-Saden, U. Sinha, and A. Yuille, "Efficient multilevel brain tumor segmentation with integrated bayesian model classification," *IEEE Transactions on Medical Imaging*, vol. 27, pp. 629-640, 2008.

[18] I. Njeh, L. Sallemi, I. B. Ayed, K. Chtourou, S. Lehericy, D. Galanaud, *et al.*, "3D multimodal MRI brain glioma tumor and edema segmentation: A graph cut distribution matching approach," *Computerized Medical Imaging and Graphics*, vol. 40, pp. 108-119, 2015.

[19] E. I. Zacharaki, S. Wang, S. Chawla, D. Soo Yoo, R. Wolf, E. R. Melhem, *et al.*, "Classification of brain tumor type and grade using MRI texture and shape in a machine learning scheme," *Magnetic Resonance in Medicine*, vol. 62, pp. 1609-1618, 2009.

[20] J. Tohka, A. Zijdenbos, and A. Evans, "Fast and robust parameter estimation for statistical partial volume models in brain MRI," *Neuroimage*, vol. 23, pp. 84-97, 2004.

[21] W. Speier, J. E. Iglesias, L. El-Kara, Z. Tu, and C. Arnold, "Robust skull stripping of clinical glioblastoma multiforme data," in *International Conference on Medical Image Computing and Computer-Assisted Intervention*, 2011, pp. 659-666.

[22] S. Roy, S. Nag, I. K. Maitra, and S. K. Bandyopadhyay, "A review on automated brain tumor detection and segmentation from MRI of brain," *arXiv preprint arXiv:1312.6150*, 2013.

[23] K. Usman and K. Rajpoot, "Brain tumor classification from multi-modality MRI using wavelets and machine learning," *Pattern Analysis and Applications*, pp. 1-11, 2017.

[24] V. Anitha and S. Murugavalli, "Brain tumour classification using two-tier classifier with adaptive segmentation technique," *IET Computer Vision*, vol. 10, pp. 9-17, 2016.

[25] C.-C. Chang and C.-J. Lin, "LIBSVM: a library for support vector machines," *ACM Transactions on Intelligent Systems and Technology (TIST)*, vol. 2, p. 27, 2011.

[26] D. Shen, G. Wu, D. Zhang, K. Suzuki, F. Wang, and P. Yan, "Machine learning in medical imaging," *Computerized medical imaging and graphics: the official journal of the Computerized Medical Imaging Society*, vol. 41, pp. 1-2, 2015.

[27] A. Kharrat, N. Benamrane, M. Ben Messaoud, and M. Abid, "Detection of brain tumor in medical images," in *Signals, Circuits and Systems (SCS), 2009 3rd International Conference on*, 2009, pp. 1-6.

[28] K. Asghar, G. Gilanie, M. Saddique, and Z. Habib, "Automatic Enhancement Of Digital Images Using Cubic Bézier Curve And Fourier Transformation," *Malaysian Journal of Computer Science*, vol. 30, pp. 300-310, 2017.

[29] C. A. Cocosco, A. P. Zijdenbos, and A. C. Evans, "A fully automatic and robust brain MRI tissue classification method," *Medical image analysis*, vol. 7, pp. 513-527, 2003.

[30] M. N. Ahmed, S. M. Yamany, N. Mohamed, A. Farag, and T. Moriarty, "A modified fuzzy c-means algorithm for bias field estimation and segmentation of MRI data," *IEEE Transactions on Medical Imaging*, vol. 21, pp. 193-199, 2002.

[31] J. Sachdeva, V. Kumar, I. Gupta, N. Khandelwal, and C. K. Ahuja, "Multiclass brain tumor classification using GA-SVM," in *Developments in E-systems Engineering (DeSE), 2011*, 2011, pp. 182-187.

[32] A. Padma and R. Sukanesh, "SVM based classification of soft tissues in brain CT images using wavelet based dominant gray level run length texture features," *middle-east journal of scientific research*, vol. 13, pp. 883-888, 2013.

[33] T. Logeswari and M. Karnan, "An improved implementation of brain tumor detection using segmentation based on soft computing," *Journal of Cancer Research and Experimental Oncology,* vol. 2, pp. 006-014, 2010.

[34] D. A. Dahab, S. S. Ghoniemy, and G. M. Selim, "Automated Brain Tumor Detection and Identification Using Image Processing and Probabilistic Neural Network Techniques," *International journal of image processing and visual communication,* vol. 1, pp. 1-8, 2012.

[35] G. L. Qurat-Ul-Ain, S. B. Kazmi, M. A. Jaffar, and A. M. Mirza, "Classification and segmentation of brain tumor using texture analysis," *Recent Advances In Artificial Intelligence, Knowledge Engineering And Data Bases,* pp. 147-155, 2010.

[36] S. Klöppel, C. M. Stonnington, C. Chu, B. Draganski, R. I. Scahill, J. D. Rohrer, *et al.*, "Automatic classification of MR scans in Alzheimer's disease," *Brain,* vol. 131, pp. 681-689, 2008.

[37] B. Arunadevi and S. N. Deepa, "Brain tumor tissue categorization in 3D magnetic resonance images using improved PSO for extreme learning machine," *Progress in Electromagnetics Research B,* vol. 49, pp. 31-54, 2013.

[38] I. Basheer and M. Hajmeer, "Artificial neural networks: fundamentals, computing, design, and application," *Journal of microbiological methods,* vol. 43, pp. 3-31, 2000.

[39] H. Khotanlou, O. Colliot, J. Atif, and I. Bloch, "3D brain tumor segmentation in MRI using fuzzy classification, symmetry analysis and spatially constrained deformable models," *Fuzzy Sets and Systems,* vol. 160, pp. 1457-1473, 2009.

[40] M. U. Akram and A. Usman, "Computer aided system for brain tumor detection and segmentation," in *International Conference on Computer Networks and Information Technology*, 2011, pp. 299-302.

[41] M. Attique, G. Gilanie, M. S. Mehmood, M. S. Naweed, M. Ikram, J. A. Kamran, *et al.*, "Colorization and automated segmentation of human T2 MR brain images for characterization of soft tissues," *PloS one,* vol. 7, p. e33616, 2012.

[42] M. Kanimozhi and C. H. Bindu, "Brain MR image segmentation using self organizing map," *Brain,* vol. 2, 2013.

[43] J. Sachdeva, V. Kumar, I. Gupta, N. Khandelwal, and C. K. Ahuja, "Segmentation, feature extraction, and multiclass brain tumor classification," *Journal of digital imaging,* vol. 26, pp. 1141-1150, 2013.

[44] G. Gilanie, M. Attique, S. Naweed, E. Ahmed, and M. Ikram, "Object extraction from T2 weighted brain MR image using histogram based gradient calculation," *Pattern Recognition Letters,* vol. 34, pp. 1356-1363, 2013.

[45] S. Wang, Z. Geng, J. Zhang, Y. Chen, and J. Wang, "A fuzzy C-means model based on the spatial structural information for brain MRI segmentation," *International Journal of Signal Processing, Image Processing and Pattern Recognition,* vol. 7, pp. 313-322, 2014.

[46] P. Szwarc, J. Kawa, M. Rudzki, and E. Pietka, "Automatic brain tumour detection and neovasculature assessment with multiseries MRI analysis," *Computerized Medical Imaging and Graphics,* vol. 46, pp. 178-190, 2015.

[47] D. Sångberg, "Automated Glioma Segmentation in MRI using Deep Convolutional Networks," ed, 2015.

[48] S. B. Gaikwad and M. S. Joshi, "Brain Tumor Classification using Principal Component Analysis and Probabilistic Neural Network," *International Journal of Computer Applications,* vol. 120, 2015.

[49] G. Jothi, "Hybrid Tolerance Rough Set–Firefly based supervised feature selection for MRI brain tumor image classification," *Applied Soft Computing,* vol. 46, pp. 639-651, 2016.

[50] E. Alberts, G. Tetteh, S. Trebeschi, M. Bieth, A. Valentinitsch, B. Wiestler, *et al.*, "Multi-modal Image Classification Using Low-Dimensional Texture Features for Genomic Brain Tumor Recognition," in *Graphs in Biomedical Image Analysis, Computational Anatomy and Imaging Genetics*, ed: Springer, 2017, pp. 201-209.

[51] C. S. Bartheld, J. Bahney, and S. Herculano-Houzel, "The search for true numbers of neurons and glial cells in the human brain: a review of 150 years of cell counting," *Journal of Comparative Neurology*, vol. 524, pp. 3865-3895, 2016.

[52] (2017, 14 Aug 2017). Available: http://www.childrenshospital.org/az/Site570/mainpageS570P0.html

[53] B. Menze, M. Reyes, and K. Van Leemput, "The Multimodal Brain Tumor Image Segmentation Benchmark (BRATS)," 2014.

[54] I. Scholl, T. Aach, T. M. Deserno, and T. Kuhlen, "Challenges of medical image processing," *Computer science-Research and development,* vol. 26, pp. 5-13, 2011.

[55] V. G. Jacob and S. Gupta, "Colorization of grayscale images and videos using a semiautomatic approach," in *Image Processing (ICIP), 2009 16th IEEE International Conference on*, 2009, pp. 1653-1656.

[56] Y. Rathore, A. Dhole, R. Giri, and U. Agrawal, "Colorization of gray scale images using fully automated approach," 2010.

[57] C. Sauvaget, S. Manuel, J.-N. Vittaut, J. Suarez, and V. Boyer, "Segmented images colorization using harmony," in *Signal-Image Technology and Internet-Based Systems (SITIS), 2010 Sixth International Conference on*, 2010, pp. 153-160.

[58] V. Bochko, P. Välisuo, T. M. Alho, S. Sutinen, J. Parkkinen, and J. T. Alander, "Medical image colorization using learning," in *Conference on Colour in Graphics, Imaging, and Vision*, 2010, pp. 70-74.

[59] G. Holland and P. Bottomley, "A colour display technique for NMR imaging," *Journal of physics E: Scientific instruments,* vol. 10, p. 714, 1977.

[60] M. Documentation. (2016, 15 January). *MatLab Documentation.* Available: http://www.mathworks.com/access/helpdesk/help/techdoc/matlab.shtml.

[61] K. L. Weiss, Q. Dong, W. J. Weadock, R. C. Welsh, and G. V. Shah, "Multiparametric Color-encoded Brain MR Imaging in Talairach Space 1," *Radiographics,* vol. 22, pp. e3-e3, 2002.

[62] K. Weiss, S. Stiving, E. Herderick, J. Cornhill, and D. Chakeres, "Hybrid color MR imaging display," *American Journal of Roentgenology,* vol. 149, pp. 825-829, 1987.

[63] M. d. C. V. Hernández, K. J. Ferguson, F. M. Chappell, and J. M. Wardlaw, "New multispectral MRI data fusion technique for white matter lesion segmentation: method and comparison with thresholding in FLAIR images," *European radiology,* vol. 20, pp. 1684-1691, 2010.

[64] A. Popowicz and B. Smolka, "Overview of Grayscale Image Colorization Techniques," in *Color Image and Video Enhancement*, ed: Springer, 2015, pp. 345-370.

[65] T. Tan, K. Sim, C. Tan, and A. Chong, "CT Image Enhancement by Colorization for Brain Infarct Detection," ed: Citeseer, 2008.

[66] A. A. Shah, G. Mikita, and K. M. Shah, "Medical image colorization using optimization technique," 2013.

[67] H. Ajmal and M. Waraich, "Ultrasound of the Eye and Orbit," *Canadian Journal on Medicine,* vol. 2, 2011.

[68] L. Palm Dzung, X. Chenyang, and L. Prince Jerry, "A survey of current methods in medical image segmentation," 1998.

[69] S. Wang, Z. Geng, J. Zhang, Y. Chen, and J. Wang, "A Fuzzy C-means Model Based on the Spatial Structural Information for Brain MRI Segmentation," *International Journal of Signal Processing, Image Processing and Pattern Recognition,* vol. 7, p. 313, 2014.

[70] H. M. School. (2016, 23 May 2016). *Harvard Medical School.* Available: (http://med.harvard.edu/AANLIB/)

[71] I. Fogel and D. Sagi, "Gabor filters as texture discriminator," *Biological cybernetics,* vol. 61, pp. 103-113, 1989.

[72] T. S. Lee, "Image representation using 2D Gabor wavelets," *IEEE Transactions on Pattern Analysis and Machine Intelligence,* vol. 18, pp. 959-971, 1996.

[73] G. K. Wallace, "The JPEG still picture compression standard," *IEEE Transactions on Consumer Electronics,* vol. 38, pp. xviii-xxxiv, 1992.

[74] K. Ito and K. Xiong, "Gaussian filters for nonlinear filtering problems," *IEEE Transactions on Automatic Control,* vol. 45, pp. 910-927, 2000.

[75] H. Zhu, F. H. Chan, and F. K. Lam, "Image contrast enhancement by constrained local histogram equalization," *Computer vision and image understanding,* vol. 73, pp. 281-290, 1999.

[76] C. S. Rao and S. T. Babu, "Image Authentication Using Local Binary Pattern on the Low Frequency Components," in *Microelectronics, Electromagnetics and Telecommunications*, ed: Springer, 2016, pp. 529-537.

[77] L. Liu, Y. Long, P. W. Fieguth, S. Lao, and G. Zhao, "BRINT: Binary rotation invariant and noise tolerant texture classification," *IEEE Transactions on Image Processing,* vol. 23, pp. 3071-3084, 2014.

[78] J. Chen, S. Shan, C. He, G. Zhao, M. Pietikäinen, X. Chen, *et al.*, "WLD: A robust local image descriptor," *Pattern Analysis and Machine Intelligence, IEEE Transactions on,* vol. 32, pp. 1705-1720, 2010.

[79] R. M. Haralick, K. Shanmugam, and I. H. Dinstein, "Textural features for image classification," *IEEE Transactions on Systems, Man and Cybernetics,* pp. 610-621, 1973.

[80] Y. Zhao, W. Jia, R.-X. Hu, and H. Min, "Completed robust local binary pattern for texture classification," *Neurocomputing*, vol. 106, pp. 68-76, 2013.

[81] J. Chen, S. Shan, C. He, G. Zhao, M. Pietikainen, X. Chen, *et al.*, "WLD: A robust local image descriptor," *IEEE transactions on pattern analysis and machine intelligence*, vol. 32, pp. 1705-1720, 2010.

[82] H. Dawood, H. Dawood, and P. Guo, "Texture Image Classification with Improved Weber Local Descriptor," in *International Conference on Artificial Intelligence and Soft Computing*, 2014, pp. 684-692.

[83] R. C. Gonzalez, R. E. Woods, and S. L. Eddins, *Digital Image Processing Using MATLAB®*: McGraw Hill Education, 2010.

[84] M. A. Hearst, S. T. Dumais, E. Osman, J. Platt, and B. Scholkopf, "Support vector machines," *IEEE Intelligent Systems and their Applications*, vol. 13, pp. 18-28, 1998.

[85] J. Barker, A. Hoogi, A. Depeursinge, and D. L. Rubin, "Automated classification of brain tumor type in whole-slide digital pathology images using local representative tiles," *Medical image analysis*, vol. 30, pp. 60-71, 2016.

[86] E.-S. A. El-Dahshan, T. Hosny, and A.-B. M. Salem, "Hybrid intelligent techniques for MRI brain images classification," *Digital Signal Processing*, vol. 20, pp. 433-441, 2010.

[87] F. G. Zöllner, K. E. Emblem, and L. R. Schad, "SVM-based glioma grading: optimization by feature reduction analysis," *Zeitschrift für medizinische Physik*, vol. 22, pp. 205-214, 2012.

[88] H. Ohgaki and P. Kleihues, "The definition of primary and secondary glioblastoma," *Clinical cancer research*, vol. 19, pp. 764-772, 2013.

[89] E. H. Herskovits, R. Itoh, and E. R. Melhem, "Accuracy for detection of simulated lesions: comparison of fluid-attenuated inversion-recovery, proton density-weighted, and T2-weighted synthetic brain MR imaging," *American Journal of Roentgenology*, vol. 176, pp. 1313-1318, 2001.

[90] G. Gilanie, H. Ullah, M. Mahmood, U. I. Bajwa, and Z. Habib, "Colored Representation of Brain Gray Scale MRI Images to potentially underscore the variability and sensitivity of images," *Current Medical Imaging Reviews*, vol. 14, pp. 555-560, 2018.

[91] G. Jothi, "Hybrid Tolerance Rough Set–Firefly based supervised feature selection for MRI brain tumor image classification," *Applied Soft Computing*, 2016.

[92] L.-K. Soh and C. Tsatsoulis, "Texture analysis of SAR sea ice imagery using gray level co-occurrence matrices," *IEEE Transactions on geoscience and remote sensing,* vol. 37, pp. 780-795, 1999.

[93] D. A. Clausi, "An analysis of co-occurrence texture statistics as a function of grey level quantization," *Canadian Journal of remote sensing,* vol. 28, pp. 45-62, 2002.

[94] N. Petkov and M. B. Wieling. (2017, 03 February 2017). *Gabor filter for image processing and computer vision*. Available: http://matlabserver.cs.rug.nl/

[95] Y. Zhang, Z. Dong, L. Wu, and S. Wang, "A hybrid method for MRI brain image classification," *Expert Systems with Applications,* vol. 38, pp. 10049-10053, 2011.

[96] S. Das, M. Chowdhury, and M. K. Kundu, "Brain MR image classification using multiscale geometric analysis of ripplet," *Progress In Electromagnetics Research,* vol. 137, pp. 1-17, 2013.

[97] T. Logeswari and M. Karnan, "An enhanced implementation of brain tumor detection using segmentation based on soft computing," in *Signal Acquisition and Processing, 2010. ICSAP'10. International Conference on*, 2010, pp. 243-247.

[98] E. Geremia, O. Clatz, B. H. Menze, E. Konukoglu, A. Criminisi, and N. Ayache, "Spatial decision forests for MS lesion segmentation in multi-channel magnetic resonance images," *NeuroImage,* vol. 57, pp. 378-390, 2011.

[99] M. A. Mahjoub, "Image segmentation by adaptive distance based on EM algorithm," *arXiv preprint arXiv:1204.1629,* 2012.

[100] A. Hamamci and G. Unal, "Multimodal brain tumor segmentation using the tumor-cut method on the BraTS dataset," *Proc. MICCAI-BRATS,* pp. 19-23, 2012.

# Appendix-A: State-of-the-art (2008~2018)

| Serial No | Reference | Problem addressed | Methodology | Dataset used | Evaluation Measures | Limitations |
|---|---|---|---|---|---|---|
| 1. | [17] | Brain Tumor Segmentation | Integrated Bayesian Model | Custom Datasets (Henry E. Singleton Brain Cancer Research Program, University of California, Los Angeles, CA 90095 USA) | JC=.88<br>Precision=.96<br>Recall=.92 | Only segmentation of brain tumor is performed. |
| 2. | [10] | Brain Tumor Segmentation | Mean-Shift Clustering | BrainWeb<br>IBSR<br>And<br>Custom Dataset (Multiple Sclerosis unit of Sheba Medical Center in Tel-Hashomer, Israel) | DSC<br>(GM=.96<br>WM=.97) | No classification performed, simulated dataset used, robustness issue |
| 3. | [39] | Brain Tumor Segmentation | Fuzzy Classification, Symmetry Plane Analysis And Spatially Constrained Deformable Models | Custom Dataset (Lariboisière Hospital, Paris, France and Salpétrière Hospital, Paris, France) | TP=.93<br>FP =7.58<br>Similarity Index (SI)=93<br>Hausdorff distance (HD)=4.39 | No classification and grade of tumor has been addressed |

| | | | | | | |
|---|---|---|---|---|---|---|
| | | | | And<br>ISBR | | |
| 4. | [19] | Classification of Brain Tumor<br>Primary Glioma from Metastasis<br>Grading of Gliomas | SVM, LDA, KNN | Custom Dataset (MAGNETOM Trio Tim System, Siemens Medical Systems, Erlangen, Germany) | Accuracy<br>SVM=91.2%<br>KNN(k=3) =89.8%<br>LDA=85.5% | Accuracy not 100% |
| 5. | [35] | Segmentation and Classification of Brain Tumor | Texture Features (Co-occurrence) and SVM | Custom (Holy Family Hospital, Rawalpindi)<br>And<br>Harvard Medical School | Accuracy=99% | Two class classification (Benign and Malignant) |
| 6. | [97] | Brain Tumor Detection | Fuzzy C-Means clustering algorithm and Hierarchical Self Organizing Map (HSOM) | Custom Dataset (KMC Hospital in Coimbatore, India) | N/A | No classification problem is addressed. |
| 7. | [98] | MS lesion segmentation | Random Decision Forest Framework | MICCAI Grand Challenge 2008 dataset | Accuracy=82.13 | Only MS lesion segmentation problem is addressed. |
| 8. | [40] | Computer Aided Brain Tumor | Global Thresholding | Custom Dataset | Accuracy=97.00% | Only detection |

| | | | | | | |
|---|---|---|---|---|---|---|
| | | Detection and Segmentation | | | | and segmentation problem of brain tumor is addressed. |
| 9. | [99] | Image Segmentation | Gaussian Mixture Expectation Maximizer (EM) Algorithm | Custom Dataset | N/A | No classification problem is addressed |
| 10. | [34] | Automated Brain Tumor Detection and Identification | *modified* Probabilistic Neural Network (PNN) model based on learning vector quantization (LVQ) | Custom Dataset | Accuracy=100% | No classification is addressed. |
| 11. | [41] | Segmentation of Brain Primary Components | Clustering Algorithm with Prior Anatomical knowledge for seed selection from histogram | Custom Dataset (Bahawal Victoria Hospital, Bahawalpur, Pakistan) and BrainWeb | JC (GM=0.029) (WM=0.026) (CSF=0.052) | No classification of brain tumor problem addressed |
| 12. | [100] | Brain Tumor Segmentation | Tumor-cut Method | BraTS 2012 | Dice Overlap (0.36±0.25 for edema | No classification problem is addressed |

| | | | | | | |
|---|---|---|---|---|---|---|
| | | | | | 0.69±0.20 for tumor)<br>JC<br>(0.25±0.20 for edema<br>0.56±0.23 for tumor) | |
| 13. | [9] | Normal and Abnormal Slices Classification | DWT+Spider web plots+PNN | Harvard Medical School | Accuracy=100% | Dataset small (75 images only and only T2w) robustness issue |
| 14. | [42] | Brain Segmentation from MR Images | Wavelet Transformation, Unsupervised Self-Organizing Map | IBSR | Quantization error=.63<br>Topological error=0.15 | Only segmentation not classification |
| 15. | [37] | Brain tumor tissue categorization | GLCM+RLM custom Genetic Algorithm + PSO + ELM | Custom Dataset (PSG IMSR & Hospitals) with T1 processed in 1.5 Tesla Siemens Machine | Sensitivity=95.9%<br>Specificity=98.88%<br>Accuracy w/o feature selection=94.88%<br>Accuracy with feature selection=98.05% | Diagnosed of glioma, meningioma and metastasis, of T1 contrast images only |

| | | | | | | |
|---|---|---|---|---|---|---|
| 16. | [43] | Brain Tumor Classification | PCA+ANN | Custom Dataset (PGIMER) with 3.0 Tesla Siemens Machine | Accuracy=91% | Accuracy and robustness issue |
| 17. | [44] | Brain Primary Regions Segmentation | Multilevel Thresholding by Histogram Filteration | Custom Dataset (Bahawal Victoria Hospital, Pakistan) and BrainWeb | JC (GM=0.002) (WM=0.012) (CSF=0.018) | Only Tumor Detection problem was addressed no classification issues has been fixed |
| 18. | [69] | MR Image Segmentation | Fuzzy C-means Model and Spatial Structural Information | Custom Dataset (McConnell Brain Imaging Center at the Montreal Neurological Institute, McGill University, QC H3A 2B4, Canada | Noise Level (NL)<br>NL Tissue JC<br>3% GM 93.19<br>WM 98.97<br>5% GM 92.03<br>WM 85.4<br>7% GM 89.49<br>WM 80.68 | Only segmentation problem is addressed |
| 19. | [7] | MRI image classification as normal and abnormal | DWT+PCA+NN | Harvard Medical School | Accuracy=99% | Only 101 images were used to train the model. Small data set, only T2 weighted images are |

| | | | | | | |
|---|---|---|---|---|---|---|
| | | | | | | used robustness issue |
| 20. | [13] | Tumor Detection from Brain MR | Regional Features (Mean and Variance) and non-linear SVM with RBF kernel | Custom Dataset (Seoul National University, Korea) | Precision=.96<br>Recall=.92<br>F-Measure=.85 | Only brain tumor detection is presented |
| 21. | [18] | 3D multimodal MRI brain glioma tumor and edema segmentation | Graph Cut Distribution Matching Approach | BraTS2012. | **Mean Dice**<br>Real Cases=.77<br>Simulated Cases=.88 | Only glioma and edema segmentation |
| 22. | [8] | Brain Tumor Detection and Neo-vasculature Assessment from Multi-series MRI | Regional Cerebral Blood Volume (RCBV) perfusion maps. | Custom Data Set (Radiodiagnostics Department of the Maria Sklodowska-Curie Memorial Cancer Centre and Institute of Oncology, Gliwice Branch,Poland) | DSC=.94 | No classification of brain tumor |
| 23. | [24] | Brain tumor segmentation and classification | SOM+KNN | Customized data sets ( Frederick National Laboratory) | Dataset1 Accuracy=85%<br>Dataset 2 Accuracy=96.6% | Only two class classification problem has been |

| | | | | | | |
|---|---|---|---|---|---|---|
| | | | | | Dataset3 Accuracy=94.28% | addressed (normal and abnormal) |
| 24. | [48] | Brain tumor classification | PCA-PNN | Customized data sets (Government hospital of Aurangabad, Sahyadri Hospital of Pune, Maharashtra India) | Accuracy=97.14 to 100% | Local datasets are used and can only diagnose 2 types of tumor. |
| 25. | [49] | Brain tumor image classification | STRSFF-QR | National Cancer Institute, United States | | |
| 26. | [50] | Brain tumor glioblastomas classification | LBP + BRIEF + HOG + AE | The Cancer Imaging Archive (TCIA) database | Accuracy =83% | evaluation measures are not up to mark. |
| 27. | [23] | Classification of brain tumor using multi-modality images | Wavelet ,random forest | MICCAI BraTS | | Quantitative measures are not up to mark |

| | | | | | | |
|---|---|---|---|---|---|---|
| 28. | [4] | Classification of brain MRI slices as normal or abnormal | Gabor texture and SVM | Custom dataset (Bahawal Victoria Hospital, Bahawalpur, Pakistan) and Harvard Medical School | Dataset 1<br>Accuracy =97.5%<br>Sensitivity = 99%<br>specificity =92%<br>Dataset 2<br>Accuracy =96.5%<br>Sensitivity = 98%<br>specificity =92% | Only defines slices as normal or abnormal not types of abnormalities |

# Appendix-B: Results of dataset, orientation, sequence, abnormality type wise experiments performed for multi class classification of brain tumor

Table 1: Five class (Normal, Cerebrovascular diseases, Degenerative diseases, Inflammatory diseases, and Neoplastic diseases) classification on HMS dataset axial orientation

| S# | Sequence | Classes and no. of slices used for training and testing | | Accuracy (%) | Sensitivity (TPR/Recall /Probability of detection) (%) | Specificity (TNR) (%) | Precision (Positive Predictive Value) (%) | AUC-value |
|---|---|---|---|---|---|---|---|---|
| | | Class | No. of Slices | | | | | |
| 1. | T1 | Normal | 113 | 96.6 | 91.8 | 100 | 100 | 0.95 |
| 2. | | Cerebrovascular | 167 | | 100 | 99.9 | 99.1 | 0.95 |
| 3. | | Degenerative | 74 | | 93 | 100 | 100 | 0.96 |
| 4. | | Inflammatory | 50 | | 89.4 | 100 | 100 | 0.94 |
| 5. | | Neoplastic | 142 | | 96 | 100 | 100 | 0.95 |
| 6. | T2 | Normal | 112 | 96.2 | 93.6 | 100 | 100 | 0.96 |
| 7. | | Cerebrovascular | 365 | | 100 | 99.9 | 89.7 | 0.96 |
| 8. | | Degenerative | 233 | | 95.4 | 100 | 100 | 0.97 |
| 9. | | Inflammatory | 207 | | 92.6 | 100 | 100 | 0.96 |
| 10. | | Neoplastic | 144 | | 91.7 | 100 | 100 | 0.95 |
| 11. | MR-GAD | Cerebrovascular | 25 | 98.1 | 100 | 100 | 100 | 1.0 |
| 12. | | Inflammatory | 96 | | 94.7 | 100 | 100 | 0.97 |
| 13. | | Neoplastic | 272 | | 100 | 99.9 | 98.2 | 0.98 |
| 14. | PDW | Normal | 84 | 96.1 | 96.9 | 99.9 | 94 | 0.97 |
| 15. | | Cerebrovascular | 180 | | 100 | 99.9 | 87.6 | 0.95 |
| 16. | | Inflammatory | 120 | | 88 | 100 | 100 | 0.94 |
| 17. | | Neoplastic | 90 | | 81 | 99.9 | 96.6 | 0.90 |

Table 2: Four class (Cerebrovascular, Degenerative, Inflammatory, and Neoplastic) classification on HMS dataset axial orientation

| S# | Sequence | Classes and no. of slices used for training and testing | | Accuracy (%) | Sensitivity (TPR/Recall /Probability of detection) (%) | Specificity (TNR) (%) | Precision (Positive Predictive Value) (%) | AUC-value |
|---|---|---|---|---|---|---|---|---|
| | | Class | No. of Slices | | | | | |
| 1. | T1 | Cerebrovascular | 167 | 96.3 | 100 | 99.9 | 89.1 | 0.96 |
| 2. | | Degenerative | 74 | | 90.1 | 100 | 100 | 0.95 |
| 3. | | Inflammatory | 50 | | 89.4 | 100 | 100 | 0.95 |
| 4. | | Neoplastic | 142 | | 94.2 | 100 | 100 | 0.97 |
| 5. | T2 | Cerebrovascular | 365 | 95.6 | 100 | 99.9 | 87.3 | 0.95 |
| 6. | | Degenerative | 233 | | 89.9 | 100 | 100 | 0.95 |
| 7. | | Inflammatory | 207 | | 90.5 | 100 | 100 | 0.95 |
| 8. | | Neoplastic | 144 | | 90.9 | 100 | 100 | 0.96 |
| 9. | PDW | Cerebrovascular | 180 | 97.1 | 100 | 99.9 | 90.3 | 0.95 |
| 10. | | Inflammatory | 120 | | 92.3 | 100 | 100 | 0.96 |
| 11. | | Neoplastic | 90 | | 88.5 | 100 | 100 | 0.94 |

Table 3: Neoplastic Class (Glioma, Meningioma, Metastatic Adenocarcinoma, Metastatic Bronchogenic carcinoma, and Sarcoma) classification on HMS dataset axial orientation

| S# | Sequence | Classes and no. of slices used for training and testing | | Accuracy (%) | Sensitivity (TPR/Recall/Probability of detection) (%) | Specificity (TNR) (%) | Precision (Positive Predictive Value) (%) | AUC-value |
|---|---|---|---|---|---|---|---|---|
| | | Class | No. of slices | | | | | |
| 1. | T1 | Glioma | 42 | 99.7 | 100 | 100 | 100 | 1.0 |
| 2. | | Sarcoma | 42 | | 100 | 100 | 100 | 1.0 |
| 3. | T2 | Glioma | 42 | 96.3 | 92.6 | 99.9 | 86.2 | 0.93 |

| | | | | | | | | |
|---|---|---|---|---|---|---|---|---|
| 4. | | Meningioma | 46 | | 96.2 | 99.9 | 92.6 | 0.97 |
| 5. | | Metastatic Adenocarcinoma | 28 | | 85.7 | 100 | 100 | 0.93 |
| 6. | | Metastatic Bronchogenic carcinoma | 24 | | 90.9 | 100 | 100 | 0.96 |
| 7. | | Sarcoma | 34 | | 100 | 100 | 100 | 1.0 |
| 8. | MR-GAD | Glioma | 44 | 96.8 | 100 | 98.4 | 90.1 | 0.90 |
| 9. | | Meningioma | 44 | | 78.4 | 100 | 100 | 0.90 |
| 10. | | Metastatic Adenocarcinoma | 40 | | 83.3 | 100 | 100 | 0.92 |
| 11. | | Metastatic Bronchogenic carcinoma | 40 | | 78.3 | 100 | 100 | 0.90 |
| 12. | | Sarcoma | 46 | | 78.3 | 100 | 100 | 0.90 |
| 13. | PDW | Glioma | 42 | 98.2 | 87.8 | 100 | 100 | 0.94 |
| 14. | | Meningioma | 42 | | 100 | 99.9 | 84.3 | 0.95 |
| 15. | | Metastatic Bronchogenic carcinoma | 44 | | 86.4 | 100 | 100 | 0.93 |
| 16. | | Sarcoma | 48 | | 100 | 100 | 100 | 1.0 |

Table 4: Neoplastic Class (Primary Tumor (Glioma, Meningioma, Sarcoma) and Secondary Tumor (Metastatic Adenocarcinoma, Metastatic Bronchogenic carcinoma) classification on HMS dataset axial orientation

| S # | Sequence | Classes and no. of slices used for training and testing | | Accuracy (%) | Sensitivity (TPR/Recall/Probability of detection) (%) | Specificity (TNR) (%) | Precision (Positive Predictive Value) (%) | AUC-value |
|---|---|---|---|---|---|---|---|---|
| | | Class | No. of slices | | | | | |
| 1. | T2 | Primary tumors | 122 | 99.6 | 100 | 100 | 100 | 1.0 |
| 2. | | Secondary tumors | 52 | | 100 | 100 | 100 | 1.0 |
| 3. | MR-GAD | Primary tumors | 134 | 98.6 | 100 | 99.9 | 98.5 | 0.96 |
| 4. | | Secondary tumors | 80 | | 91.5 | 100 | 100 | 0.96 |
| 5. | PDW | Primary tumors | 132 | | 100 | 98.8 | 96.4 | 0.90 |
| 6. | | Secondary tumors | 44 | | 81.8 | 100 | 100 | 0.90 |

Table 5: Neoplastic and Non-neoplastic (Cerebrovascular, Degenerative, and Inflammatory abnormality) classification on HMS dataset axial orientation

| S # | Sequence | Classes and no. of slices used for training and testing | | Accuracy (%) | Sensitivity (TPR/Recall/Probability of detection) (%) | Specificity (TNR) (%) | Precision (Positive Predictive Value) (%) | AUC-value |
|---|---|---|---|---|---|---|---|---|
| | | Class | No. of slices | | | | | |
| 1. | T1 | Neoplastic | 142 | 97.9 | 95.7 | 100 | 100 | 0.98 |
| 2. | | Non-Neoplastic | 241 | | 100 | 99.9 | 97.9 | 0.98 |
| 3. | T2 | Neoplastic | 144 | 96.8 | 92.6 | 100 | 100 | 0.96 |

| | | | | | | | | |
|---|---|---|---|---|---|---|---|---|
| 4. | | Non-Neoplastic | 805 | | 100 | 99.9 | 98.8 | 0.96 |
| 5. | MR-GAD | Neoplastic | 272 | 96.2 | 100 | 99.8 | 94.4 | 0.93 |
| 6. | | Non-Neoplastic | 121 | | 86.6 | 100 | 100 | 0.93 |
| 7. | PDW | Neoplastic | 90 | 97.8 | 97.7 | 100 | 100 | 0.99 |
| 8. | | Non-Neoplastic | 300 | | 100 | 99.9 | 99.3 | 0.99 |

Table 6: Neoplastic Class (Glioma, Meningioma, Metastatic Adenocarcinoma, Metastatic Bronchogenic carcinoma, Sarcoma) classification on BVHB dataset axial orientation

| **S#** | **Sequence** | **Classes and no. of slices used for training and testing** | | **Accuracy (%)** | **Sensitivity (TPR/Recall/ Probability of detection) (%)** | **Specificity (TNR) (%)** | **Precision (Positive Predictive Value) (%)** | **AUC-value** |
|---|---|---|---|---|---|---|---|---|
| | | **Class** | **No. of slices** | | | | | |
| 1. | T1 | Glioma | 50 | 95.1 | 98 | 95.7 | 96 | 0.98 |
| 2. | | Meningioma | 50 | | 87 | 96 | 98 | 0.99 |
| 3. | | Metastatic Adenocarcinoma | 50 | | 96 | 89.3 | 88 | 0.98 |
| 4. | | Metastatic Bronchogenic carcinoma | 50 | | 77 | 97.8 | 97 | 0.95 |
| 5. | | Sarcoma | 50 | | 93 | 87.9 | 88 | 1.0 |
| 6. | T2 | Glioma | 50 | 96.9 | 99 | 98.3 | 97 | 0.99 |
| 7. | | Meningioma | 50 | | 93 | 94.8 | 95 | 0.99 |
| 8. | | Metastatic Adenocarcinoma | 50 | | 91 | 95 | 95 | 0.98 |
| 9. | | Metastatic Bronchogenic carcinoma | 50 | | 87 | 96.4 | 97 | 0.98 |

| | | | | | | | | |
|---|---|---|---|---|---|---|---|---|
| 10. | | Sarcoma | 50 | | 96 | 99.5 | 100 | 1.0 |
| 11. | T1C | Glioma | 50 | 95.2 | 97 | 97 | 98 | 0.98 |
| 12. | | Meningioma | 50 | | 96 | 89 | 88 | 0.98 |
| 13. | | Metastatic Adenocarcinoma | 50 | | 92 | 93 | 92 | 0.97 |
| 14. | | Metastatic Bronchogenic carcinoma | 50 | | 91 | 96 | 95 | 0.99 |
| 15. | | Sarcoma | 50 | | 91 | 89.3 | 87 | 0.98 |
| 16. | PDW | Glioma | 50 | 96.3 | 99 | 98.3 | 97 | 1.0 |
| 17. | | Meningioma | 50 | | 85 | 100 | 100 | 0.97 |
| 18. | | Metastatic Adenocarcinoma | 50 | | 87 | 92 | 91 | 0.98 |
| 19. | | Metastatic Bronchogenic carcinoma | 50 | | 97 | 87.6 | 88 | 0.99 |
| 20. | | Sarcoma | 50 | | 93 | 100 | 100 | 1.0 |
| 21. | FLAIR | Glioma | 50 | 94.3 | 97 | 98 | 98 | 0.97 |
| 22. | | Meningioma | 50 | | 88 | 89.8 | 89 | 0.95 |
| 23. | | Metastatic Adenocarcinoma | 50 | | 92 | 83 | 81 | 0.97 |
| 24. | | Metastatic Bronchogenic carcinoma | 50 | | 87 | 89 | 87 | 0.98 |
| 25. | | Sarcoma | 50 | | 96 | 98 | 96 | 0.99 |

Table 7: Neoplastic Class (Glioma, Meningioma, Metastatic Adenocarcinoma, Metastatic Bronchogenic carcinoma, Sarcoma) classification on BVHB dataset coronal orientation

| S# | Sequence | Classes and no. of slices used for training and testing | | Accuracy (%) | Sensitivity (TPR/Recall/ Probability of detection) (%) | Specificity( TNR) (%) | Precision (Positive Predictive Value) (%) | AUC-value |
|---|---|---|---|---|---|---|---|---|
| | | Class | No. of slices | | | | | |
| 1. | T1 | Glioma | 50 | 96.1 | 99 | 95.7 | 96 | 0.99 |
| 2. | | Meningioma | 50 | | 88 | 96 | 97 | 0.99 |
| 3. | | Metastatic Adenocarcinoma | 50 | | 96 | 96 | 94 | 0.99 |
| 4. | | Metastatic Bronchogenic carcinoma | 50 | | 82 | 94 | 97 | 0.97 |
| 5. | | Sarcoma | 50 | | 96 | 98 | 96 | 1.0 |
| 6. | T2 | Glioma | 50 | 96.8 | 99 | 95 | 97 | 0.99 |
| 7. | | Meningioma | 50 | | 88 | 94.6 | 95 | 0.98 |
| 8. | | Metastatic Adenocarcinoma | 50 | | 91 | 94.6 | 93 | 0.99 |
| 9. | | Metastatic Bronchogenic carcinoma | 50 | | 92 | 93.4 | 92 | 0.99 |
| 10. | | Sarcoma | 50 | | 96 | 98 | 100 | 1.0 |
| 11. | T1C | Glioma | 50 | 96.2 | 98 | 99 | 98 | 0.97 |
| 12. | | Meningioma | 50 | | 93 | 91 | 90 | 0.99 |
| 13. | | Metastatic Adenocarcinoma | 50 | | 96 | 92 | 92 | 0.97 |
| 14. | | Metastatic Bronchogenic carcinoma | 50 | | 87 | 95.3 | 95 | 0.99 |
| 15. | | Sarcoma | 50 | | 95 | 98 | 100 | 0.99 |

| | | | | | | | | |
|---|---|---|---|---|---|---|---|---|
| 16. | PDW | Glioma | 50 | 95.4 | 99 | 96.7 | 95 | 0.98 |
| 17. | | Meningioma | 50 | | 82 | 99.2 | 98 | 0.98 |
| 18. | | Metastatic Adenocarcinoma | 50 | | 96 | 94 | 94 | 0.99 |
| 19. | | Metastatic Bronchogenic carcinoma | 50 | | 85 | 98.9 | 100 | 0.97 |
| 20. | | Sarcoma | 50 | | 87 | 97.6 | 98 | 1.0 |
| 21. | FLAIR | Glioma | 50 | 92.5 | 96 | 96.4 | 94 | 0.97 |
| 22. | | Meningioma | 50 | | 79 | 97 | 95 | 0.96 |
| 23. | | Metastatic Adenocarcinoma | 50 | | 91 | 83.2 | 82 | 0.98 |
| 24. | | Metastatic Bronchogenic carcinoma | 50 | | 85 | 89.1 | 89 | 0.92 |
| 25. | | Sarcoma | 50 | | 87 | 92.4 | 91 | 0.99 |

Table 8: Neoplastic Class (Glioma, Meningioma, Metastatic Adenocarcinoma, Metastatic Bronchogenic carcinoma, Sarcoma) classification on BVHB dataset sagittal orientation

| **S#** | **Sequence** | **Classes and no. of slices used for training and testing** | | **Accuracy (%)** | **Sensitivity (TPR/Recall/ Probability of detection) (%)** | **Specificity( TNR) (%)** | **Precision (Positive Predictive Value) (%)** | **AUC-value** |
|---|---|---|---|---|---|---|---|---|
| | | **Class** | **No. of slices** | | | | | |
| 1. | T1 | Glioma | 50 | 94.2 | 99 | 96.5 | 95 | 0.99 |
| 2. | | Meningioma | 50 | | 84 | 94 | 95 | 0.98 |
| 3. | | Metastatic Adenocarcinoma | 50 | | 83 | 91 | 90 | 0.95 |
| 4. | | Metastatic Bronchogenic carcinoma | 50 | | 77 | 87.2 | 86 | 0.91 |

| | | | | | | | | |
|---|---|---|---|---|---|---|---|---|
| 5. | | Sarcoma | 50 | | 91 | 99.3 | 100 | 1.0 |
| 6. | T2 | Glioma | 50 | 94.9 | 97 | 96.2 | 96 | 0.99 |
| 7. | | Meningioma | 50 | | 87 | 93 | 92 | 0.99 |
| 8. | | Metastatic Adenocarcinoma | 50 | | 91 | 89.2 | 88 | 0.98 |
| 9. | | Metastatic Bronchogenic carcinoma | 50 | | 85 | 93 | 92 | 0.94 |
| 10. | | Sarcoma | 50 | | 98 | 94 | 96 | 1.0 |
| 11. | T1C | Glioma | 50 | 96 | 99 | 94 | 97 | 0.99 |
| 12. | | Meningioma | 50 | | 90 | 95.2 | 95 | 0.99 |
| 13. | | Metastatic Adenocarcinoma | 50 | | 100 | 93 | 94 | 1.0 |
| 14. | | Metastatic Bronchogenic carcinoma | 50 | | 87 | 92 | 91 | 0.92 |
| 15. | | Sarcoma | 50 | | 89 | 99.6 | 100 | 0.98 |
| 16. | PDW | Glioma | 50 | 94.4 | 98 | 94 | 96 | 0.99 |
| 17. | | Meningioma | 50 | | 93 | 96 | 97 | 0.99 |
| 18. | | Metastatic Adenocarcinoma | 50 | | 91 | 84 | 86 | 0.99 |
| 19. | | Metastatic Bronchogenic carcinoma | 50 | | 72 | 83 | 88 | 0.94 |
| 20. | | Sarcoma | 50 | | 87 | 94 | 93 | 1.0 |
| 21. | FLAIR | Glioma | 50 | 95.1 | 98 | 97 | 96 | 0.98 |
| 22. | | Meningioma | 50 | | 91 | 93 | 95 | 0.99 |
| 23. | | Metastatic Adenocarcinoma | 50 | | 91 | 92 | 91 | 0.99 |

| | | | | | | | | |
|---|---|---|---|---|---|---|---|---|
| 24. | | Metastatic Bronchogenic carcinoma | 50 | | 87 | 93 | 92 | 0.98 |
| 25. | | Sarcoma | 50 | | 89 | 95.2 | 93 | 1.0 |

Table 9: Neoplastic Class (Primary Tumor (Glioma, Meningioma, Sarcoma) and Secondary Tumor (Metastatic Adenocarcinoma, Metastatic Bronchogenic carcinoma) classification on BVHB dataset axial orientation

| **S#** | **Sequence** | **Classes and no. of slices used for training and testing** | | **Accuracy (%)** | **Sensitivity/ TPR/Recall/Probability of detection** | **Sensitivity/ TNR** | **Precision/ Positive Predictive Value** | **AUC-value** |
|---|---|---|---|---|---|---|---|---|
| | | **Class** | **No. of slices** | | | | | |
| 1. | T1 | Primary tumors | 150 | 98.6 | 99 | 98 | 99 | 0.99 |
| 2. | | Secondary tumors | 100 | | 93 | 99 | 98 | 0.99 |
| 3. | T2 | Primary tumors | 150 | 98.5 | 99 | 97 | 99 | 0.97 |
| 4. | | Secondary tumors | 100 | | 94 | 94 | 95 | 0.97 |
| 5. | T1C | Primary tumors | 150 | 97.9 | 99 | 98 | 99 | 0.98 |
| 6. | | Secondary tumors | 100 | | 96 | 98 | 96 | 0.98 |
| 7. | PDW | Primary tumors | 150 | 98 | 99 | 95 | 98 | 0.96 |
| 8. | | Secondary tumors | 100 | | 84 | 98 | 96 | 0.96 |
| 9. | FLAIR | Primary tumors | 150 | 98.7 | 99 | 96 | 99 | 0.99 |

| | | | | | | | | |
|---|---|---|---|---|---|---|---|---|
| 10. | | Secondary tumors | 100 | | 98 | 94 | 94 | 0.99 |

Table 10: Neoplastic Class (Primary Tumor (Glioma, Meningioma, Sarcoma) and Secondary Tumor (Metastatic Adenocarcinoma, Metastatic Bronchogenic carcinoma) classification BVHB dataset coronal orientation

| **S#** | **Sequence** | **Classes and no. of slices used for training and testing** | | **Accuracy (%)** | **Sensitivity/ TPR/Recall/Probability of detection** | **Sensitivity/ TNR** | **Precision/ Positive Predictive Value** | **AUC-value** |
|---|---|---|---|---|---|---|---|---|
| | | **Class** | **No. of slices** | | | | | |
| 1. | T1 | Primary tumors | 150 | 98.8 | 99 | 98 | 99 | 0.99 |
| 2. | | Secondary tumors | 100 | | 95 | 97 | 96 | 0.99 |
| 3. | T2 | Primary tumors | 150 | 97.8 | 99 | 95 | 98 | 0.99 |
| 4. | | Secondary tumors | 100 | | 88 | 97 | 96 | 0.99 |
| 5. | T1C | Primary tumors | 150 | 95.8 | 97 | 96 | 97 | 1.0 |
| 6. | | Secondary tumors | 100 | | 92 | 93 | 92 | 1.0 |
| 7. | PDW | Primary tumors | 150 | 98.5 | 99 | 99 | 99 | 0.99 |
| 8. | | Secondary tumors | 100 | | 94 | 94 | 95 | 0.99 |
| 9. | FLAIR | Primary tumors | 150 | 98.7 | 100 | 98 | 99 | 0.98 |
| 10. | | Secondary tumors | 100 | | 88 | 94 | 100 | 0.98 |

Table 11: Neoplastic Class (Primary Tumor (Glioma, Meningioma, Sarcoma) and Secondary Tumor (Metastatic Adenocarcinoma, Metastatic Bronchogenic carcinoma) classification on BVHB dataset sagittal orientation

| S# | Sequence | Classes and no. of slices used for training and testing | | Accuracy (%) | Sensitivity /TPR/Recall/Probability of detection | Sensitivity /TNR | Precision /Positive Predictive Value | AUC - value |
|---|---|---|---|---|---|---|---|---|
| | | Class | No. of slices | | | | | |
| 1. | T1 | Primary tumors | 150 | 98.8 | 99 | 98 | 99 | 0.99 |
| 2. | | Secondary tumors | 100 | | 96 | 94 | 95 | 0.99 |
| 3. | T2 | Primary tumors | 150 | 99.2 | 99 | 98 | 99 | 1.0 |
| 4. | | Secondary tumors | 100 | | 96 | 97 | 98 | 1.0 |
| 5. | T1C | Primary tumors | 150 | 95.8 | 96 | 99 | 99 | 0.99 |
| 6. | | Secondary tumors | 100 | | 96 | 90 | 89 | 0.99 |
| 7. | PDW | Primary tumors | 150 | 99.3 | 99 | 99 | 99 | 1.0 |
| 8. | | Secondary tumors | 100 | | 98 | 99 | 98 | 1.0 |
| 9. | FLAIR | Primary tumors | 150 | 97.7 | 99 | 99 | 99 | 0.97 |
| 10. | | Secondary tumors | 100 | | 88 | 91 | 89 | 0.97 |

Table 12: Neoplastic and Non-neoplastic (Cerebrovascular, Degenerative, and Inflammatory abnormality) classification on BVHB dataset axial orientation

| S # | Sequence | Classes and no. of slices used for training and testing | | Accuracy (%) | Sensitivity (TPR/Recall/Probability of detection) (%) | Specificity (TNR) (%) | Precision (Positive Predictive Value) (%) | AUC - value |
|---|---|---|---|---|---|---|---|---|
| | | Class | No. of slices | | | | | |
| 1. | T1 | Neoplastic | 250 | 99.2 | 98 | 100 | 99 | 1.0 |
| 2. | | Non-Neoplastic | 500 | | 99 | 99 | 99 | 1.0 |
| 3. | T2 | Neoplastic | 250 | 96.5 | 83 | 92 | 93 | 0.97 |
| 4. | | Non-Neoplastic | 500 | | 99 | 98 | 97 | 0.97 |
| 5. | T1C | Neoplastic | 250 | 97.3 | 83 | 96 | 97 | 0.99 |
| 6. | | Non-Neoplastic | 500 | | 99 | 96 | 97 | 0.99 |
| 7. | PDW | Neoplastic | 250 | 98.1 | 94 | 97 | 98 | 0.98 |
| 8. | | Non-Neoplastic | 500 | | 99 | 99 | 98 | 0.98 |
| 9. | FLAIR | Neoplastic | 250 | 98.3 | 99 | 96 | 98 | 1.0 |
| 10. | | Non-Neoplastic | 500 | | 95 | 97 | 99 | 1.0 |

Table 13: Neoplastic and Non-neoplastic (Cerebrovascular, Degenerative, and Inflammatory abnormality) classification on BVHB dataset coronal orientation

| **S #** | **Sequence** | **Classes and no. of slices used for training and testing** | | **Accuracy (%)** | **Sensitivity (TPR/Recall/Probability of detection) (%)** | **Specificity (TNR) (%)** | **Precision (Positive Predictive Value) (%)** | **AUC-value** |
|---|---|---|---|---|---|---|---|---|
| | | **Class** | **No. of slices** | | | | | |
| 1. | T1 | Neoplastic | 250 | 99.7 | 100 | 98 | 99 | 1.0 |
| 2. | | Non-Neoplastic | 500 | | 99 | 99 | 100 | 1.0 |
| 3. | T2 | Neoplastic | 250 | 97.1 | 88 | 94 | 93 | 0.98 |
| 4. | | Non-Neoplastic | 500 | | 99 | 96 | 98 | 0.98 |

| | | | | | | | | |
|---|---|---|---|---|---|---|---|---|
| 5. | T1C | Neoplastic | 250 | 97.1 | 84 | 98 | 94 | 0.99 |
| 6. | | Non-Neoplastic | 500 | | 99 | 95 | 97 | 0.99 |
| 7. | PDW | Neoplastic | 250 | 96.9 | 93 | 99 | 94 | 0.96 |
| 8. | | Non-Neoplastic | 500 | | 98 | 98 | 98 | 0.96 |
| 9. | FLAIR | Neoplastic | 250 | 98.7 | 99 | 97 | 98 | 1.0 |
| 10. | | Non-Neoplastic | 500 | | 96 | 99 | 99 | 1.0 |

Table 14: Neoplastic and Non-neoplastic (Cerebrovascular, Degenerative, and Inflammatory abnormality) classification on BVHB dataset sagittal orientation

| S # | Sequence | Classes and no. of slices used for training and testing | | Accuracy (%) | Sensitivity (TPR/Recall/Probability of detection) (%) | Specificity (TNR) (%) | Precision (Positive Predictive Value) (%) | AUC - value |
|---|---|---|---|---|---|---|---|---|
| | | Class | No. of slices | | | | | |
| 1. | T1 | Neoplastic | 250 | 99.2 | 100 | 99 | 98 | 1.0 |
| 2. | | Non-Neoplastic | 500 | | 99 | 98 | 100 | 1.0 |
| 3. | T2 | Neoplastic | 250 | 97.6 | 86 | 99 | 98 | 0.98 |
| 4. | | Non-Neoplastic | 500 | | 99 | 96 | 98 | 0.98 |
| 5. | T1C | Neoplastic | 250 | 96.9 | 82 | 95 | 95 | 0.97 |
| 6. | | Non-Neoplastic | 500 | | 99 | 97 | 97 | 0.97 |
| 7. | PDW | Neoplastic | 250 | 97.2 | 95 | 92 | 93 | 0.98 |
| 8. | | Non-Neoplastic | 500 | | 98 | 97 | 98 | 0.98 |
| 9. | FLAIR | Neoplastic | 250 | 99.2 | 100 | 99 | 99 | 0.99 |
| 10. | | Non-Neoplastic | 500 | | 97 | 98 | 100 | 0.99 |

Table 15: Five class (Normal, Cerebrovascular diseases, Degenerative diseases, Inflammatory diseases, and Neoplastic diseases) classification on BVHB dataset axial orientation

| S # | Sequence | Classes and no. of slices used for training and testing | | Accuracy (%) | Sensitivity (TPR/Recall /Probability of detection) (%) | Specificity(TNR) (%) | Precision (Positive Predictive Value) (%) | AUC-value |
|---|---|---|---|---|---|---|---|---|
| | | Class | No. of Slices | | | | | |
| 1. | T1 | Normal | 250 | 97.8 | 100 | 99 | 100 | 1.0 |
| 2. | | Cerebrovascular | 250 | | 97 | 98 | 97 | 0.99 |
| 3. | | Degenerative | 250 | | 97 | 94 | 95 | 1.0 |
| 4. | | Inflammatory | 250 | | 88 | 95 | 95 | 0.98 |
| 5. | | Neoplastic | 250 | | 100 | 98 | 98 | 1.0 |
| 6. | T2 | Normal | 250 | 94.8 | 98 | 98 | 99 | 1.0 |
| 7. | | Cerebrovascular | 250 | | 94 | 93 | 93 | 0.99 |
| 8. | | Degenerative | 250 | | 98 | 97 | 97 | 1.0 |
| 9. | | Inflammatory | 250 | | 93 | 94 | 93 | 0.99 |
| 10. | | Neoplastic | 250 | | 92 | 96 | 96 | 0.99 |
| 11. | T1C | Normal | 250 | 97 | 100 | 99 | 99 | 1.0 |
| 12. | | Cerebrovascular | 250 | | 97 | 97 | 96 | 0.99 |
| 13. | | Degenerative | 250 | | 97 | 99 | 99 | 0.99 |
| 14. | | Inflammatory | 250 | | 98 | 97 | 97 | 0.99 |
| 15. | | Neoplastic | 250 | | 94 | 96 | 95 | 0.98 |
| 16. | PDW | Normal | 250 | 93.7 | 100 | 98 | 98 | 1.0 |
| 17. | | Cerebrovascular | 250 | | 95 | 93 | 91 | 0.98 |
| 18. | | Degenerative | 250 | | 88 | 95 | 95 | 0.96 |
| 19. | | Inflammatory | 250 | | 93 | 94 | 93 | 0.97 |
| 20. | | Neoplastic | 250 | | 93 | 92 | 92 | 0.97 |
| 21. | FLAIR | Normal | 250 | 98.2 | 100 | 99 | 98 | 1.0 |

| | | | | | | | | |
|---|---|---|---|---|---|---|---|---|
| 22. | | Cerebrovascular | 250 | | 100 | 98 | 98 | 1.0 |
| 23. | | Degenerative | 250 | | 97 | 95 | 95 | 0.99 |
| 24. | | Inflammatory | 250 | | 97 | 98 | 97 | 0.99 |
| 25. | | Neoplastic | 250 | | 98 | 99.5 | 99 | 0.99 |

Table 16: Five class (Normal, Cerebrovascular diseases, Degenerative diseases, Inflammatory diseases, and Neoplastic diseases) classification on BVHB dataset coronal orientation

| S # | Sequence | Classes and no. of slices used for training and testing | | Accuracy (%) | Sensitivity (TPR/Recall /Probability of detection) (%) | Specificity (TNR) (%) | Precision (Positive Predictive Value) (%) | AUC-value |
|---|---|---|---|---|---|---|---|---|
| | | Class | No. of Slices | | | | | |
| 1. | T1 | Normal | 250 | 98.5 | 100 | 98 | 100 | 1.0 |
| 2. | | Cerebrovascular | 250 | | 99 | 99 | 98 | 1.0 |
| 3. | | Degenerative | 250 | | 98 | 96 | 97 | 1.0 |
| 4. | | Inflammatory | 250 | | 91 | 97 | 98 | 0.98 |
| 5. | | Neoplastic | 250 | | 100 | 95 | 98 | 1.0 |
| 6. | T2 | Normal | 250 | 95.2 | 99 | 98 | 98 | 1.0 |
| 7. | | Cerebrovascular | 250 | | 95 | 94 | 94 | 0.98 |
| 8. | | Degenerative | 250 | | 97 | 98 | 97 | 1.0 |
| 9. | | Inflammatory | 250 | | 93 | 94 | 94 | 0.99 |
| 10. | | Neoplastic | 250 | | 94 | 95 | 96 | 0.99 |
| 11. | T1C | Normal | 250 | 97.1 | 98 | 99.5 | 100 | 1.0 |
| 12. | | Cerebrovascular | 250 | | 97 | 96 | 96 | 0.99 |
| 13. | | Degenerative | 250 | | 97 | 99 | 99 | 1.0 |
| 14. | | Inflammatory | 250 | | 96 | 97 | 97 | 1.0 |
| 15. | | Neoplastic | 250 | | 98 | 95 | 94 | 0.99 |
| 16. | PDW | Normal | 250 | 96.9 | 100 | 99 | 99 | 1.0 |
| 17. | | Cerebrovascular | 250 | | 97 | 98 | 95 | 0.99 |
| 18. | | Degenerative | 250 | | 95 | 97 | 97 | 0.99 |

| | | | | | | | | |
|---|---|---|---|---|---|---|---|---|
| 19. | | Inflammatory | 250 | | 95 | 97 | 99 | 0.98 |
| 20. | | Neoplastic | 250 | | 100 | 98 | 98 | 1.0 |
| 21. | FLAIR | Normal | 250 | 98.9 | 100 | 98 | 100 | 1.0 |
| 22. | | Cerebrovascular | 250 | | 100 | 99 | 100 | 0.99 |
| 23. | | Degenerative | 250 | | 97 | 98 | 98 | 1.0 |
| 24. | | Inflammatory | 250 | | 99 | 98 | 99 | 0.99 |
| 25. | | Neoplastic | 250 | | 97 | 99 | 99 | 1.0 |

Table 17: Five class (Normal, Cerebrovascular diseases, Degenerative diseases, Inflammatory diseases, and Neoplastic diseases) classification on BVHB dataset sagittal orientation

| **S #** | **Sequence** | **Classes and no. of slices used for training and testing** | | **Accuracy (%)** | **Sensitivity (TPR/Recall /Probability of detection) (%)** | **Specificity (TNR) (%)** | **Precision (Positive Predictive Value) (%)** | **AUC-value** |
|---|---|---|---|---|---|---|---|---|
| | | **Class** | **No. of Slices** | | | | | |
| 1. | T1 | Normal | 250 | 99.6 | 99 | 99.7 | 100 | 1.0 |
| 2. | | Cerebrovascular | 250 | | 99 | 100 | 100 | 1.0 |
| 3. | | Degenerative | 250 | | 100 | 98.9 | 98 | 1.0 |
| 4. | | Inflammatory | 250 | | 100 | 98.7 | 100 | 1.0 |
| 5. | | Neoplastic | 250 | | 100 | 99 | 99 | 1.0 |
| 6. | T2 | Normal | 250 | 95.9 | 100 | 97 | 97 | 1.0 |
| 7. | | Cerebrovascular | 250 | | 95 | 96 | 95 | 0.98 |
| 8. | | Degenerative | 250 | | 98 | 97 | 98 | 1.0 |
| 9. | | Inflammatory | 250 | | 94 | 94 | 95 | 0.99 |
| 10. | | Neoplastic | 250 | | 94 | 96 | 95 | 0.99 |
| 11. | T1C | Normal | 250 | 96.4 | 100 | 99.6 | 100 | 1.0 |
| 12. | | Cerebrovascular | 250 | | 98 | 97 | 96 | 1.0 |
| 13. | | Degenerative | 250 | | 95 | 97 | 98 | 1.0 |
| 14. | | Inflammatory | 250 | | 96 | 95 | 98 | 0.99 |
| 15. | | Neoplastic | 250 | | 91 | 97 | 95 | 0.99 |
| 16. | PDW | Normal | 250 | 96.4 | 100 | 94 | 98 | 1.0 |

| | | | | | | | | |
|---|---|---|---|---|---|---|---|---|
| 17. | | Cerebrovascular | 250 | | 97 | 98 | 95 | 0.99 |
| 18. | | Degenerative | 250 | | 93 | 94 | 97 | 0.97 |
| 19. | | Inflammatory | 250 | | 95 | 95 | 95 | 0.97 |
| 20. | | Neoplastic | 250 | | 96 | 97 | 96 | 0.99 |
| 21. | FLAIR | Normal | 250 | 97.8 | 100 | 99 | 100 | 1.0 |
| 22. | | Cerebrovascular | 250 | | 100 | 93 | 95 | 1.0 |
| 23. | | Degenerative | 250 | | 96 | 97 | 95 | 0.99 |
| 24. | | Inflammatory | 250 | | 95 | 98 | 98 | 1.0 |
| 25. | | Neoplastic | 250 | | 98 | 97 | 97 | 0.98 |

Table 18: Four class (Cerebrovascular, Degenerative, Inflammatory, and Neoplastic) classification on BVHB dataset axial orientation

| S# | Sequence | Classes and no. of slices used for training and testing | | Accuracy (%) | Sensitivity (TPR/Recall/ Probability of detection) (%) | Specificity (TNR) (%) | Precision (Positive Predictive Value) (%) | AUC-value |
|---|---|---|---|---|---|---|---|---|
| | | Class | No. of Slices | | | | | |
| 1. | T1 | Cerebrovascular | 250 | 98.8 | 100 | 98 | 99 | 1.0 |
| 2. | | Degenerative | 250 | | 96 | 99 | 100 | 0.99 |
| 3. | | Inflammatory | 250 | | 98 | 97 | 98 | 1.0 |
| 4. | | Neoplastic | 250 | | 99 | 96 | 98 | 1.0 |
| 5. | T2 | Cerebrovascular | 250 | 94.2 | 95 | 94 | 93 | 0.98 |
| 6. | | Degenerative | 250 | | 96 | 99 | 98 | 0.99 |
| 7. | | Inflammatory | 250 | | 93 | 92 | 90 | 0.98 |
| 8. | | Neoplastic | 250 | | 90 | 94 | 98 | 0.98 |
| 9. | T1C | Cerebrovascular | 250 | 96.3 | 97 | 96 | 96 | 0.98 |
| 10. | | Degenerative | 250 | | 97 | 95 | 96 | 1.0 |
| 11. | | Inflammatory | 250 | | 95 | 97 | 97 | 0.99 |
| 12. | | Neoplastic | 250 | | 97 | 96 | 97 | 1.0 |
| 13. | PDW | Cerebrovascular | 250 | 96 | 96 | 97 | 97 | 0.99 |
| 14. | | Degenerative | 250 | | 96 | 95 | 95 | 0.98 |

| | | | | | | | | |
|---|---|---|---|---|---|---|---|---|
| 15. | | Inflammatory | 250 | | 97 | 96 | 94 | 0.98 |
| 16. | | Neoplastic | 250 | | 98 | 96 | 96 | 0.99 |
| 17. | FLAIR | Cerebrovascular | 250 | 97.1 | 95 | 99 | 100 | 1.0 |
| 18. | | Degenerative | 250 | | 92 | 95 | 95 | 0.98 |
| 19. | | Inflammatory | 250 | | 99 | 97 | 97 | 0.99 |
| 20. | | Neoplastic | 250 | | 97 | 99 | 98 | 0.96 |

Table 19: Four class (Cerebrovascular, Degenerative, Inflammatory, and Neoplastic) classification on HMS dataset coronal orientation

| S# | Sequence | Classes and no. of slices used for training and testing | | Accuracy (%) | Sensitivity (TPR/Recall/ Probability of detection) (%) | Specificity (TNR) (%) | Precision (Positive Predictive Value) (%) | AUC-value |
|---|---|---|---|---|---|---|---|---|
| | | Class | No. of Slices | | | | | |
| 1. | T1 | Cerebrovascular | 250 | 98.8 | 100 | 96 | 97 | 1.0 |
| 2. | | Degenerative | 250 | | 100 | 99 | 100 | 1.0 |
| 3. | | Inflammatory | 250 | | 97 | 98 | 100 | 0.99 |
| 4. | | Neoplastic | 250 | | 97 | 100 | 100 | 1.0 |
| 5. | T2 | Cerebrovascular | 250 | 94.6 | 95 | 94 | 93 | 0.97 |
| 6. | | Degenerative | 250 | | 96 | 94 | 95 | 0.99 |
| 7. | | Inflammatory | 250 | | 93 | 95 | 94 | 0.99 |
| 8. | | Neoplastic | 250 | | 94 | 96 | 97 | 0.98 |
| 9. | T1C | Cerebrovascular | 250 | 97.2 | 98 | 98 | 97 | 0.99 |
| 10. | | Degenerative | 250 | | 97 | 93 | 97 | 0.99 |
| 11. | | Inflammatory | 250 | | 97 | 95 | 97 | 0.99 |
| 12. | | Neoplastic | 250 | | 95 | 98 | 95 | 0.99 |
| 13. | PDW | Cerebrovascular | 250 | 96.2 | 96 | 98 | 98 | 0.98 |
| 14. | | Degenerative | 250 | | 97 | 95 | 95 | 0.98 |
| 15. | | Inflammatory | 250 | | 97 | 94 | 94 | 0.99 |
| 16. | | Neoplastic | 250 | | 99 | 96 | 96 | 0.97 |
| 17. | FLAIR | Cerebrovascular | 250 | 97.5 | 95 | 94 | 91 | 1.0 |

| | | | | | | | | |
|---|---|---|---|---|---|---|---|---|
| 18. | | Degenerative | 250 | | 98 | 94 | 94 | 1.0 |
| 19. | | Inflammatory | 250 | | 98 | 99 | 99 | 0.99 |
| 20. | | Neoplastic | 250 | | 97 | 96 | 97 | 0.98 |

Table 20: Four class (Cerebrovascular, Degenerative, Inflammatory, and Neoplastic) classification on BVHB dataset sagittal orientation

| **S#** | **Sequence** | **Classes and no. of slices used for training and testing** | | **Accuracy (%)** | **Sensitivity (TPR/Recall/ Probability of detection) (%)** | **Specificity (TNR) (%)** | **Precision (Positive Predictive Value) (%)** | **AUC-value** |
|---|---|---|---|---|---|---|---|---|
| | | **Class** | **No. of Slices** | | | | | |
| 1. | T1 | Cerebrovascular | 250 | 98.7 | 100 | 96 | 97 | 0.94 |
| 2. | | Degenerative | 250 | | 92 | 99 | 100 | 0.95 |
| 3. | | Inflammatory | 250 | | 100 | 100 | 100 | 0.96 |
| 4. | | Neoplastic | 250 | | 85 | 98 | 100 | 0.95 |
| 5. | T2 | Cerebrovascular | 250 | 92.9 | 93 | 96 | 94 | 0.98 |
| 6. | | Degenerative | 250 | | 95 | 94 | 95 | 0.99 |
| 7. | | Inflammatory | 250 | | 92 | 93 | 91 | 0.98 |
| 8. | | Neoplastic | 250 | | 92 | 91 | 90 | 0.97 |
| 9. | T1C | Cerebrovascular | 250 | 96.1 | 98 | 93 | 95 | 0.99 |
| 10. | | Degenerative | 250 | | 96 | 98 | 99 | 0.99 |
| 11. | | Inflammatory | 250 | | 96 | 96 | 95 | 0.99 |
| 12. | | Neoplastic | 250 | | 91 | 99 | 98 | 0.99 |
| 13. | PDW | Cerebrovascular | 250 | 95.3 | 89 | 92 | 90 | 0.89 |
| 14. | | Degenerative | 250 | | 93 | 94 | 93 | 0.91 |
| 15. | | Inflammatory | 250 | | 91 | 91 | 89 | 0.88 |
| 16. | | Neoplastic | 250 | | 93 | 93 | 92 | 0.91 |
| 17. | FLAIR | Cerebrovascular | 250 | 96.9 | 86 | 99.5 | 100 | 0.97 |
| 18. | | Degenerative | 250 | | 92 | 98.6 | 99 | 0.99 |
| 19. | | Inflammatory | 250 | | 99 | 96 | 96 | 1.0 |
| 20. | | Neoplastic | 250 | | 97 | 97 | 96 | 0.98 |